TÉCNICO LISBOA

Estimation of Aerodynamic and Control Derivatives of Small Fixed-Wing Aircraft using Numerical Simulations and Wind Tunnel Experiments

Carlos Alberto Almeida Seixas

Thesis to obtain the Master of Science Degree in

Aerospace Engineering

Supervisor: Prof. André Calado Marta

Examination Committee

Chairperson: Prof. Afzal Suleman

Supervisor: Prof. André Calado Marta

Member of the Committee: Prof. José Raul Carreira Azinheira

November 2022

Dedicated to the single lady looking for a man to take her to the moon, I´m just a few steps away from getting my license..

Acknowledgments

Firstly, I would like to express a special eternal thanks to my Family for their unconditional support over the years to make this course a reality, especially to my Mother, Father, Sister and Girlfriend, who have always supported me.

Secondly, a big thanks for all the transmitted knowledge and rational tools acquired, for my two engineering schools, ”Instituto Superior Técnico da Universidade de Lisboa” and ”Faculdade de Engenharia da Universidade do Porto”, I would like to thank Prof. Marta for being an outstanding advisor. From the beginning of my journey in the Aerospace Degree, to graduate master school, Prof. Marta believed in me and gave me confidence that I could finish this thesis in one school year as well as make a seamless transition from a different undergraduate background. Prof. Marta was very supportive of my rigid graduation timeline and his optimism fueled my efforts in producing a successful final result. Also to all the teachers who directly or indirectly contributed to my knowledge, a really special thanks to all the lecturers in Aerodynamics, Structures, Flight Stability, Aeroacoustics, Material Strength, Propulsion, Aeroelasticity, Hydraulics, Fluid Mechanics, Statistics and Management, which have become my favorite subjects. A special thanks to all my university colleagues, especially to the ”AeroTéc” and ”FSTLisboa” team, who were always present during the wind tunnel experiments, allowing them to provide the necessary hardware tools and materials to make the wind tunnel tests possible, thank you very much!

Thirdly, I am very grateful to my country, Portugal, which gave me all the necessary tools of knowledge, for a solid engineering background to form me, so that one day later I can contribute significantly to the Portuguese society.

Resumo

Nos últimos anos, o uso de pequenos VANT (Veículos Aéreos Não Tripulados) em atividades recreativas e comerciais experimentou um crescimento significativo. Os benefícios dos VANTs vêm principalmente da sua elevada autonomia usando sistemas automáticos de orientação e controle.

O desempenho de tais sistemas depende muito da qualidade do modelo de aeronave identificado, isso torna-se de extrema importância para o processo geral.

O objetivo desta Tese é estabelecer as etapas necessárias para a conceção de um VANT, construindo um novo modelo em XFLR5 ”Test Aircraft” e recriando na integra o modelo elaborado fisicamente para análise no Túnel de Vento, assim é possível comparar os resultados para validação dos mesmos, tornando possível a análise de qualquer modelo, assim é possível construir a identificação do modelo, incorporando estimativas analíticas e respetivas simulações numéricas. Será seguido por ensaios em túnel de vento.

Em primeira instância serão determinadas as derivadas aerodinâmicas e de controle para serem usadas em equações simplificadas de movimento longitudinal e lateral usando aproximações analíticas encontradas na literatura base para a presente atividade.

Posteriormente, usando as ferramentas numéricas disponíveis, como XFLR5 ou Start-CCM +, melhores estimativas são calculadas com base numa definição geométrica mais detalhada do VANT selecionado para o caso de estudo.

Finalmente, um modelo VANT preliminar é identificado, que pode ser validado em túnel de vento.

Palavras-chave: VANT, Aerodinâmica, Derivadas Aerodinâmicas e de Controlo, Dinâmica de Voo, Estabilidade de Voo e Controlo de Voo.

Abstract

In recent years, the use of small UAVs (Unmanned Aerial Vehicles) in recreational and commercial activities has experienced significant growth. The benefits of UAVs mainly come from their high autonomy using automatic guidance and control systems.

The performance of such systems depends a lot on the quality of the identified aircraft model, which becomes extremely important for the general process.

The objective of this Thesis is to establish the necessary steps for the conception of a UAV, building a new model in XFLR5 ”Test Aircraft” and completely recreating the model physically elaborated for analysis in the Wind Tunnel, so it is possible to compare the results for validation of the themselves, making it possible to analyze any model, so that it is possible to build the identification of the model, incorporating analytical estimates and respective numerical simulations. It will be followed by wind tunnel tests.

In the first instance, the aerodynamic and control derivatives will be determined to be used in simplified equations of longitudinal and lateral motion using analytical approximations. found in the base literature for the present activity.

Later, using available numerical tools, such as XFLR5 or Start-CCM+, best estimates are calculated based on a more detailed geometric definition of the UAV selected for the case study.

Finally, a preliminary UAV model is identified, which can be validated in a wind tunnel.

Keywords: UAV, Aerodynamics, Aerodynamic and Control Derivatives, Flight Dynamics, Flight Stability, Flight Control.

Contents

Resumo vii
Abstract ix
List of Tables xv
List of Figures xvii
Nomenclature xxi
Glossary 1

1 Introduction **1**
1.1 Motivation 1
1.2 Topic Overview 3
1.3 Objectives and Deliverables 4
1.4 Thesis Outline 5

2 Formulation of Stability Equations **7**
2.1 Equations of Motion 7
2.1.1 Aircraft Body Axes 7
2.1.2 Euler Angles 8
2.1.3 Trajectory Equations 10
2.1.4 Aircraft's Rotational Dynamics 11
2.1.5 Aircraft's Translational Dynamics 13
2.2 Forces and Moments 14
2.3 Control Derivatives of Linearized Equations 16
2.4 Stability Control Models 17
2.4.1 Longitudinal Stability Model 17
2.4.2 Lateral Stability Model 18
2.5 Identification of Relevant Stability Derivatives 19
2.5.1 Longitudinal Mode: 19
2.5.2 Lateral Mode: 19

3 Estimation of Stability Derivatives **20**
3.1 Aerodynamic Derivatives of Linearized Equations 20
3.1.1 Longitudinal Derivatives 22

3.1.2 Lateral Derivatives . . . 22
3.2 Numerical Models . . . 24
3.3 Computational Fluid Dynamics . . . 26
3.3.1 Vortex Lattice Method (VLM) . . . 26
3.3.2 XFLR5 . . . 27
3.4 Wind Tunnel . . . 29
3.4.1 Force Balance . . . 31

4 Design and Building of Aircraft Models **33**
4.1 Test Aircraft Model Design . . . 33
4.1.1 Airfoil Profile Design . . . 33
4.2 Test Aircraft Model Building . . . 37
4.3 F35 Model Design . . . 41
4.4 F35 Model Building . . . 42

5 Calibration of Force Balance **47**
5.1 Structure Assembly . . . 47
5.2 Calibration Results . . . 49
5.3 Calibration Equations . . . 52

6 Longitudinal and Lateral Derivatives **54**
6.1 Test Aircraft . . . 54
6.1.1 Test Aircraft Geometry . . . 55
6.1.2 Test Aircraft Input Values for Calculations . . . 56
6.1.3 Test Aircraft Results . . . 58
6.1.4 Test Aircraft Discussion of Numerical and Qualitative Model Analysis . . . 66
6.2 F35 Aircraft . . . 69
6.2.1 F35 Aircraft Geometry . . . 69
6.2.2 F35 Aircraft Input Values for Calculations . . . 71
6.2.3 F35 Aircraft Results . . . 72
6.2.4 F35 Aircraft Discussion of Numerical and Qualitative Model Analysis . . . 75

7 Conclusions **77**
7.1 Achievements . . . 77
7.2 Future Work . . . 78

Bibliography **79**

A Excel Final Results - XFLR5 **81**
A.1 Tables - Stability Derivatives - Test Aircraft - XFLR5 . . . 81
A.2 Tables - Control Derivatives - Test Aircraft - XFLR5 . . . 82
A.3 Excel - Control Derivatives - Test Aircraft - XFLR5 . . . 83

B Excel Final Results - Wind Tunnel **87**

B.1 Excel - Stability Derivatives - Test Aircraft - Wind Tunnel 88

B.2 Excel - Stability Derivatives - F35 Aircraft - Wind Tunnel 93

B.3 Excel - Control Derivatives - Test Aircraft - Wind Tunnel 97

B.4 Procedure Guide for Balance of Forces 100

List of Tables

4.1 Model Test Reference Values 33
4.2 F35 Model Specifications 41

5.1 Calibration Equations Table - Matlab 53

6.1 Inertia Aircraft Table 56
6.2 Test Aircraft Values 57
6.3 Reference Values - Test Aircraft 57
6.4 Air Properties - Test Aircraft 57
6.5 Mean Values for Different Velocities Test Aircraft Table 63
6.6 Test Aircraft - Aerodynamic Coefficients From Wind Tunnel 64
6.7 Test Aircraft - Aerodynamic Coefficients 64
6.8 Stability Derivatives Test Aircraft - XFLR5 66
6.9 Stability Derivatives Test Aircraft - Wind Tunnel 67
6.10 Control Derivatives Test Aircraft - XFLR5 and Wind Tunnel 68
6.11 Air Properties - F35 Aircraft 71
6.12 F35 Model Specifications 71
6.13 Reference Values - F35 Aircraft 71
6.14 F35 Aircraft - Aerodynamic Coefficients From Wind Tunnel 73
6.15 F35 Aircraft - Aerodynamic Coefficients 74
6.16 Stability Derivatives F35 Aircraft - Wind Tunnel 75

A.1 Test Aircraft - Data From Excel - XFLR5 81

B.1 Test Aircraft - Data From Excel - Wind Tunnel 87
B.2 F35 Aircraft - Data From Excel - Wind Tunnel 87

List of Figures

1.1 Main Areas in Aircraft Design 2
1.2 Wind Tunnel Test Aircraft Model 3
1.3 Logical System of Interference in an Aircraft Read by Sensors and Answered by Actuators to Maintain Trim Flight - Since the Aerodynamic and Control Derivatives are Essential to Quantify the Necessary Changes in the Wings and Ailerons to Maintain Trim Flight 4

2.1 Body and Earth Reference Frames [2] 7
2.2 Aircraft Reference Frame [3] 8
2.3 Aircraft Trajectory Example 10
2.4 Symmetry Aircraft Plane 12
2.5 Applied Forces and Moments in Aircraft [14] 14
2.6 Control Model System Example MIMO 17

3.1 Model Characterization 21
3.2 Finite Difference 25
3.3 Vortex Lattice Method (VLM) 27
3.4 3D Panel Method 27
3.5 Grid of Panels 28
3.6 Wind Tunnel Types 30
3.7 Balance of Forces Components [29] 31
3.8 Balance of Forces [29] 32

4.1 Profile SD7062 (14%) 34
4.2 Profile S8036 (16%) 35
4.3 C_L vs C_D Polars for $Re = 100000$ and $Re = 200000$ 35
4.4 Profile NACA 0015 36
4.5 C_L vs C_D Polars for $Re = 100000$ and $Re = 200000$, Profile NACA 0015 36
4.6 Cutting Profiles in XPS 37
4.7 Support Wings Building 37
4.8 Ailerons Cut 38
4.9 Ailerons Attachment to Main Wing 38
4.10 Installation of Servos Mechanisms 38

4.11 Tail Wing and Fin Building . . . 39
4.12 Servo Mechanisms Test . . . 39
4.13 Main Wing and Tail Wing Calibration . . . 40
4.14 Final Test Aircraft . . . 40
4.15 F35 . . . 41
4.16 F35 Cockpit Building . . . 42
4.17 F35 Fuselage Building . . . 42
4.18 F35 Fuselage Final . . . 43
4.19 F35 Rear Wings Installation . . . 43
4.20 F35 Front Overview . . . 44
4.21 F35 Aircraft Final - Front View . . . 45
4.22 F35 Aircraft Final - Left View . . . 46
4.23 F35 Aircraft Final - Right View . . . 46

5.1 Positioning the Balance of Forces in the Wind Tunnel . . . 47
5.2 Calibration Structure . . . 48
5.3 Force and Moment Calibration Process . . . 48
5.4 Force and Moment Calibration Process . . . 49
5.5 Calibration Block Diagram used for the Present Master Thesis . . . 49
5.6 Calibration Results for Force ”Fx” Positive . . . 50
5.7 Calibration Results for Moment ”My” Positive . . . 50
5.8 Calibration Results for Compose Forces ”Fx” and ”Fz” Negative . . . 51
5.9 Calibration Results for Combined Forces and Moments ”Fx”, ”Fz” and ”My” Negative . . . 51

6.1 Real Test Aircraft Geometry and Mass Distribution . . . 54
6.2 CFD Test Aircraft Model . . . 55
6.3 Profile SD 7062 . . . 55
6.4 Profile NACA 0015 . . . 55
6.5 Graphics Foil in 2D for SD 7062 Analysis relative to Test Aircraft . . . 58
6.6 Graphics Foil in 2D for NACA 0015 Analysis relative to Test Aircraft . . . 59
6.7 C_p Distribution for Different Angles of Attack $\alpha = -2°$ and $\alpha = 0°$ . . . 59
6.8 C_p Distribution for Different Angles of Attack $\alpha = 1.5°$ and $\alpha = 3°$ . . . 60
6.9 C_p Distribution for Different Angles of Attack $\alpha = 5°$ and $\alpha = 7°$ . . . 60
6.10 C_p Distribution for Different Angles of Attack $\alpha = 9°$ and $\alpha = 11°$ . . . 61
6.11 3D Aerodynamic Coefficients Graphics C_L ,C_D, C_m, with variation of $-2° < \alpha < 11°$ . . . 61
6.12 Test Aircraft Geometry and Inertia Distribution . . . 62
6.13 Reference Values for Zero Speed in Wind Tunnel . . . 63
6.14 C$_{D_u}$ . . . 64
6.15 C$_{L_u}$ . . . 65
6.16 C$_{m_u}$ . . . 65

6.17 Test Aircraft δ_a Variation 68
6.18 F35 Aircraft Wind Tunnel Assembly 69
6.19 F35 Aircraft Cruise Flight 69
6.20 F35 Aircraft 70
6.21 F35 Aircraft Back View 70
6.22 Wind Tunnel F35 Aircraft 72
6.23 F35 Aircraft - Reference Values 72
6.24 F35 Aircraft in Wind Tunnel 73
6.25 F35 Aircraft Speed Variation - 0 m/s, 6.3 m/s, 10 m/s, 15 m/s, 20m/s, 25m/s, 0 m/s 74

A.1 Speed 10 m/s 81
A.2 $\alpha = 0°$ 82
A.3 δ_e Variation 82
A.4 δ_a Variation 82
A.5 δ_r Variation 82
A.6 Test Aircraft δ_e Variation 83
A.7 Test Aircraft δ_a Variation 84
A.8 Test Aircraft δ_r Variation 85

B.1 Test Aircraft Speed Variation 88
B.2 Test Aircraft Angle of Attack Variation 89
B.3 Test Aircraft β Variation 90
B.4 Test Aircraft Pitch Moment Variation 91
B.5 Test Aircraft Turning Moment Variation 92
B.6 Test Aircraft Rolling Moment Variation 92
B.7 F35 Aircraft Speed Variation 93
B.8 F35 Aircraft Angle of Attack Variation 94
B.9 F35 Aircraft β Variation 95
B.10 F35 Aircraft Pitch Moment Variation 96
B.11 F35 Aircraft Yaw Moment Variation 96
B.12 F35 Aircraft Rolling Moment Variation 96
B.13 Test Aircraft δ_e Variation 97
B.14 Test Aircraft δ_a Variation 98
B.15 Test Aircraft δ_r Variation 99

Nomenclature

Greek symbols

α	Angle of attack.
β	Angle of side-slip.
μ	Molecular viscosity coefficient.
ρ	Density.

Roman symbols

C_D	Coefficient of drag.
C_L	Coefficient of lift.
C_M	Coefficient of moment.
C_{D_i}	Coefficient of induced drag.
p	Pressure.
U	Aircraft velocity.
u, v, w	Velocity Cartesian components.

Subscripts

∞	Free-stream condition.
AR	Aspect Ratio.
b	Wing Span.
c	Wing chord.
D	Drag.
g	Gravity Acceleration.
i, j, k	Computational indexes.
L	Lift.

M_a	Mach Number.
n	Normal component.
R_e	Reynolds Number.
S	Wing Area.
T	Trust.
W	Weight.
x, y, z	Cartesian components.
ref	Reference values.

Chapter 1

Introduction

In this chapter, a brief introduction to the subject under study in this Master's Thesis will be presented, divided into four sections, Motivation, that summarizes the reasons for the elaboration of the Thesis on the present theme, Topic Overview, a small summary of the subjects discussed later, Objectives and Deliverable, which summarizes the proposed objectives that will be achieved, and finally Thesis Outline a very general summary about each chapter.

1.1 Motivation

Aircraft design it is a very complex procedure, so there are many tools to help its analyse and design. Systems engineering is one off the most used technique in engineering fields such as control engineering, industrial engineering, and interface design, to deal with the complex projects.

So we use tools to modeling, simulation, analysis and scheduling. Apart from this overlapping between technical and human disciplines everything can be managed with system engineering, creating tools in project manager and computational services that helps to handle with time and costs. And for the main reason to make the best dimensionless and estimations in the different areas of concept and production. In Figure 1.1, we can see a diagram elaborated for the present work in a general view the main areas of aircraft design, however, in this master thesis we will focus on the estimation of the aerodynamic models and equations of motion and their relation with the aircraft body axes, to calculate the parameters to estimate the right variable values.

A design phase consists of many compromises such as technical and economical factors. New methods that allow engineers to achieve a design at low cost and time have to be developed. In the aircraft industry the main challenge is to improve the best that we can design, lower production time and most importantly the cost. Also the importance of determining the aircraft stability and control derivatives from flight test data has been recognized for a long time.

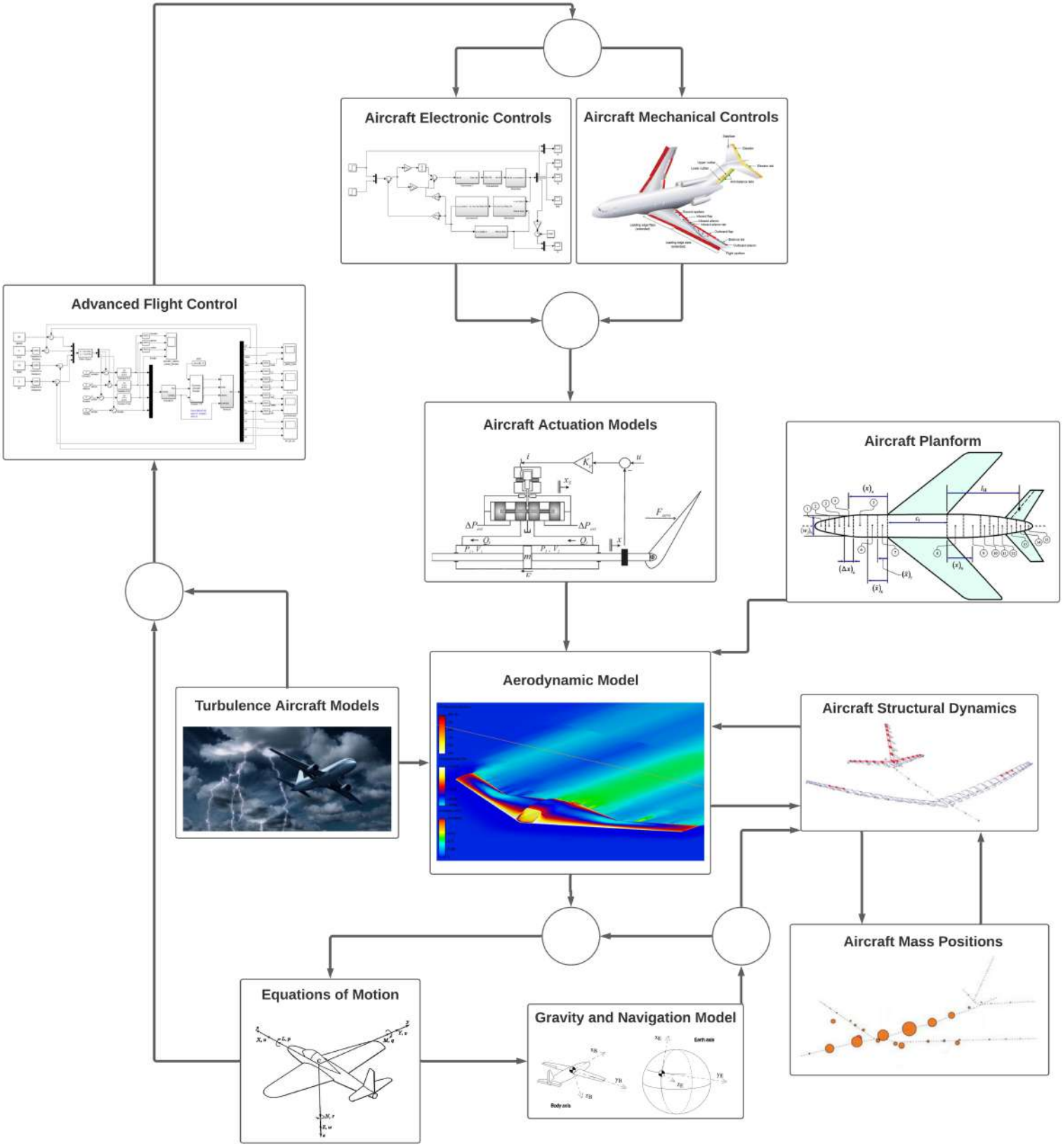

Figure 1.1: Main Areas in Aircraft Design

1.2 Topic Overview

The drive for aircraft efficiency and minimum environmental impact is requiring the aerospace industry to generate technologically innovative and highly integrated aircraft concepts.

This thesis describes the parameters and the development of a nonlinear flight dynamics model for a small, fixed-wing unmanned Aerial Vehicle (UAV). Models developed for UAVs are usually used in many different applications including risk analysis, controls system design and flight simulators such as described in Figure 1.1.

We find a very large challenge spectrum for system identification of small fixed wing, because we will talk about small aircraft including an increased sensitivity to atmospheric disturbances and decreased data quality from a cost-appropriate instrumentation system. These challenges result in many problems about the development of the project, such as the model structure and all the parameters estimations that they are crucial to a good estimation of the final values.

The small size also limit the scale of flight test experiments and the consequent information content of the data from which the model is developed. Present to improve the accuracy of system identification that will include data conditioning, data selection and calculus. The last parameter estimation and uncertainty analysis was developed from the time domain formulation of the output-error method using the fully nonlinear aircraft equations of motion. This thesis will only cover the Aerodynamic effects, rigid body flight dynamics, and inertial forces, chosen by the generic and diversified spectrum that we have in science to identify the fields and areas to analyse aircraft behavior.

In Figure 1.2, we can see the Test Aircraft Model in wind tunnel for future analysis, for a small fixed wing UAV that will be made latter on this Thesis.

Figure 1.2: Wind Tunnel Test Aircraft Model

1.3 Objectives and Deliverables

The objective according to title, is to determine the derivatives of stability and control derivatives of an aircraft through numerical simulations and wind tunnel experiments.

In more detail the study model of the master's thesis "Test Aircraft" goes through the construction of a simple model in CFD-XFLR5, to later replicate its characteristics, building a real model of "Test Aircraft", completely equal to the virtual model to analyze in the Wind Tunnel.

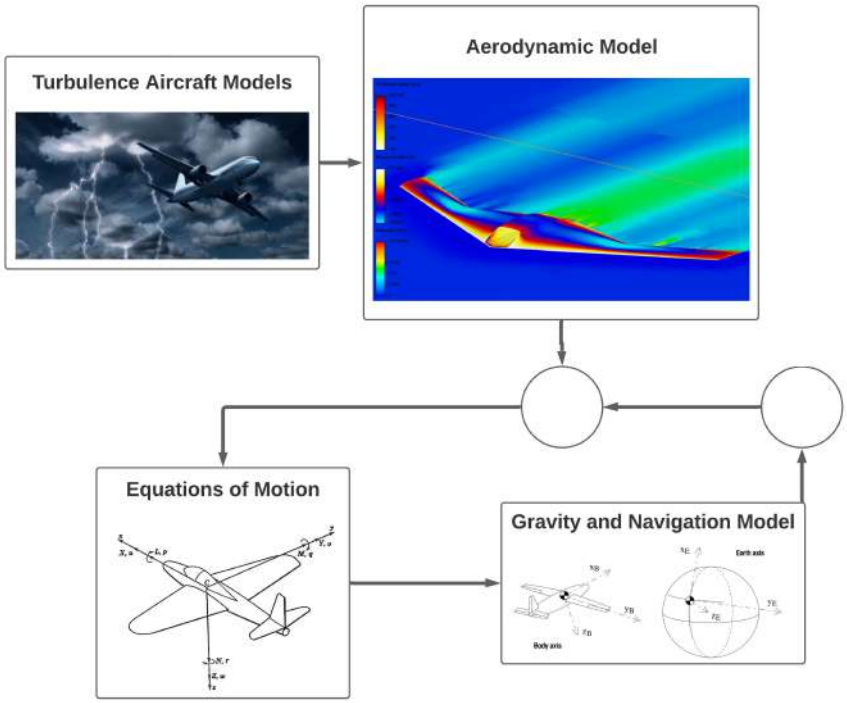

Figure 1.3: Logical System of Interference in an Aircraft Read by Sensors and Answered by Actuators to Maintain Trim Flight - Since the Aerodynamic and Control Derivatives are Essential to Quantify the Necessary Changes in the Wings and Ailerons to Maintain Trim Flight

Thus, it is possible to validate the results obtained in both the CFD-XFLR5 and the Wind Tunnel and make a comparison of the values, thus a perception of the oscillations and variations of the values obtained allow to fully characterize the same model by two distinct forms CFD-XFLR5 and Wind Tunnel, and to equate the observed variations.

After validation of the results obtained with the "Test Aircraft", it is possible to determine with a high degree of certainty the derivatives of stability and control derivatives in any model, only with tests in wind tunnel, in this master's thesis was built a replica of an F35, "F35 Aircraft", to calculate its derivatives of stability and control.

These two aircraft models, "Test Aircraft" and "F35 Aircraft", were the first two aircraft models to be tested in the Wind Tunnel with balance of forces at Instituto Superior Técnico, and perhaps in Portugal.

1.4 Thesis Outline

This thesis is divided in **7 chapters**, including introduction, and structured as follows:

Chapter 1: Introduction In this chapter, a brief introduction to the subject under study in this Master's Thesis will be presented, divided into four sections, Motivation, that summarizes the reasons for the elaboration of the Thesis on the present theme, Topic Overview, a small summary of the subjects discussed later, Objectives and Deliverable, which summarizes the proposed objectives that will be achieved, and finally Thesis Outline a very general summary about each chapter.

Chapter 2: Formulation of Stability Equations This section provides a systematic background of the derivation of the equations of motion for a flight vehicle and their linearization. The relationship between dimensional stability derivatives and dimensionless aerodynamic coefficients is presented and the principal contributions to all important stability derivatives for flight vehicles having left/right symmetry are explained.

Chapter 3: Estimation of Stability Derivatives The equations of motion (for small perturbations) were written in dimensional form, using the stability derivatives in dimensional form. However, the derivatives are normally obtained in dimensionless form, for example, by means of testing of models in wind tunnel. It is therefore necessary to relate the dimensional stability derivatives with the non-dimensional ones.

Chapter 4: Design and Building Aircraft This chapter describes the construction process of the two models that will be analyzed in the wind tunnel and CFD by XFLR5 software, as well as the manufacturing processes of the models with special detail for the construction with illustrative images of both models, concluding with the final result of the construction.

Chapter 5: Balance of Forces Calibration This chapter describe and discuss the calibration of the force balance, where it is possible to see all the process, reported with pictures and also the data collected to calculate the equations for the axial force for the different angles measured in each bar of the force balance.

Chapter 6: Longitudinal and Lateral Derivatives In this chapter, the results obtained in the study of both models in the wind tunnel and in CFD-XFLR5 software are presented, the Longitudinal and Lateral aerodynamic derivatives are presented as well as a detailed quantitative and qualitative discussion of the results.

Chapter 7: Conclusions Presents the overall conclusions and introduces future work to improve the estimations of the aerodynamic stability derivatives.

Chapter 2

Formulation of Stability Equations

This section provides a systematic background of the derivation of the equations of motion for a flight vehicle and their linearization. The relationship between dimensional stability derivatives and dimensionless aerodynamic coefficients is presented and the principal contributions to all important stability derivatives for flight vehicles having left/right symmetry are explained.

2.1 Equations of Motion

The present section is divided into five subsections in which the study and calculation process to obtain stability derivatives will be explained in detail with the respective quantitative equations.

2.1.1 Aircraft Body Axes

The aircraft equations of motion contain kinematic and dynamic relationships which describe translational and rotational motion for a wide variety of fixed-wing aircraft. The dynamic equations are related to external aerodynamic forces and moments on the aircraft, which are generally the primary interest of aircraft model identification. Background equations of motion are well defined, the model for the aerodynamic forces and moments on the aircraft will change between individual aircraft and flight conditions. The main task of system identification for an aircraft involves modeling these aerodynamic forces and moments [1].

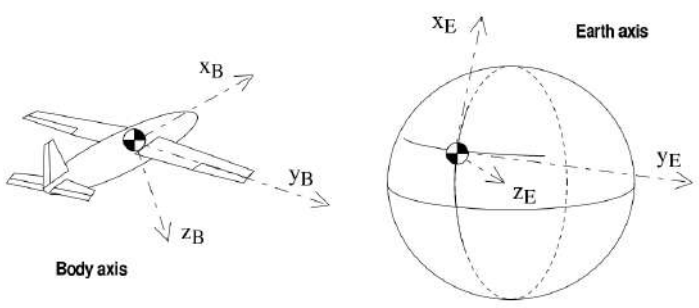

Figure 2.1: Body and Earth Reference Frames [2]

Before formulating the equations of motion, it is necessary to choose the references used and present the associated nomenclature. Two references are essentially needed in flight mechanics Figure 2.1:

• the fixed reference frame, connected to the earth's surface (Earth axis), with the first two axes tangent to the meridian and parallel: in the notation the index E (x_E, y_E, z_E) is used or, more explicitly, is called NED $(North - East - Down)$ frame (N, E, D): the fixed frame is considered inertial, the rotation of the earth is particularly neglected

• the body frame of reference (of the body, local or relative), connected to the rigid body of the plane (Body axis, index B), originating from the center of gravity $(c.g.)$, sometimes called ABC $(Aircraft\ Body\ Centered)$ (x_B, y_B, z_B): [2]

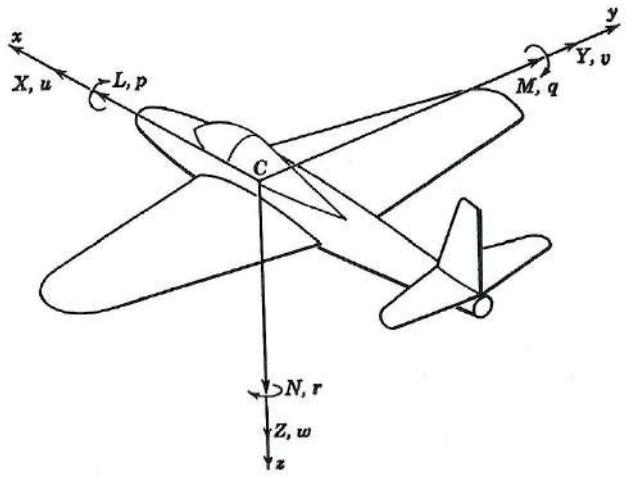

Figure 2.2: Aircraft Reference Frame [3]

The components according to Figure 2.2, and to (x , y , z) of linear velocity $\vec{v}$ are denoted by $\vec{v} = (u, v, w)$.

The components of angular velocity are $\vec{w} = (p, q, r)$.

So, p is the rolling angular velocity (roll), q is the pitch angular velocity (pitch) and r is the yaw angular velocity (yaw) [4].

Relative to the axes of the aircraft, the x, y and z components of the forces applied to the aircraft will be designated simply by $\vec{F} = (X, Y, Z)$ while the components of the moments are $\vec{M} = (L, M, N)$, where L is the rolling moment, M is the pitch moment and N the yaw moment [4].

2.1.2 Euler Angles

Attitude angles of the aircraft are also called the Euler angles. The angles in flight simulation can be usually solved by a single set of the Euler equations. This is a simple and old method but it is the most exact and feasible method in general. [5]

The old method has difficulty in solving the all-attitude simulation and serious effects on solution accuracy due to natural defect of the singularity in the Euler angle system, Though it is possible to solve all-attitude simulation by use of a dead band fixed-value method, it can not fully remove the errors of the singular areas so that the classical equations of the single-Euler method is very difficult to suit for solving

all- attitude of the aircraft. In the past, there were many substitute methods to overcome the difficulty in calculating in the neighborhood of the singular points. [5]

One of the substitute methods, the quaternion method, used to solve all- attitude simulation in nine cases out of ten, But the quaternion method is not very perfect. Besides leading into simplified hypothesis and conditions, there are frequent phenomena out of the boundary owing to integrating to get parameters of field of definitions. Due to all these factors of principle defect, the quaternion method will produce method errors. After the correcting process, it still can not fully remove the errors and only gets an approximate solution. Other methods are not better than the quaternion method. So there are defects in all these methods. In order to fully overcome the singularity, in 1978, a dual-set of the Euler equations was presented by use of separating the Euler angle system into two kind of areas with new the method of the alternating calculation. It is called a dual-Euler method. Due to the concept simplicity, straightforwardness, convenience in application it is an ideal all-attitude equations. [5]

The spectrum of variance of Euler angles is given by the following range of values,

• Rolling Angle ($roll$): $\phi \in [-\pi; \pi](rad)$

• Pitch Angle ($pitch$): $\theta \in [-\frac{\pi}{2}; \frac{\pi}{2}](rad)$

• Yaw Angle (yaw): $\psi \in [0; 2\pi](rad)$

The transformation matrix from Earth axes to body axes, also called attitude matrix are given by the following equations,

For a rotation of an angle ϕ around the "Ox" axis the rotation matrix 2.1 is: [4]

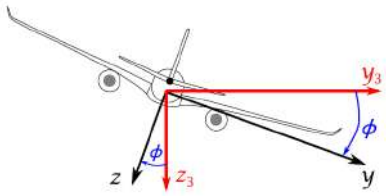

$$R_x(\phi) = \begin{bmatrix} 1 & 0 & 0 \\ 0 & \cos\phi & \sin\phi \\ 0 & -\sin\phi & \cos\phi \end{bmatrix} \tag{2.1}$$

For a rotation of an angle θ around the "Oy" axis the rotation matrix 2.2 is: [4]

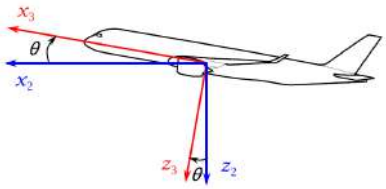

$$R_x(\theta) = \begin{bmatrix} \cos\theta & 0 & -\sin\theta \\ 0 & 1 & 0 \\ \sin\theta & 0 & \cos\theta \end{bmatrix} \tag{2.2}$$

For a rotation of an angle ψ around the "Oz" axis the rotation matrix 2.3 is: [4]

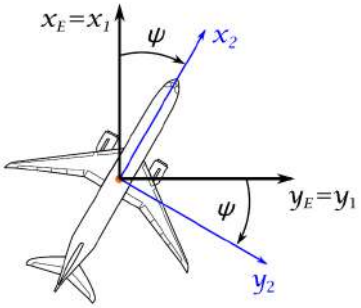

$$R_x(\psi) = \begin{bmatrix} \cos\psi & \sin\psi & 0 \\ -\sin\psi & \cos\psi & 0 \\ 0 & 0 & 1 \end{bmatrix} \tag{2.3}$$

To obtain the rotation matrix of the fixed frame on Earth NED $(North-East-Down)$ frame (N, E, D), for the frame fixed on the aircraft ABC $(Aircraft\ Body\ Centered)$ (x_B, y_B, z_B), just apply multiply (from right to left) the matrices corresponding to the roll ϕ, pitch θ and yaw ψ rotations, from matrice 2.1.2, [4]

$$R_{BE} = R_x(\phi) * R_y(\theta) * R_z(\psi) =$$

$$= \begin{bmatrix} \cos\theta\cos\psi & \cos\theta\sin\psi & -\sin\theta \\ \sin\phi\sin\theta\cos\psi - \cos\phi\sin\psi & \sin\phi\sin\theta\sin\psi + \cos\phi\cos\psi & \sin\phi\cos\theta \\ \cos\phi\sin\theta\cos\psi + \sin\phi\sin\psi & \cos\phi\sin\theta\sin\psi - \sin\phi\cos\psi & \cos\phi\cos\theta \end{bmatrix} \quad (2.4)$$

2.1.3 Trajectory Equations

The movement of an aircraft could be expressed by a 6 Degrees of Freedom (6DoF) or a 3DoF. The first model is the most complete model due to the fact that it has into consideration both rotational and translational motion. Commercial aircraft trajectories involve small aircraft rotation axes and also the angle of sideslip could be considered negligible because of the turn coordinator system that is installed into almost the whole commercial aircraft.[6]

A trajectory or flight path is the path that an object with mass in motion follows through space as a function of time. In classical mechanics, a trajectory is defined by $HamiltonianMechanics$ via canonical coordinates, hence, a complete trajectory is defined by position and momentum, simultaneously. [7]

The mass might be a projectile or a satellite or a aircraft. For example, it can be an orbit — the path of a planet, asteroid, or comet as it travels around a central mass.

In control theory, a trajectory is a time-ordered set of states of a dynamical system. In discrete mathematics, a trajectory is a sequence $(f^k(x))_{k\in\mathbb{N}}$ of values calculated by the iterated application of a mapping f to an element x of its source, a example of a trajectoty is given by Figure 2.3 [7]

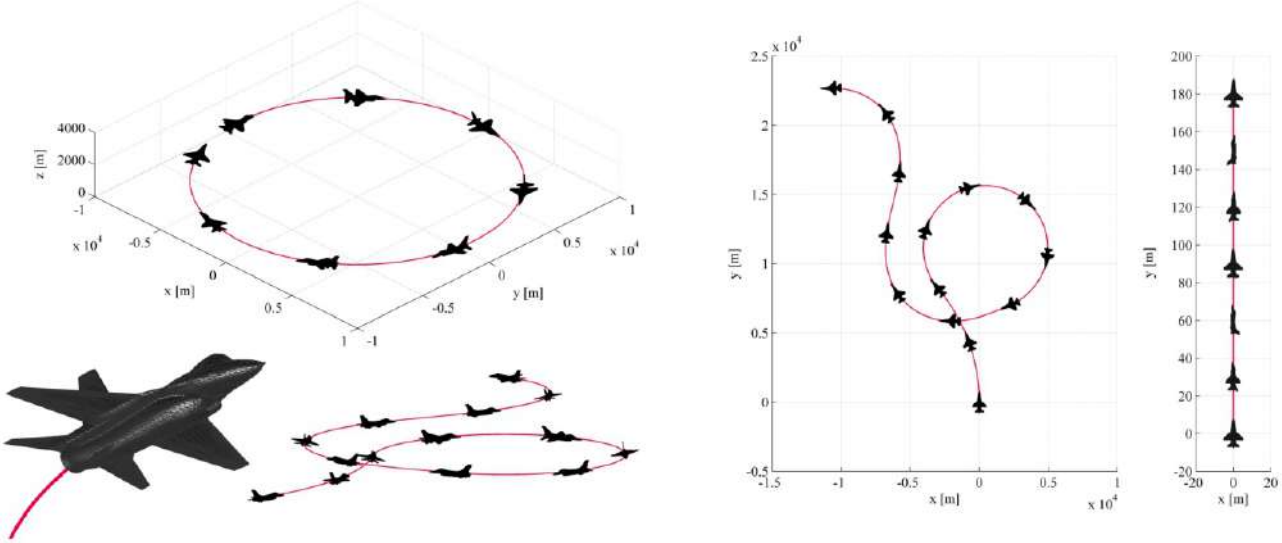

Figure 2.3: Aircraft Trajectory Example

Equations (2.5 to 2.7) describe the aircraft's translational kinematics and are used to calculate the inertial position of the aircraft's center of gravity, x, y and z. Equations (2.8 - 2.10) describe the aircraft's rotational kinematics and are used to calculate the aircraft's orientation angles, roll attitude ϕ, pitch attitude θ and yaw attitude ψ . The quantities p, q and r are the aircraft's roll rate, pitch rate and yaw rate in the body frame, respectively [8].

The kinematic equations or trajectory equations are as follows:

$$\dot{x} = u\cos\theta\cos\psi + v(\sin\theta\cos\psi\sin\phi - \sin\psi\cos\phi) + w(\sin\theta\cos\psi\cos\phi + \sin\psi\sin\phi) \tag{2.5}$$

$$\dot{y} = u\cos\theta\sin\psi + v(\sin\theta\sin\psi\sin\phi + \cos\psi\cos\phi) + w(\sin\theta\sin\psi\cos\phi - \cos\psi\sin\phi) \tag{2.6}$$

$$\dot{z} = -u\sin\theta + v\cos\theta\sin\phi + w\cos\theta\cos\phi \tag{2.7}$$

$$\dot{\phi} = p + (q\sin\phi + r\cos\phi)\tan\theta \tag{2.8}$$

$$\dot{\theta} = q\cos\phi - r\sin\phi \tag{2.9}$$

$$\dot{\psi} = (q\sin\phi + r\cos\phi)\sec\theta \tag{2.10}$$

In order to accept the model as an aircraft, an adequate validation is needed. According to a validation process involves: the evaluation of the software used, the airframe and the pilot. This Thesis is focused on the software and aircraft model validation. To evaluate the accuracy of the model, it could be developed from an experimental flight test to an aircraft observation during several parameters are modified.

For this reason, the uncertainties of the model should be delimited. The data used to perform the validation of the model is obtained from actual flights, and it allows checking the differences between the real variables from real Flight Data Recorder (FDR) and the ones defined by the aircraft. A similar method has been used, for Unmanned Aerial Vehicles (UAV) model based on a 6DoF has been validated through the comparison at the same inputs of the real aircraft response and the software model. Also, a flight test program will be designed to validate a 6DoF flight model. [6]

2.1.4 Aircraft's Rotational Dynamics

Flight test maneuvers and dynamic modeling techniques were developed for determining aircraft moments of inertia from flight test data. Full nonlinear rigid-body rotational equations of motion were used in the analysis, with aerodynamic moment dependencies modeled by linear expansions in the aircraft states and controls. Aerodynamic parameters were estimated simultaneously with inertia parameters

using equation-error modeling applied to flight test data from maneuvers designed specifically for this problem.

The matrix in Equation 2.11 is the inertia tensor (Etkin, 1959) expressed in the body-axis system, and in Figure 2.4 we can see the symmetric plane of an aircraft, [9]

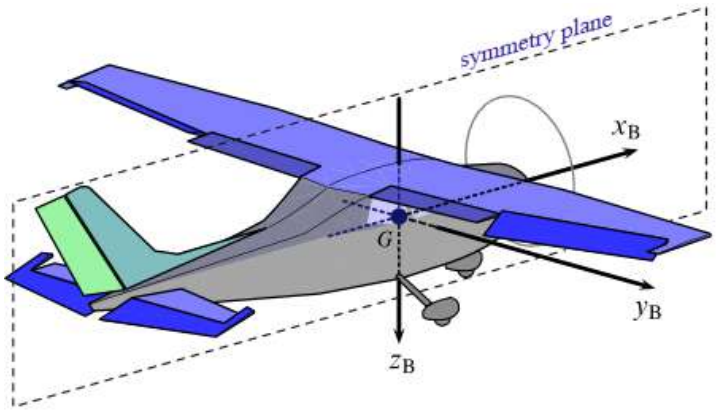

Figure 2.4: Symmetry Aircraft Plane

Accurate estimates of aircraft inertia characteristics, the location of the center of gravity, the moments and products of inertia—are crucial in linear and nonlinear simulation, analysis of stall-spin characteristics, control system design, and dynamic flight testing. Throughout the past 60 years, experimental techniques for the determination of inertia characteristics have been developed and continuously improved.

These techniques have the following in common: the rolling, pitching, and yawing moments of inertia are derived from the measured characteristic frequencies of one-degree-of-freedom oscillations about the corresponding axes. The resulting data have to be corrected for the distance between the axis of oscillation and the corresponding body axis through the aircraft center of gravity.

Separate experiments must be carried out to locate the center of gravity. For the determination of the inertia product in the XZ plane of symmetry, Figure 2.4, additional oscillation measurements are required at different aircraft attitudes. In all cases, a symmetrical mass distribution is assumed, and the effects of oscillatory damping is neglected.

Although the literature has been concerned with improved techniques with respect to accuracy, no significant reduction has been gained regarding the complexity of these methods. The separate one-degree-of-freedom oscillations and center of gravity measurements require time-consuming re configurations of the experiment setups. Extreme care in conducting the various experiments is considered essential to obtain good results. [10]

It is very important to know that ”Inertia” can be defined as the resistant capacity of a mass body experiences face of change movement, in aircraft structures it is the capacity of a structure to support bending, or shear, with no deformation, the most higher is the Inertia more difficult is that a body deformed.

The aircraft inertia matrix is given by Equation 2.11, [9]

$$[I_B] = \begin{bmatrix} I_{xx} & -I_{xy} & -I_{xz} \\ -I_{xy} & I_{yy} & -I_{yz} \\ -I_{xz} & -I_{yz} & I_{zz} \end{bmatrix} \tag{2.11}$$

Replacing all these expressions in the rotation dynamics equation 2.12 as components according to x, y and z are given by, [4]

$$\begin{cases} L = I_{xx}\dot{p} - Iyz(q^2 - r^2) - I_{zx}(\dot{r} + pq) - I_{xy}(\dot{q} - rp) - (I_{yy} - Izz)qr \\ M = I_{yy}\dot{q} - I_{zx}(r^2 - p^2) - I_{xy}(\dot{p} + qr) - I_{yz}(\dot{r} - pq) - (I_{zz} - I_{xx})rp \\ N = I_{zz}\dot{r} - I_{xy}(p^2 - q^2) - I_{yz}(\dot{q} + rp) - I_{zx}(\dot{p} - qr) - (I_{xx} - I_{yy})pq \end{cases} \tag{2.12}$$

Equations 2.12 describe the aircraft's rotational dynamics which are dependent on the external aerodynamic moments exerted on the aircraft, L, M and N. The moments and product of inertia (I_{xx}, I_{yy}, I_{zz}, I_{xy}, I_{xz}, I_{yz}) as well as the body-axis angular rates (p, q, r) and their time derivatives ($\dot{p}$, $\dot{q}$, $\dot{r}$) also appear in these equations [11].

2.1.5 Aircraft's Translational Dynamics

The translational velocity at the center of gravity of the aircraft in the body frame are given as u, v and w [11]. The aircraft dynamic equations, which include the aerodynamic forces and moments exerted on the aircraft, are:

$$\begin{cases} X = m(\dot{u} + qw - rv) - T + mg\sin\theta \\ Y = m(\dot{v} + ru - pw) - mg\cos\theta\sin\phi \\ Z = m(\dot{w} + pv - qu) - mg\cos\theta\cos\phi \end{cases} \tag{2.13}$$

Equations 2.13 describe the aircraft's translational dynamics which are dependent on the external aerodynamic forces exerted on the aircraft, X, Y and Z. The thrust force T is assumed to be acting along the x body-axis through the aircraft's center of gravity $(c.g.)$. Other quantities appearing in the equations are the aircraft mass m, gravitational acceler-ation $g = 9.81m^2/s$, the time derivative of the body-axis velocity components ($\dot{u}$, $\dot{v}$, $\dot{w}$), and identified state variables ϕ, θ, ψ , p, q, r, u, v, w. [11]

$$X = \frac{\rho V_a^2}{2} S C_x \qquad Y = \frac{\rho V_a^2}{2} S C_y \qquad Z = \frac{\rho V_a^2}{2} S C_z \tag{2.14}$$

$$L = \frac{\rho V_a^2}{2} b S C_l \qquad M = \frac{\rho V_a^2}{2} \bar{c} S C_m \qquad N = \frac{\rho V_a^2}{2} b S C_n \tag{2.15}$$

Equation 2.14 and 2.15 shows the conversion between dimensional forces and moments, and the non-dimensional force and moment coefficients C_x, C_y , C_z, C_l, C_m, C_n [12]. In these conversions, ρ is the air density, S is the wing reference area, $\bar{c}$ is the mean aerodynamic chord, b is the wing span and V_a is the airspeed.

2.2 Forces and Moments

A study has been made of the forces and moments acting on a small aircraft while it is flying. Preliminary analysis of the expected ranges of forces and moments were made using available theoretical methods and confirming experiments were performed. The range of positions of the small model relative to the large model extended laterally to a big scale. Consideration was given to the problem of maintaining steady position at a point that provided a maximum increase in the lift to drag ratio of the small aircraft. [13]

The present study was undertaken to provide information on the improved range and endurance to be obtained by small aircraft or drone, the forces are represented in Figure 2.5,

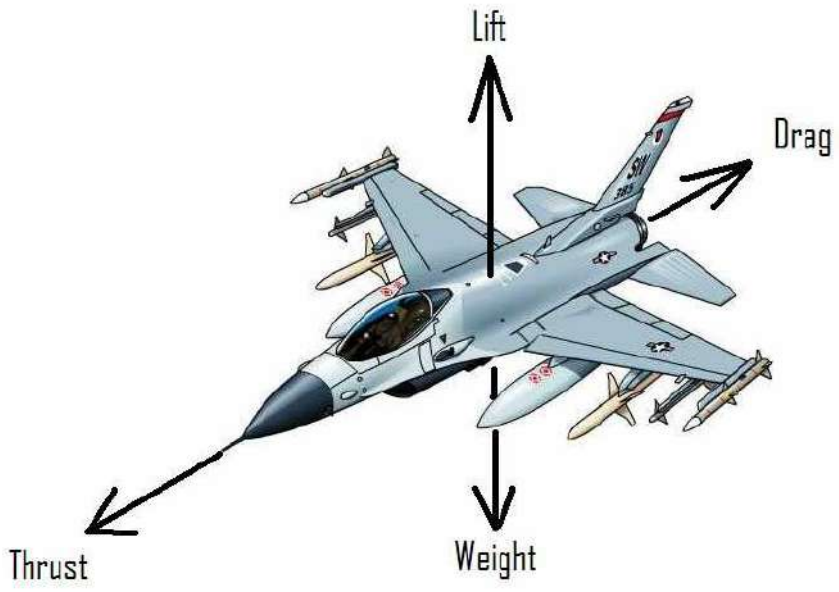

Figure 2.5: Applied Forces and Moments in Aircraft [14]

The optimal control technique linear quadratic regulator (LQR) is chosen to design a controller for the longitudinal motion of a small fixed-wing type UAV. Kalman filter technique is then applied to see how the controller is affected by disturbances. The effectiveness of the controller with and without the Kalman filter is also shown through simulations. Linear quadratic control is an optimal control technique that is used for controlling the aircraft. This control technique aims to decrease the energy that is used to control the aircraft. This technique can be applied together with a filtering technique (Kalman filter etc.) in cases where some of the states are not available for measurement or when the measurements are noisy.

In this study the longitudinal motion of the small UAV is investigated. We can find the longitudinal equations of motion for the UAV by linearizing the equations for wings-level flight. For longitudinal model we will use the following equation 2.16, [15]

$$\begin{cases} X = X_A + \Delta X_C \\ Z = Z_A + \Delta Z_C \\ M = M_A + \Delta M_C \end{cases} \tag{2.16}$$

Where X_A, Z_A, M_A, ΔX_C, ΔZ_C and ΔM_C is given by,

$$\begin{cases} X_A = X_u u + X_w w + X_q q + X_{\dot{w}} \dot{w} \\ Z_A = Z_u u + Z_w w + Z_q q + Z_{\dot{w}} \dot{w} \\ M_A = M_u u + M_w w + M_q q + M_{\dot{w}} \dot{w} \end{cases}, \qquad \begin{cases} \Delta X_C = X_{\delta_e} \delta_e + X_{\delta_t} \delta_t \\ \Delta Z_C = Z_{\delta_e} \delta_e + Z_{\delta_t} \delta_t \\ \Delta M_C = M_{\delta_e} \delta_e + M_{\delta_t} \delta_t \end{cases},$$

In general we found that the roots of the lateral-directional characteristic equation composed of two real roots and a pair of complex roots. Lateral directional equations of motion consist of the side force, rolling moment and yawing moment equations of motion. For the lateral state-space equations, the state is given by, "lateral model" we will use the following equation 2.18,

$$\begin{cases} Y = Y_A + \Delta Y_C \\ L = L_A + \Delta L_C \\ N = N_A + \Delta N_C \end{cases} \tag{2.18}$$

Where Y_A, L_A, N_A, ΔY_C, ΔL_C and ΔN_C is given by,

$$\begin{cases} Y_A = Y_v v + Y_p p + Y_r r \\ L_A = L_v v + L_p p + L_r r \\ N_A = N_v v + N_p p + N_r r \end{cases}, \qquad \begin{cases} \Delta Y_C = Y_{\delta_a} \delta_a + Y_{\delta_r} \delta_r \\ \Delta L_C = L_{\delta_a} \delta_a + L_{\delta_r} \delta_r \\ \Delta N_C = N_{\delta_a} \delta_a + N_{\delta_r} \delta_r \end{cases},$$

Forces and moments applied on the aircraft UAV is subjected to external forces and moments due to gravity, propulsion, and aerodynamics. After applying the newton's second law for translational motion, the applied forces are combined and expressed in the body frame.

For rotational motion the applied moments are combined and expressed in the body frame. Momentum is defined as the product of inertia matrix 2.11 and the angular velocity vector.

Six degrees of freedom 12-state equations of motion are obtained, but they are not complete, the external forces and moments are not defined yet. The modeling of the forces and moments can be utilized to get finally the nonlinear 12- state equations of motion. The gravity g, aerodynamic, and propeller T forces are the composition of the total forces applied on the body frame. Aerodynamic, and propeller T moments is the composition of the total moments applied on the body frame (L, M ,N), there are no moments produced by the gravity. The above forces will be represented in the stability chapters. [16]

2.3 Control Derivatives of Linearized Equations

Control derivative - measures how much change occurs in a force or moment acting on the vehicle when there is a small change in the deflection of a control surface such as the ailerons, elevator, and rudder.

The control derivatives consist of the pitching moment due to elevator deflection δ_e [17].

$$M_{\delta_e} = \frac{\frac{1}{2}\rho V^2 S\bar{c}}{I_y} C_{m\delta_e} \tag{2.20}$$

The rolling moment due to aileron deflection δ_a [17]

$$L_{\delta_a} = \frac{\frac{1}{2}\rho V^2 Sb}{I_x} C_{l\delta_a} \tag{2.21}$$

And the yawing moment due to rudder deflection δ_r [17]

$$N_{\delta_r} = \frac{\frac{1}{2}\rho V^2 Sb}{I_z} C_{n\delta_r} \tag{2.22}$$

There also can be significant cross-coupling of the rudder and aileron control moments. The yawing moment due to aileron deflection [17].

$$N_{\delta_a} = \frac{\frac{1}{2}\rho V^2 Sb}{I_z} C_{n\delta_a} \tag{2.23}$$

Is called adverse yaw, since this derivative usually is negative, leading to a tendency to rotate the nose to the left when the vehicle rolls to the right. The rolling moment due to rudder deflection [17]

$$L_{\delta_r} = \frac{\frac{1}{2}\rho V^2 Sb}{I_x} C_{l\delta_r} \tag{2.24}$$

Also tends to be unfavorable, as it tends to roll the vehicle to the left when trying to turn to the right [17] .

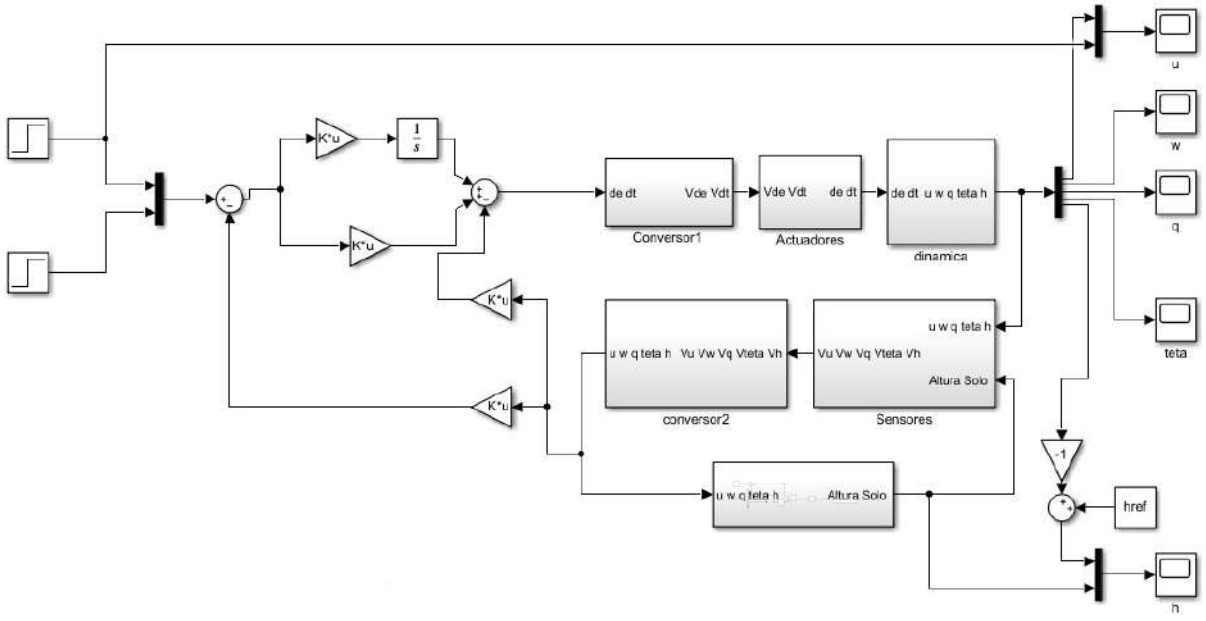

Figure 2.6: Control Model System Example MIMO

2.4 Stability Control Models

This section provides a brief background in modern control theory and its application to the equations of motion for a flight vehicle. The description is meant to provide the basic background in linear algebra for understanding how modern tools for the analysis of linear systems work, and provide examples of their application to flight vehicle dynamics and control.

2.4.1 Longitudinal Stability Model

In flight dynamics, longitudinal static stability is the stability of an aircraft in the longitudinal, or pitching, plane under steady flight conditions. This characteristic is important in determining whether a human pilot will be able to control the aircraft in the pitching plane without requiring excessive attention or excessive strength [18].

As some derivatives are usually negligible we can simplify equation 2.16, assuming,

$X_{\dot{u}} \approx X_q \approx X_{\dot{q}} \approx X_{\dot{w}} \approx Z_{\dot{u}} \approx Z_q \approx Z_{\dot{q}} \approx Z_{\dot{w}} \approx M_{\dot{u}} \approx M_{\dot{q}} \approx 0$

The longitudinal stability of an aircraft, also called pitch stability, refers to the aircraft's stability in its plane of symmetry, about the lateral axis (the axis along the wingspan). One important aspect of the handling qualities of the aircraft, it is one of the main factors determining the ease with which the pilot is able to maintain trim.

In this simplified Equation 2.25, we have the system identification that will be used to calculate the longitudinal variables, taking into account all the variables and expressions to describe the most detailed model about the project aircraft [19].

$$\begin{cases} X = X_u u + X_w w + X_{\delta_e}\delta_e + X_{\delta_t}\delta_t \\ Z = Z_u u + Z_w w + Z_{\delta_e}\delta_e + Z_{\delta_t}\delta_t \\ M = M_u u + M_w w + M_{\dot{w}}\dot{w} + M_q q + M_{\delta_e}\delta_e + M_{\delta_t}\delta_t \end{cases} \tag{2.25}$$

If an aircraft is longitudinally stable, a small increase in angle of attack will create a negative (nose-down) pitching moment on the aircraft so that the angle of attack decreases. Similarly, a small decrease in angle of attack will create a positive (nose-up) pitching moment so that the angle of attack increases [18].

Unlike motion about the other two axes and in the other degrees of freedom of the aircraft (sideslip translation, rotation in roll, rotation in yaw), which are usually heavily coupled, motion in the longitudinal degrees of freedom is planar and can be treated as two-dimensional.

Near the cruise condition, most of the lift force is generated by the wings, with ideally only a small amount generated by the fuselage and tail. We may analyse the longitudinal static stability by considering the aircraft in equilibrium under wing lift, tail force, and weight. The moment equilibrium condition is called trim, and we are generally interested in the longitudinal stability of the aircraft about this trim condition [19].

2.4.2 Lateral Stability Model

With a symmetrical rocket, the directional stability in yaw is the same as the pitch stability, it resembles the short period pitch oscillation, with yaw plane equivalents to the pitch plane stability derivatives. For this reason, pitch and yaw directional stability are collectively known as the ”weathercock” stability of the missile.

Aircraft lack the symmetry between pitch and yaw, so that directional stability in yaw is derived from a different set of stability derivatives. The yaw plane equivalent to the short period pitch oscillation, which describes yaw plane directional stability is called Dutch roll. Unlike pitch plane motions, the lateral modes involve both roll and yaw motion [18].

As some derivatives are usually negligible, we can simplify the Equation 2.18, assuming,

$Y_{\dot{v}} \approx Y_{\dot{p}} \approx Y_{\dot{r}} \approx Y_{\delta_A} \approx L_{\dot{v}} \approx L_{\dot{p}} \approx L_{\dot{r}} \approx N_{\dot{v}} \approx N_{\dot{p}} \approx N_{\dot{r}} \approx 0$

Leading to,

$$\begin{cases} Y = Y_v v + Y_p p + Y_r r + Y_{\delta_a}\delta_a + Y_{\delta_r}\delta_r \\ L = L_v v + L_p p + L_r r + L_{\delta_a}\delta_a + L_{\delta_r}\delta_r \\ N = N_v v + N_p p + N_r r + N_{\delta_a}\delta_a + N_{\delta_r}\delta_r \end{cases} \tag{2.26}$$

In Equation 2.26, we have the system identification that will be use to calculate the lateral variables it will be take into account all the variables and expressions to described the most detailed model.

Directional or weathercock stability is concerned with the static stability of the airplane about the z axis. Just as in the case of longitudinal stability it is desirable that the aircraft should tend to return to

an equilibrium condition when subjected to some form of yawing disturbance. For this the slope of the yawing moment curve must be positive. An airplane possessing this mode of stability will always point towards the relative wind, hence the name weathercock stability [19].

2.5 Identification of Relevant Stability Derivatives

Stability derivative measures how much change occurs in a force or moment acting on the vehicle when there is a small change in a flight condition parameter such as angle of attack, airspeed, altitude.

2.5.1 Longitudinal Mode:

In order to solve the equations describing longitudinal vehicle motions, we need to be able to evaluate all the coefficients. This means we need to be able to provide estimates for the derivatives of X, Z, and M with respect to the relevant independent variables u, w, $\dot{w}$, and q. These dimensional stability derivatives usually are expressed in terms of dimensionless aerodynamic coefficient derivatives as,

$$X_u = \rho u_0 S C_{w_0} \sin\theta_0 + \frac{1}{2}\rho u_0 S C_{x_u} \qquad Z_u = -\rho u_0 S C_{w_0} \cos\theta_0 + \frac{1}{2}\rho u_0 S C_{z_u} \qquad M_u = \frac{1}{2}\rho u_0 \bar{c} S C_{m_u}$$
$$X_w = \frac{1}{2}\rho u_0 S C_{x_\alpha} \qquad Z_w = \frac{1}{2}\rho u_0 S C_{z_\alpha} \qquad M_w = \frac{1}{2}\rho u_0 S \bar{c} C_{m_\alpha}$$
$$X_q = \frac{1}{4}\rho u_0 S \bar{c} C_{x_q} \qquad Z_q = \frac{1}{4}\rho u_0 S \bar{c} C_{z_q} \qquad M_q = \frac{1}{4}\rho u_0 S \bar{c}^2 C_{m_q}$$

Where the dimensionless derivatives (C_{x_u}, C_{z_u}...) are described in section 3.

2.5.2 Lateral Mode:

In order to solve the equations describing lateral/directional vehicle motions, we need to be able to evaluate all the coefficients. This means we need to be able to provide estimates for the derivatives of Y , L, and N with respect to the relevant independent variables v, p, and r. As for the longitudinal case, these stability derivatives usually are expressed in terms of dimensionless aerodynamic coefficient derivatives as,

$$Y_v = \frac{1}{2}\rho u_0 S C_{y_\beta} \qquad Y_p = \frac{1}{4}\rho u_0 S b C_{y_p} \qquad Y_r = \frac{1}{4}\rho u_0 S b C_{y_r}$$
$$L_v = \frac{1}{2}\rho u_0 S b C_{l_\beta} \qquad L_p = \frac{1}{4}\rho u_0 S b^2 C_{l_p} \qquad L_r = \frac{1}{4}\rho u_0 S b^2 C_{l_r}$$
$$N_v = \frac{1}{2}\rho u_0 S b C_{n_\beta} \qquad N_p = \frac{1}{4}\rho u_0 S b^2 C_{n_p} \qquad N_r = \frac{1}{4}\rho u_0 S b^2 C_{n_r}$$

Where the dimensionless derivatives (C_{y_β}, C_{l_β}...) are described in section 3.

Chapter 3

Estimation of Stability Derivatives

The equations of motion (for small perturbations) were written in dimensional form, using the stability derivatives in dimensional form. However, the derivatives are normally obtained in dimensionless form, for example, by means of testing of models in wind tunnel. It is therefore necessary to relate the dimensional stability derivatives with the non-dimensional ones.

3.1 Aerodynamic Derivatives of Linearized Equations

The forces and moments derivatives corresponding to the small perturbation are given by equations 3.1, also here the derivatives are calculated in the steady state for Trim condition.

$$Z_u = \left(\frac{\partial Z}{\partial u}\right)_0 \qquad Z_w = \left(\frac{\partial Z}{\partial w}\right)_0 \qquad Z_q = \left(\frac{\partial Z}{\partial q}\right)_0 \qquad Z_{\dot{w}} = \left(\frac{\partial Z}{\partial \dot{w}}\right)_0 \tag{3.1}$$

In dimensionless form, the velocity components are expressed as 3.2:

$$\hat{u} = \frac{u}{u_0} \qquad \hat{v} = \frac{v}{u_0} \qquad \hat{w} = \frac{w}{u_0} \tag{3.2}$$

And some examples of the dimensionless derivatives are them expressed as 3.3:

$$C_{Zu} = \left(\frac{\partial C_Z}{\partial \hat{u}}\right)_0 \qquad C_{Z\alpha} = \left(\frac{\partial C_Z}{\partial \alpha}\right)_0 \qquad C_{Zq} = \left(\frac{\partial C_x}{\partial \hat{q}}\right)_0 \qquad C_{Z\hat{\alpha}} = \left(\frac{\partial C_Z}{\partial \hat{\alpha}}\right)_0 \tag{3.3}$$

In the design phase it is important to have approximate expressions for the derivatives of dimensionless stability in function of the characteristics of the aircraft. We will try to find these expressions by treating separately, as usual, the cases of longitudinal movement and lateral movement.

Derivatives with respect to u translate the changes in forces and moments when varies the horizontal speed, assuming , T, etc. constants. The C_L and C_D coefficients depend on u due to compressibility effects (that is, depend on the Mach M_a number), to aeroelastic effects and the interaction of propulsion with the airframe (wing and fuselage), especially in the case of propeller propulsion.

The derivatives in order to q are calculated keeping constants α and the others variables. The most important contribution is that of the tail; the contribution of the wing is less important and more difficult to estimate. It is common practice to estimate the wing contribution as 10% of the tail contribution, and in this report we will take that 10% assumption for the main wing.

The estimation of aerodynamic derivatives from flight test measurements is an established and well developed experimental process. However, derivative estimates are usually obtained indirectly since it is not possible to measure the aerodynamic components of force and moment acting on the airframe directly. Also, since the aircraft has six degrees of freedom, it is not always possible to perturb the single motion variable of interest without perturbing some, or all, of the others as well. However, as in wind tunnel testing, some derivatives are easily estimated from flight test experiments with a good degree of confidence, whereas others can be notoriously difficult to estimate.

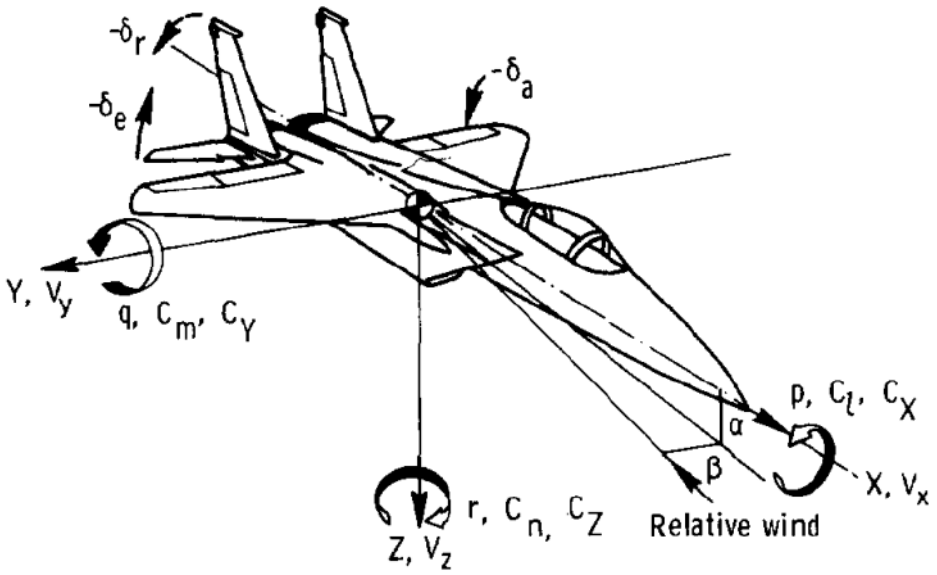

Figure 3.1: Model Characterization

Although it is relatively easy to set up approximately steady conditions in flight from which direct estimates of some derivatives can be made, the technique often produces results of indifferent accuracy and has limited usefulness. Today parameter identification techniques are commonly used in which measurements are made following the deliberate excitation of multi-variable dynamic conditions. Complex multivariable response analysis then follows, from which it is possible to derive a complete estimate of the mathematical model of the aircraft corresponding with the flight condition at which the measurements were made. Parameter identification is an analytical process in which full use is made of state-space computational tools to estimate the aircraft state description that best matches the input-output response measured in flight. It is essentially a multi-variable curve fitting procedure, and the computational output consists of the coefficients in the aircraft state equation from which estimates of the aerodynamic stability and control derivatives may be obtained. This method is complex, and success depends, to a considerable extent, on the correct choice of computational algorithm appropriate to the experiment. [10]

3.1.1 Longitudinal Derivatives

The longitudinal aerodynamic coefficients of motion acts in the plane which is called pitch plane and affected by the lift force L, Drag force D, and pitch moment m. The effectiveness of these forces and moments are measured by lift coefficient C_L, drag coefficient C_D, and pitch moment coefficient C_m. These coefficients influenced by the angle of attack α, pitch angular rate q, and elevator deflection δ_e, but they are nonlinear in the angle of attack. For small α the flow over the wings remain laminar, so no stall conditions will be happened, then we will linearize the equations about this linear zone. [16]

Some non dimensional Derivatives can be analytically estimated as:

$$C_{x_u} = C_{T_u} - C_{D_u} \qquad C_{z_u} = -C_{L_u}$$
$$C_{x_\alpha} = C_{L_1} - C_{D_\alpha} \qquad C_{z_\alpha} = -(C_{L_\alpha} + C_{D_1})$$
$$C_{z_{\dot{\alpha}}} = -C_{L_{\dot{\alpha}}} \qquad C_{z_q} = -C_{L_q}$$

$$\begin{cases} C_x = C_T + C_L\alpha_x - C_D \\ C_z = -(C_L + C_D\alpha_x) \end{cases} \tag{3.4}$$

$$\begin{cases} C_{T_u} = -2C_{T_0} \\ C_{T_u} = -3C_{T_0} \\ C_{T_0} = C_{D_1} + C_{W_0}\sin\theta_0 \end{cases} \tag{3.5}$$

$$\begin{cases} (C_{L_q})_{Tail} = 2V_H a_t \\ (C_{m_q})_{Tail} = -2V_H a_t \frac{l_t}{\bar{c}} \end{cases} \tag{3.6}$$

$$\begin{cases} (C_{L_q})_{Foil} \approx -2C_{L_\alpha}(h - h_0) \\ (C_{m_q})_{Foil} = \bar{C_{m_q}} - 2C_{L_\alpha}(h - \bar{h})^2 \end{cases} \tag{3.7}$$

3.1.2 Lateral Derivatives

The lateral aerodynamic coefficients of motion which is responsible of the yaw and roll motions. It's affected by the side force F_y, yaw moment n, and roll moment l. The effectiveness of these forces and moments are measured by side force coefficient C_y, yaw moment coefficient C_n, and roll moment coefficient C_n. These coefficients influenced by sideslip angle , yaw angular rate r, roll angular rate p, aileron deflection δ_a, and rudder deflection δ_r, but they are nonlinear in these parameters. All of these coefficients should be determined by wind tunnel. Linear approximations for these coefficients and their derivatives are acceptable for modeling purposes and accurate, the linearization is produced by the

first-Taylor approximation, and non-dimensionalize of the aerodynamic coefficients of the angular rates. [16]

In necessary cases, it is important to know the stability derivatives that they result from the sum of the main wing and the tail wing. Next, the generic equation is presented with "i" and "j" representing the developed series of equations, and "k" the sum of the different contributions to both the wing and the tail that add up to the total contribution of the element, some non dimensional Derivatives can be analytically estimated as:

$$(C_{i_j})_{Total} = \sum_{k=1}^{N}(C_{i_j})_{MainWing} + \sum_{k=1}^{N}(C_{i_j})_{TailWing} \tag{3.8}$$

Tail contributions:

$$(C_{y_\beta})_{tail} = -a_F\left(1 - \frac{\partial\sigma}{\partial\beta}\right)\frac{S_F}{S} \tag{3.9}$$

$$(C_{y_p})_{tail} = -a_F\frac{S_F}{S}\left(\frac{2z_F}{b} - \frac{\partial\sigma}{\partial\hat{p}}\right) \tag{3.10}$$

$$(C_{y_r})_{tail} = a_F\frac{S_F}{S}\left(2\frac{l_F}{b} + \frac{\partial\sigma}{\partial\hat{r}}\right) \tag{3.11}$$

$$(C_{l_\beta})_{tail} \approx -a_F\frac{S_F z_F}{Sb}\left(1 - \frac{\partial\sigma}{\partial\beta}\right) \tag{3.12}$$

$$(C_{l_p})_{tail} \approx -a_F\frac{S_F}{S}\left(\frac{2z_F}{b} - \frac{\partial\sigma}{\partial\hat{p}}\right)\frac{z_F}{b} \tag{3.13}$$

$$(C_{l_r})_{tail} = a_F\frac{S_F}{S}\frac{z_F}{b}\left(2\frac{l_F}{b} + \frac{\partial\sigma}{\partial\hat{r}}\right) \tag{3.14}$$

$$(C_{n_\beta})_{tail} = a_F V_V\left(1 - \frac{\partial\sigma}{\partial\beta}\right) \tag{3.15}$$

$$(C_{n_p})_{tail} = a_F V_V\left(\frac{2z_F}{b} - \frac{\partial\sigma}{\partial\hat{p}}\right) \tag{3.16}$$

$$(C_{n_r})_{tail} = -a_F V_V\left(2\frac{l_F}{b} + \frac{\partial\sigma}{\partial\hat{r}}\right) \tag{3.17}$$

Wing contributions:

$$(C_{l_\beta})_{diedro} \approx -\frac{1+2\lambda}{6(1+\lambda)} a_0 \Gamma \tag{3.18}$$

$$(C_{l_\beta})_{offset} \approx -\frac{1+2\lambda}{3(1+\lambda)} C_l \tan\Lambda \tag{3.19}$$

$$(C_{l_\beta})_{wingposition} \approx \begin{cases} = -0.00016/^\circ \\ = 0 \\ = +0.00016/^\circ \end{cases} \tag{3.20}$$

$$(C_{l_p})_{wing} \approx -\frac{a_w}{12}\frac{1+3\lambda}{1+\lambda}, \qquad rectangular wings \qquad (C_{l_p})_{wing} \approx -\frac{a_w}{6} \tag{3.21}$$

$$(C_{l_r})_{wing} \approx \frac{C_l}{6}\frac{1+3\lambda}{1+\lambda} \tag{3.22}$$

$$(C_{n_p})_{wing} \approx -\frac{C_l}{8} \tag{3.23}$$

3.2 Numerical Models

A numerical model is a combination of a large number of mathematical equations that depends upon computers to find an approximate solution to the underlying physical problem. Using the first few terms of a Taylor Series to get an approximate value for a function, however, numerical models are not always limited to the Taylor expansion.

Taylor series is the series of functions of the form [20]:

$$f(x) = \sum_{n=0}^{\infty} a_n (x-a)^n \qquad \text{since} \qquad a_n = \frac{f^n(a)}{n!} \tag{3.24}$$

Where $f(x)$ is a given analytic function. In this case, the series above is said to be the Taylor series of $f(x)$ around the point $x = a$. Associated, the Taylor polynomial of order n around $x = a$ of a given n-times differentiable function at this point is given by[21]:

$$p(x) = f(a) + f'(a)\frac{(x-a)^1}{1!} + f''(a)\frac{(x-a)^2}{2!} + f'''(a)\frac{(x-a)^3}{3!} + ... + f^n(a)\frac{(x-a)^n}{n!} \tag{3.25}$$

To better estimate the stability derivatives will be use the method of finite [22] difference that is a mathematical expression of the form $f(x+b) - f(x+a)$. If a finite difference is divided by $b-a$, one gets a difference quotient. The approximation of derivatives by finite differences plays a central role in finite difference methods for the numerical solution of differential equations, especially boundary value

problems.

The difference operator, commonly denoted Δ is the operator that maps a function f to the function $\Delta|f|$ defined by [23]:

$$\Delta|f|(x) = f(x+1) - f(x)\Delta|f|(x) = f(x+1) - f(x) \tag{3.26}$$

A difference equation is a functional equation that involves the finite difference operator in the same way as a differential equation involves derivatives. There are many similarities between difference equations and differential equations, specially in the solving methods. Certain recurrence relations can be written as difference equations by replacing iteration notation with finite differences.

In numerical analysis, finite differences are widely used for approximating derivatives, and the term ”finite difference” is often used as an abbreviation of ”finite difference approximation of derivatives”. Finite difference approximations are finite difference quotients in the terminology employed above [24].

$$f'(x) = \frac{f(x+\Delta x) - f(x)}{\Delta x} + O(\Delta x) \tag{3.27}$$

$$f'(x) = \frac{f(x+\Delta x) - f(x-\Delta x)}{2\Delta x} + O(\Delta x^2) \tag{3.28}$$

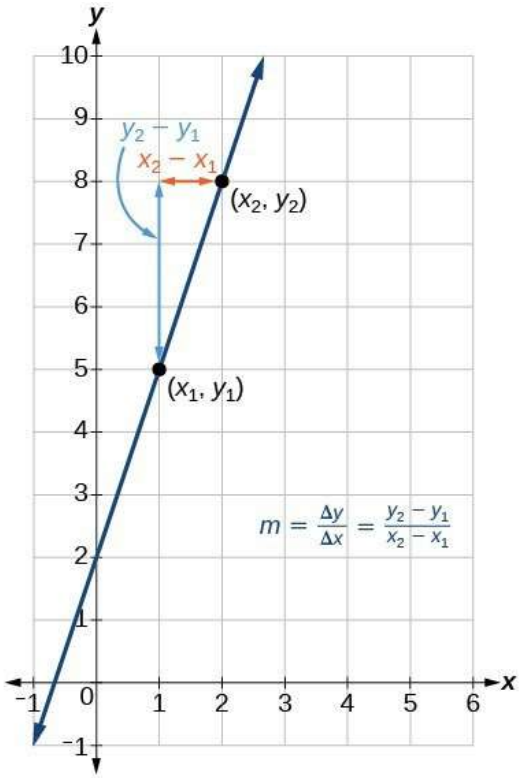

Figure 3.2: Finite Difference

3.3 Computational Fluid Dynamics

Computational Fluid Dynamics or Computational Fluid Dynamics (CFD), can be described in a generalized way as the numerical simulation of all those physical and/or physico-chemical processes that present flow.

The prediction of concentration fields, velocities, pressure, temperatures and turbulent properties is carried out through microscopic models based on the principles of conservation of mass, energy and momentum, in the domain of space and time.

3.3.1 Vortex Lattice Method (VLM)

The vortex lattice method (VLM) is a numerical method for the solution for flow over an arbitrary lifting surface. It is based on the ideal flow model and the solution to Laplace's equation, and thus, carries the assumptions that the flow is incompressible, inviscid and that the aerodynamic angles remain small. The effect of wing thickness is also neglected [25].

The solution can be used to compute the pressure distribution and then estimate aerodynamic characteristics and stability and control derivatives of an aircraft. VLM is a generic method in the sense that it can be used to define a wide range of aircraft geometry where methods such as lifting line theory would not be applicable.

One formulation of VLM uses a series of horseshoe vortices of variable strengths Γ to model the surface of the wing. A panel on the surface of the wing is composed of a control point at the $3/4$ chord of the panel and a vortex filament at the quarter chord of the panel which is bent 90 at the spanwise edge of the panel and extended infinitely trailing the wing. The induced velocity normal to the surface at each control point due to a vortex filament is calculated using the Biot-Savart law, Equation 3.29, where Γ is the strength of the vortex filament, ds is a differential length along the vortex filament, r is the distance to the control point and dV is the velocity induced by the vortex filament. The total normal velocity induced at a control point is calculated by summing the contributions from all horseshoe vortices on the wing. The strength of each horseshoe vortex is set by enforcing the condition that there is no component of velocity normal to the surface of the wing. This results in a linear system of equations that is solved for the strength of each vortex filament.

Another version of the vortex lattice approach models the wing surface using a series of vortex ring elements using a similar implementation. This approach has the added benefit that the boundary conditions on the wing surface can be satisfied exactly which allows more flexibility in wing shape, notably permitting the wing to be cambered.

$$dV = \frac{\Gamma}{4\pi} \frac{ds * r}{|r|^3} \tag{3.29}$$

VLM, represented in Figure 3.3 requires attention to details in its implementation to produce good results. The total number of lines defining the surface outline should be minimized, the wing tips should be parallel to the streamwise direction, and the trailing vortices from a surface cannot collide with the

control points of a trailing surface. Additionally, the effect of different panel distributions should be studied. Past results have shown that a good solution is obtained with a large amount of panels along the span compared to the number of panels along the chord. [25]

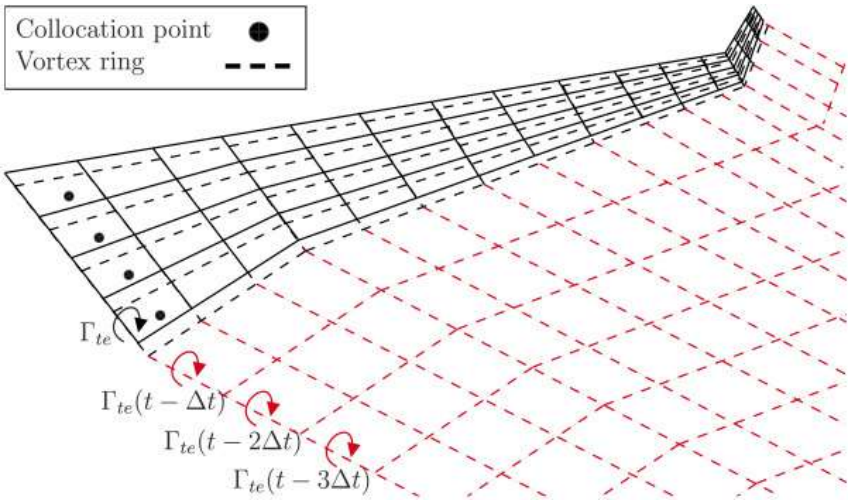

Figure 3.3: Vortex Lattice Method (VLM)

3.3.2 XFLR5

XFLR5 is an analysis tool for airfoils, wings and planes operating at low Reynolds Numbers. XFLR5 includes, XFoil's Direct and Inverse analysis capabilities Wing design and analysis capabilities based on the Lifting Line Theory, the Vortex Lattice Method, and a 3D Panel Method.

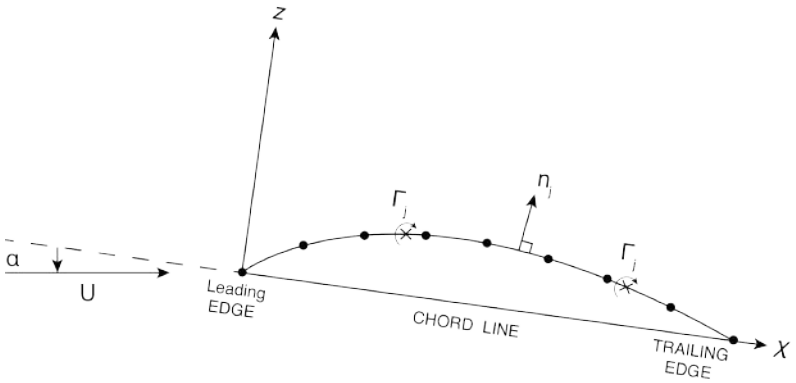

Figure 3.4: 3D Panel Method

The panel method is an analysis method that can be used to arrive at an approximate solution for the forces acting on an object in a flow. The method, as we present it here, is based on inviscid flow analysis, so it is limited to the resultant pressure forces over the surface. The panel method is basically a numerical approximation that relies on using discrete elements on the surface of an object and then prescribing a flow element (such as a vortex or doublet or source or sink) on each element that will satisfy certain boundary conditions (like no flow crosses the surface of the object). The interaction of the

elements are accounted for and must also satisfy the condition that far from the object the flow should be equal to the free stream velocity approaching the object.

The general approach is to select a “grid” which is a series of “panels” that form the surface. Here we take the panels as straight flat surfaces arranged over the real surface. In the limit of very small panels the constructed surface will simulate the actual surface. On each panel we place a distribution of flow elements (like sources, sinks, vortices, etc) that when combined together will result in a flow field that will satisfy the surface boundary condition. There are lots of ways to identify which elements to use and how they may be distributed on the panels. Here we will use vortex elements, with one placed on each panel. The net flow is the result of superposition of the flow set up by each vortex on each panel element. So at each point in the field we add together the flow caused by all of the panel elements using the superposition rule. The panels that are far away from a given point will have less and less influence on the flow because the strength of the flow caused by a flow element decreases with distance from the element origin. For instance for a “source” the velocity decreases with increasing radial position because the flow is spreading out away from the source. But the influence never really goes to zero.

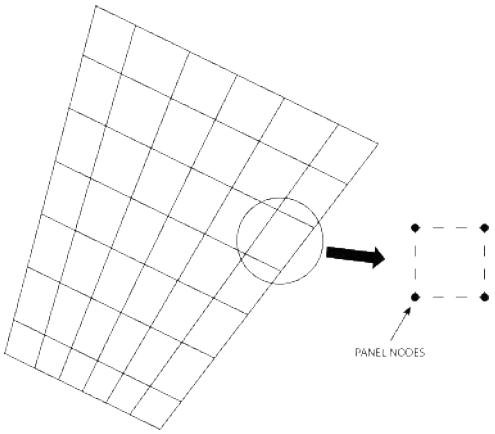

Figure 3.5: Grid of Panels

The Vortex lattice method, (VLM), is a numerical method used in computational fluid dynamics, mainly in the early stages of aircraft design and in aerodynamic education at university level. The VLM models the lifting surfaces, such as a wing, of an aircraft as an infinitely thin sheet of discrete vortices to compute lift and induced drag. The influence of the thickness and viscosity is neglected.

VLMs can compute the flow around a wing with rudimentary geometrical definition. For a rectangular wing it is enough to know the span and chord. On the other side of the spectrum, they can describe the flow around a fairly complex aircraft geometry (with multiple lifting surfaces with taper, kinks, twist, camber, trailing edge control surfaces and many other geometric features).

By simulating the flow field, one can extract the pressure distribution or as in the case of the VLM, the force distribution, around the simulated body. This knowledge is then used to compute the aerodynamic coefficients and their derivatives that are important for assessing the aircraft’s handling qualities in the conceptual design phase. With an initial estimate of the pressure distribution on the wing, the structural designers can start designing the load-bearing parts of the wings, fin and tailplane and other lifting

surfaces. Additionally, while the VLM cannot compute the viscous drag, the induced drag stemming from the production of lift can be estimated. Hence as the drag must be balanced with the thrust in the cruise configuration, the propulsion group can also get important data from the VLM simulation.

XFLR5 computes the following dimensional stability derivatives: X_u, X_w, Z_u, Z_w, Z_q, M_u, M_w, M_q, Y_v, Y_p, Y_r, L_v, L_p, L_r, N_v, N_p, N_r, and the associated non-dimensional stability derivatives. The control derivatives may also be calculated. The software also computes the longitudinal and lateral-directional state matrices and estimates of the dynamic modes of the aircraft. The stability analysis capability models the wing using the ring vortex approach. It is recommended in the code and guidelines to analyze the aircraft without the fuselage, i.e. typically only the wing and horizontal/vertical tail are defined for analysis. Omission of the body has been shown to have negligible effects on the results while avoiding potential numerical problems by including it. The results from the stability analysis have been validated against those calculated with the Athena Vortex Lattice (AVL) software [26].

$$\Delta X = X_u \Delta u + X_w w + X_{\delta e} \delta_e \tag{3.30}$$

$$\Delta Y = Y_v v + Y_p p + Y_r r + Y_{\delta a} \delta_a + Y_{\delta r} \delta_r \tag{3.31}$$

$$\Delta Z = Z_u \Delta u + Z_w w + Z_q q + X_{\delta e} \delta_e \tag{3.32}$$

$$\Delta L = L_v v + L_p p + L_r r + L_{\delta a} \delta_a + L_{\delta r} \delta_r \tag{3.33}$$

$$\Delta M = M_u \Delta u + M_w w + M_q q + X_{\delta e} \delta_e \tag{3.34}$$

$$\Delta N = N_v v + N_p p + N_r r + L_{\delta a} \delta_a + L_{\delta r} \delta_r \tag{3.35}$$

3.4 Wind Tunnel

Wind tunnels are large tubes with air moving inside. The tunnels are used to copy the actions of an object in flight. Researchers use wind tunnels to learn more about how an aircraft will fly. NASA uses wind tunnels to test scale models of aircraft and spacecraft. Some wind tunnels are big enough to hold full-size versions of vehicles. The wind tunnel moves air around an object, making it seem like the object is really flying.

Most of the time, powerful fans move air through the tube. The object to be tested is fastened in the tunnel so that it will not move. The object can be a small model of a vehicle. It can be just a piece of a vehicle. It can be a full-size aircraft or spacecraft. It can even be a common object like a tennis ball. The air moving around the still object shows what would happen if the object were moving through the air. How the air moves can be studied in different ways. Smoke or dye can be placed in the air and can be seen as it moves. Threads can be attached to the object to show how the air is moving. Special instruments are often used to measure the force of the air on the object.

NASA has more wind tunnels than any other group. The agency uses the wind tunnels in a lot of ways. One of the main ways NASA uses wind tunnels is to learn more about airplanes and how things

move through the air. One of NASA's jobs is to improve air transportation. Wind tunnels help NASA test ideas for ways to make aircraft better and safer. Engineers can test new materials or shapes for airplane parts. Then, before flying a new airplane, NASA will test it in a wind tunnel to make sure it will fly as it should. NASA also works with others that need to use wind tunnels. That way, companies that are building new airplanes can test how the planes will fly. By letting these companies use the wind tunnels, NASA helps to make air travel safer. NASA also uses wind tunnels to test spacecraft and rockets. These vehicles are made to operate in space. Space has no atmosphere. Spacecraft and rockets have to travel through the atmosphere to get to space. Vehicles that take humans into space also must come back through the atmosphere to Earth. Wind tunnels are important. NASA uses them to test the Orion spacecraft and the Space Launch System rockets. These rockets are called the SLS. Orion and SLS are new vehicles. They will take astronauts into space. NASA must test the systems in wind tunnels to see if they are safe to fly. And NASA must see what happens when Orion comes back to Earth through the atmosphere. Wind tunnels can even help engineers design spacecraft to work on other worlds. Mars has a thin atmosphere. It is important to know what the Martian atmosphere will do to vehicles that are landing there. Spacecraft designs and parachutes are tested in wind tunnels set up to be like the Martian atmosphere. NASA has many different types of wind tunnels. They are located at NASA centers all around the country. The wind tunnels come in a lot of sizes. Some are only a few inches square, and some are large enough to test a full-size airplane. Some wind tunnels test aircraft at very slow speeds. But some wind tunnels are made to test at hypersonic speeds. That is more than 4,000 miles per hour! [27]. The Wind Tunnel used for this thesis, have a section that have a maximum diameter of 1.20m and a maximum speed of 25 m/s was used.

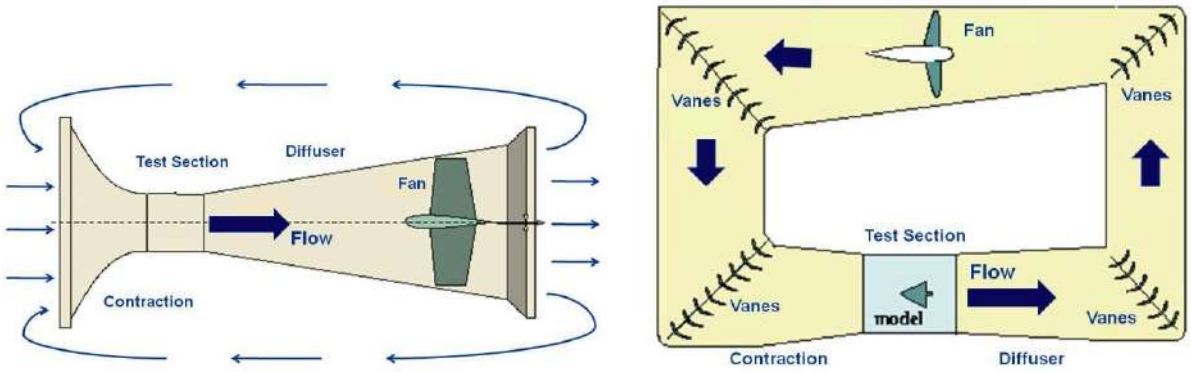

(a) Open Wind Tunnel

(b) Closed Wind Tunnel

Figure 3.6: Wind Tunnel Types

The conditions of operation in wind tunnel are set to reproduce the same results as those obtained in real aircraft operation. To guarantee this, it is necessary to analyse non-dimensional fluid motion equations. The equations are used to provide the dimensionless relations between the scale model and the normal size aircraft. Three dimensionless coefficients are found: the Reynolds number (R_e), the Mach number (M_a) and the Froude number (F_r). These parameters provide relations between the main causes of force in the flow: viscosity, inertia, elasticity and gravity, [28]

$$R_e = \frac{\rho \nu l}{\mu} = \frac{InertialForces}{ViscousForces} \tag{3.36}$$

$$M_a = \frac{\nu}{a} = \frac{InertialForces}{ElasticForces} \tag{3.37}$$

$$F_r = \sqrt{\frac{\nu^2}{lg}} = \sqrt{\frac{InertialForces}{GravitationalForces}} \tag{3.38}$$

where l represents the characteristic length in m, ν the velocity of the body in m/s, ρ the air density in kg/m^3, μ the coefficient of dynamic viscosity in $kg/(m.s)$, a the speed of sound in m/s and g the acceleration of gravity in m/s^2 .

3.4.1 Force Balance

Aerodynamicists use wind tunnels to test models of proposed aircraft and engine components. During a test, the model is placed in the test section of the tunnel and air is made to flow past the model. Various types of instrumentation are used to determine the forces on the model.

For the analysis of the UAV aircraft of the present master's thesis, the following force balance model shown in Figure 3.7 will be used,

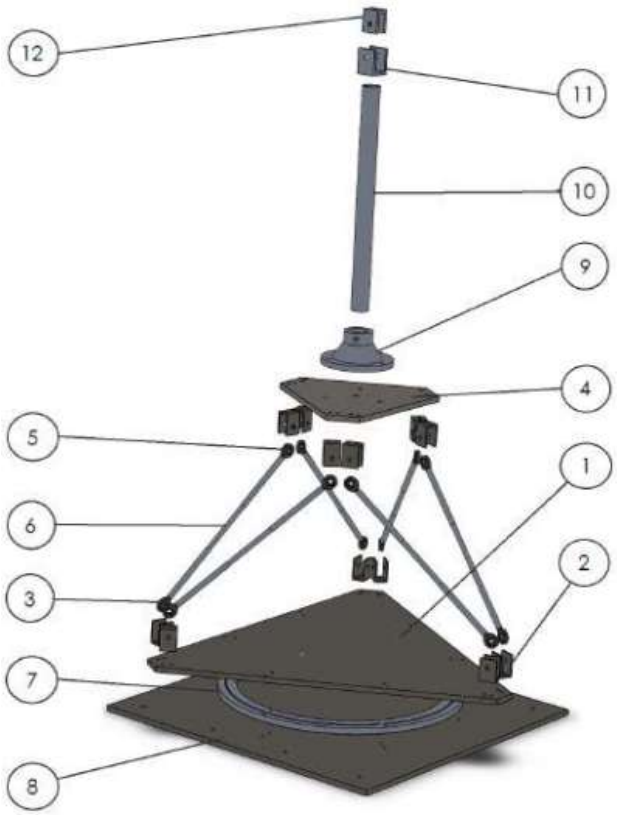

Item number	Part name	Quantity	Material
1	FixedPlatform	1	Steel 1.0037
2	Coupler	12	Alloy Steel
3	RodEndBearing_R	6	Steel 1.0503 Brass
4	NewMovingPlatform	1	Al 6082-T6
5	RodEndBearin_L	6	Steel 1.0503 Brass
6	NewSensingBar	6	Al 6063-T6
7	RotatingCollar	1	Al 2024-T4 Al 6063-T6
8	Table	1	Steel 1.0037
9	NewFlange	1	Al 7075-T6
10	NewStrut	1	Al 6063-T6
11	alphaAdjustment_1	1	Al2024-T4
12	alphaAdjustment_2	1	Al 2024-T4

Figure 3.7: Balance of Forces Components [29]

A wing model is mounted in the tunnel on a bar that passes through the side of the tunnel. The bar passes over a fulcrum and the force generated by the model is balanced by weights placed on a plate

hung from the end of the bar. With the tunnel turned off and no air passing through the test section, weights are added to the plate to balance the weight of the model. The tunnel is then turned on and air flows over the model. The model generates an aerodynamic force witch is measured by the balance. In the figure, the leading edge of the wing model is lower than the trailing edge. In this case, the wing will generate a lift force that is in the same direction as the weight of the model (downforce). The bar is no longer in balance; the end outside the tunnel is higher than the previous setting. Additional weights are added to the plate to re-balance the bar. The amount of the added weight is equal to the magnitude of the aerodynamic lift of the model. If the model had been mounted with a positive angle of attack, one would have to remove weights from the plate to bring the bar back into balance. [30]

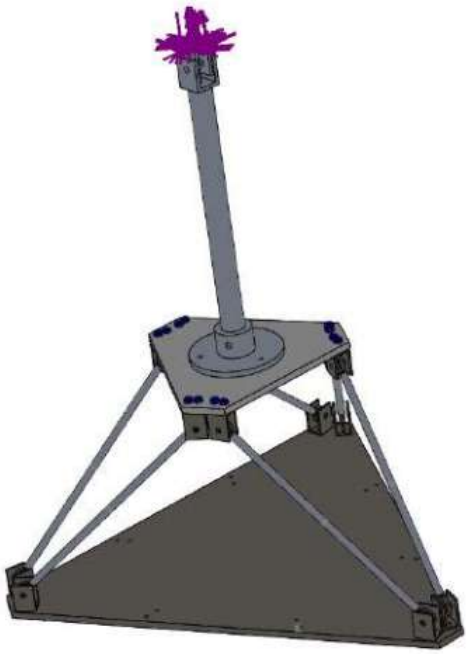

(a) Auto-CAD Balance of Forces

(b) Real Balance of Forces

Figure 3.8: Balance of Forces [29]

This very simplified mechanical method of determining lift can be used with a student-built wind tunnel. Some student wind tunnels are equipped with electronic instrumentation to determine drag. To accurately determine the aerodynamic forces and moments on an aircraft model in a ”real” wind tunnel requires much more sophisticated instrumentation. Electronic strain gages are placed inside the model, or on a measuring platform outside the tunnel. Multiple gages permit the determination of multiple forces during the same test. The axis system used was that of the aircraft, as shown in figure 3.1, in order to be able to measure the variables $F_x, F_y, F_z, M_x, M_y and M_z$, in order to adjust the parameters, V - Speed,α and β. In other tunnels, the measuring devices are placed inside the model. The location of the device affects the choice of mounting system for the model and the data reduction necessary to determine the aerodynamic forces.

Chapter 4

Design and Building of Aircraft Models

This chapter describes the construction process of the two models that will be analyzed in the wind tunnel and CFD by XFLR5 software, as well as the manufacturing processes of the models with special detail for the construction with illustrative images of both models, concluding with the final result of the construction.

4.1 Test Aircraft Model Design

The test model design will be fully purposed taking into account all the parameters that allow a high fidelity in the CFD Modeling, thus the aircraft design is intentionally kept as simple as possible.

4.1.1 Airfoil Profile Design

To choose the most suitable airfoil for the test model, it is necessary to make quantitative calculations to choose with the greatest accuracy the ideal airfoil for experimentation, considering reference values of aircraft speed V, kinematic viscosity ν and air density ρ, that can be seen in Table 4.1.

Table 4.1: Model Test Reference Values

Values	
V - Air Speed	20 m/s
ν - Kinematic Viscosity	1.51×10^{-5} m^2/s
ρ - Air Density	1.225 kg/m^3
AR - Aspect Ratio	8
b - Wingspan	1 m
g - Gravity Acceleration	9.81 m/s^2
W - Aircraft Mass	1.2 kg

Main Wing

The wing span $b = 1m$, was chosen because as the maximum allowed to be tested in the wind tunnel.

$$AR = \frac{b}{c} = 8 <=> 8 = \frac{1}{c} <=> c = 0.125m \tag{4.1}$$

Since the wing is rectangular, we obtain the wing area as.

$$S = b \times c = 1 \times 0.125 = 0.125m^2 \tag{4.2}$$

When the UAV is flying in trimming we know that Lift is equal to Weight.

$$L = W \tag{4.3}$$

So applying the general formula for the lift coefficient given by.

$$C_L = \frac{W}{\frac{1}{2}\rho V^2 S} \tag{4.4}$$

Where V is the aircraft speed, ρ is the air density, S is the surface area, c is the wing chord, b is the wing span, W is the weight of the UAV and L is the lift force in newton, replacing the values we obtain the reference lift coefficient.

$$C_L = \frac{1.2 \times 9.81}{\frac{1}{2} \times 1.225 \times 20^2 \times 0.125} = 0.384391837 \tag{4.5}$$

We calculate the reference Reynolds number by.

$$Re = \frac{Vc}{\nu} = \frac{20 \times 0.125}{1.51 \times 10^{-5}} = 165562.9139 \tag{4.6}$$

So now having the Reynolds and Lift Coefficient reference values, it is possible to chose the best low Reynolds number airfoil for the experience.

Analyzing between 2 low Reynolds numbers alar profiles that best adapt to our case, this choice was made by the conventional low Reynolds number profiles [31]

The Selig/Donovan SD7062 low Reynolds number airfoil is shown in Figure 4.1.

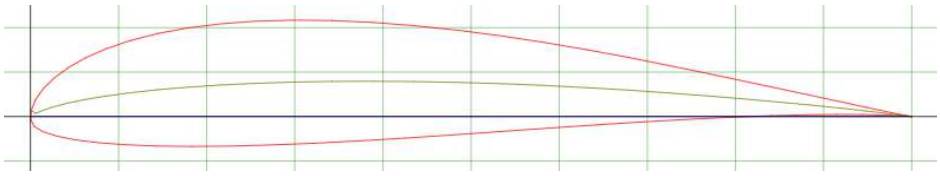

Figure 4.1: Profile SD7062 (14%)

The Selig S8036 low Reynolds number airfoil is shown in Figure 4.2.

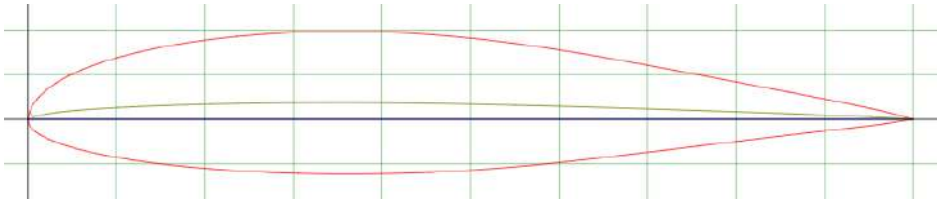

Figure 4.2: Profile S8036 (16%)

Then a comparison was made between the polar lines of the expected actuation range of Reynolds numbers, $Re = 165562.9$, consequently comparing between the lines of $Re = 100000$ and $Re = 200000$, between the two proposed 2D profiles, with the objective of verifying which of the two would have a lower drag coefficient for the expected lift coefficient.

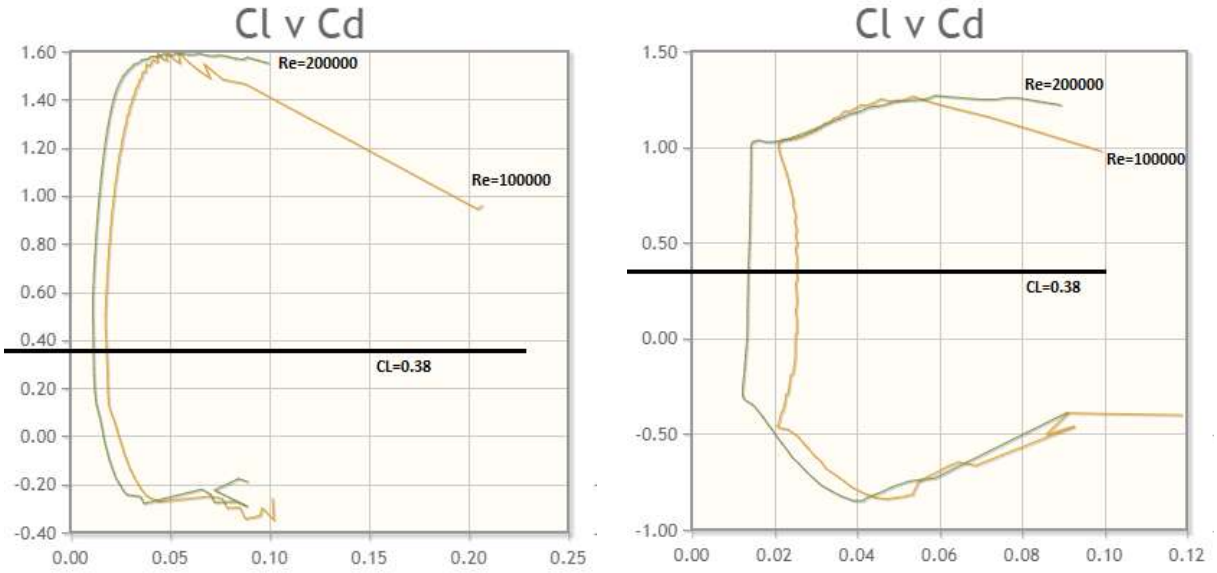

(a) SD 7062

(b) S 8036

Figure 4.3: C_L vs C_D Polars for $Re = 100000$ and $Re = 200000$

As we can see in the Figure 4.3, drawing a horizontal asymptote at $C_L = 0.38$, at the intersection of the asymptote with the polar lines of the respective Reynolds number, we observe that between the two chosen profiles, the one that presents the lowest drag coefficient is the **SD 7062** profile, so we can conclude that it is the most efficient profile for the chosen reference flight conditions, so this will be the design profile chosen for the Test Aircraft Model.

Tail and Fin Wing

For the tail wing and vertical fin, a symmetrical profile more suitable for low Reynolds numbers will be chosen, which will be the **NACA 0015** profile, illustrated in Figure 4.4. [31]

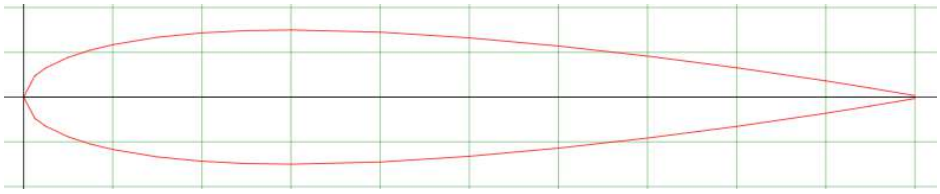

Figure 4.4: Profile NACA 0015

The NACA 0015 airfoil is symmetrical, the 00 indicating that it has no camber. The 15 indicates that the airfoil has a 15% thickness to chord length ratio: it is 15% as thick as it is long.

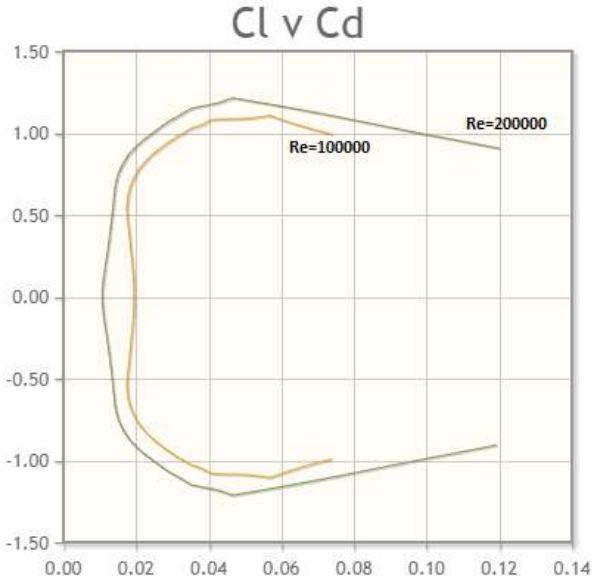

Figure 4.5: C_L vs C_D Polars for $Re = 100000$ and $Re = 200000$, Profile NACA 0015

The choice of this profile **NACA 0015** is based on being one of the most appropriate symmetrical profiles for low Reynolds numbers, which is the case, presenting very low values of the drag coefficient for the expected lift coefficient values.

4.2 Test Aircraft Model Building

In this section, we will address the construction process of the test aircraft, which was designed in the previous chapter with 2D airfoil sections for small Reynolds numbers. The main objective of the aircraft is, in scientific terms, to know with great certainty the type of real profile and the model for CFD in order to be able to compare as realistically as possible the real model with the virtual model analyzed in XFLR5. Thus, we can assure that the results obtained in the real model in the wind tunnel and in the virtual model in the XFLR5 are coherent because we are sure of the distances, profiles, wingspan and all the characteristics of the aircraft both in reality and in the virtual model, being able to guarantee a correct and appropriate validation of the results obtained, as the recreated models are exactly the same.

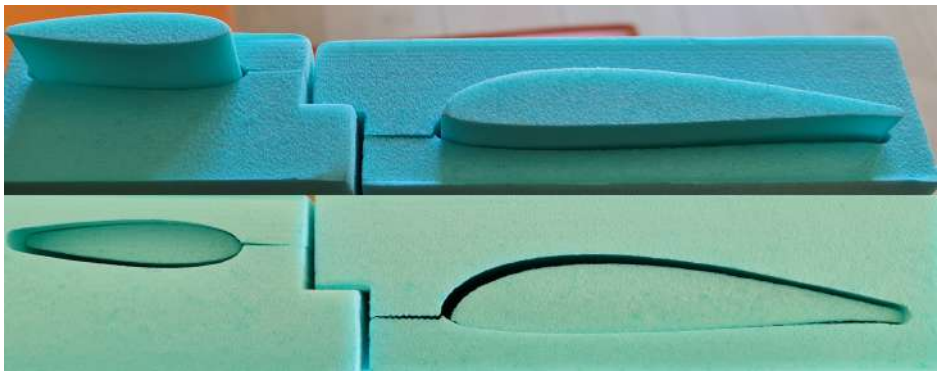

Figure 4.6: Cutting Profiles in XPS

The first phase of construction involves using XPS boards, an extremely suitable material due to its low weight and ease of working. As you can see in the Figure 4.6 the XPS plates cut in a hot wire machine, all the coordinates of the points that characterize the airfoils in two dimensions were used and thus the wings were cut in 3D with the desired span.

(a) Wing (b) Tail

Figure 4.7: Support Wings Building

Then, a wooden pole of circular section, with the surface with the lowest possible roughness so as not to influence the results in terms of increasing friction coefficient and forces consequently exerted, it was used as a support and fuselage for the XPS wings. It was necessary to wear an angle grinder in order to obtain a flat base to seat the wings of the test model, as can be seen in the Figure 4.7.

Figure 4.8: Ailerons Cut

The next process was to cut the ailerons from both the main wing Figure 4.8 and the horizontal and vertical stabilizer to be able to control the test aircraft. The ailerons' cut measures were specially dimensioned to provide the forces necessary to change the aircraft's movement, generating the necessary angular velocities, as well as in our wind tunnel test case, generating the force necessary to calculate its control derivatives.

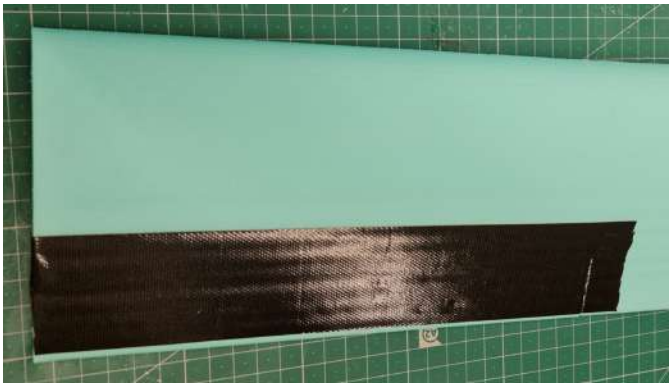

Figure 4.9: Ailerons Attachment to Main Wing

Subsequently, it was necessary to join the ailerons, Figure 4.9 so that they are movable, in order to have various combinations of aileron angles, so a high-resistance tape was used to attach the ailerons to the wing and at the same time the ailerons are movable. The same process was used for both the vertical stabilizer, Fin, and for the horizontal stabilizer, Elevator.

Figure 4.10: Installation of Servos Mechanisms

At this moment, as the ailerons and main wing are already built, it is necessary to have an electronic component to move the ailerons, as well as keep them in the same position if desired, so a servomechanism figure 4.10 was used, 1 for each aileron of the main wing , 1 for the horizontal stabilizer and 1 for the vertical stabilizer, totaling 4 servo-mechanisms needed to control the test aircraft.

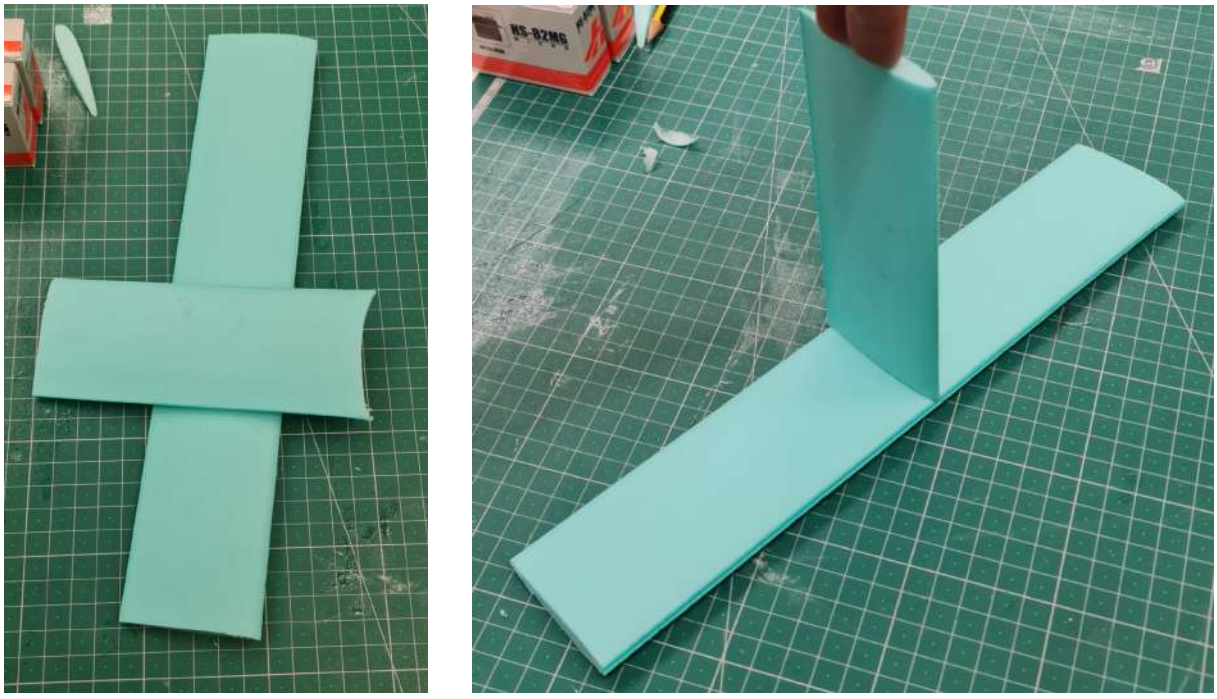

(a) Tail Wing and Fin Cutting

(b) Tail Wing and Fin Assembly

Figure 4.11: Tail Wing and Fin Building

As can be seen in the Figure 4.11 (a), in the vertical stabilizer, it was necessary to create a cut with the coordinates of the NACA 0015 profile, to create a connection between the profiles in order to ensure its stability. Subsequently, epoxy glue was applied in order to join both the vertical stabilizer and the horizontal stabilizer with an angle of 90°.

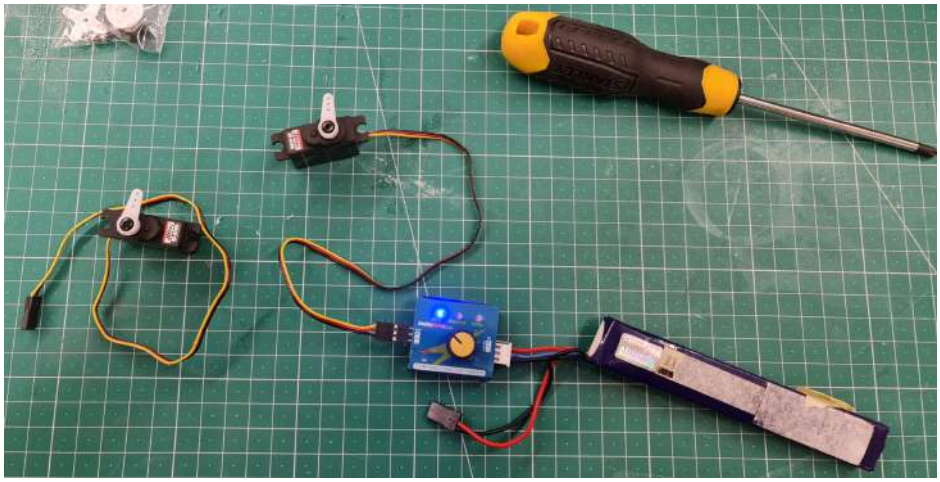

Figure 4.12: Servo Mechanisms Test

It was also necessary to test the servo-mechanisms present in figure 4.12 in order to guarantee that they were at the neutral angle, corresponding with the zero angle deflection of the aileron when coupling to the main wing, so it was possible to cover all the variable working angles from positive to negative present in the airplane wing.

Figure 4.13: Main Wing and Tail Wing Calibration

To make sure that both the main wing and the horizontal stabilizer were level and with the same angle of attack position, a level was used as seen in the Figure 4.13 in order to guarantee the level before putting in order to glue both wings to the support of the wings of both the main and the vertical stabilizer. After this process, it is only necessary to make the tie rods / connecting rods, in order to have a physical mechanical means that makes the interconnection of the movement between the servo-mechanism and the aileron, thus allowing its motion and, thus finishing the construction of the test aircraft as can be seen in the Figure 4.14.

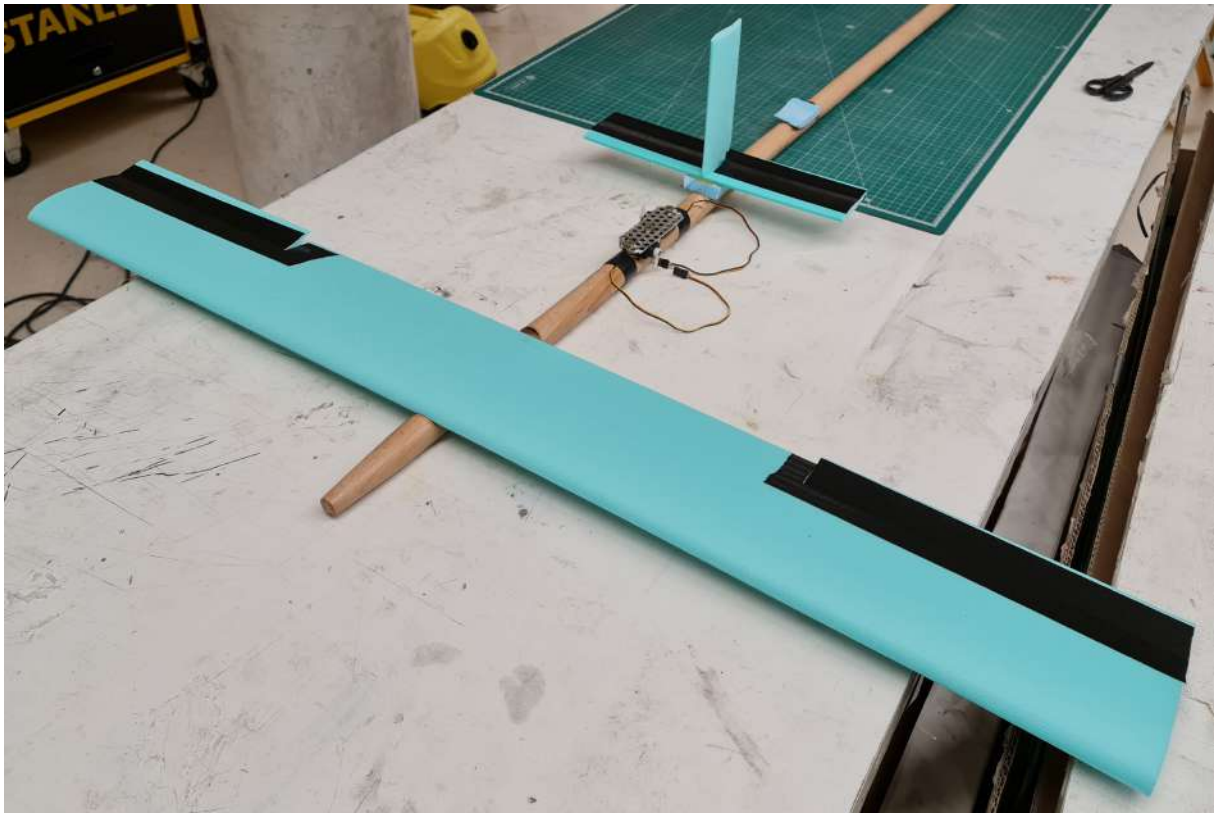

Figure 4.14: Final Test Aircraft

4.3 F35 Model Design

This aircraft was specially designed for the present master's thesis. It is a replica of the F35 Fighter Figure 4.15, the "Open Source" design project, available online **By Julius Perdana 2020 Webpage** , was used for the design base, however many changes were made in order to aesthetic and mainly aerodynamic improvements, in order to maximize its load capacity and efficiency.

(a) F35 Fighter

(b) F35 **Designed By Julius Perdana 2020**

Figure 4.15: F35

Below in Table 4.2 we can see in detail all the specifications of the F35 model, which are required for an analysis as coherent as possible in a wind tunnel, like Wing Span, Flying Weight, Wing Loading, Aspect Ratio, Wing Area and Center of Gravity position,

Table 4.2: F35 Model Specifications

Values	
Wing Span	950 mm
Flying Weight	1.235 Kg
Wing Loading	37 g/dm^2
Aspect Ratio	6.4
Wing Area	33.37 dm^2
Center of Gravity	11.5 cm from the wing root leading edge

In Figure 4.15 we can see the $3D$ model of the $F35\ Fighter$ that will be built, an overview of the construction project which is of high priority as it becomes the basis for the development of the construction, later in this thesis it will be described in detail the construction process, for now is the $Auto\ CAD\ 3D$ image of the final objective.

4.4 F35 Model Building

In the following figures of this chapter, the construction process of the F35 model will be presented, respecting its real scale, however for an increase in the model's lift since the model fly at low speeds, much lower than the real F35 Fighter, they were proportionally scaled up, respecting the Aspect Ratio, increasing the size of the main wings which allows the smaller-scale Model to fly at low speeds, producing greater lift through the increase of the wing area, allowing in consequence to reduce the speed necessary for the smaller-scale Model to fly.

(a) 2 Pieces

(b) 1 Pieces

Figure 4.16: F35 Cockpit Building

First, all the pieces that make up the model were cut to the right measure, with the help of an X act.

(a) F35 Fuselage Installation

(b) F35 Fuselage Final Rear Perspective

Figure 4.17: F35 Fuselage Building

The material used to build the small model was, INART K-Line, 5 mm, 700 x 1000 mm to build the fuselage and both wings , in which hot glue was used to connect the pieces.

For a rear perspective we have the following Figure 4.17.

Then, with hot glue, after giving the necessary shape to the pieces, the pieces from the front of the model were joined, and so the construction of the fuselage began.

Figure 4.18: F35 Fuselage Final

After the fuselage was complete, the construction of the main wings, left and right, started, a $5mm$ carbon tube was also installed on the inside of the wings and fuselage, crossing the model transversally from the left wing tip to the right wing tip, intersecting perpendicularly the fuselage in a single tube of $5mm$, thus conferring resistance to the model to when the lift force is imposed to the model and also still ensures that both wings are with the same angle of attack, with the same dihedral angle and completely perpendicular to the fuselage of the airplane model.

Finally, the main wing ailerons were made on both sides, and the rear wing responsible for the longitudinal stability of the model was installed. Both side stabilizers were also installed with the same angle in relation to the fuselage as in the real model.

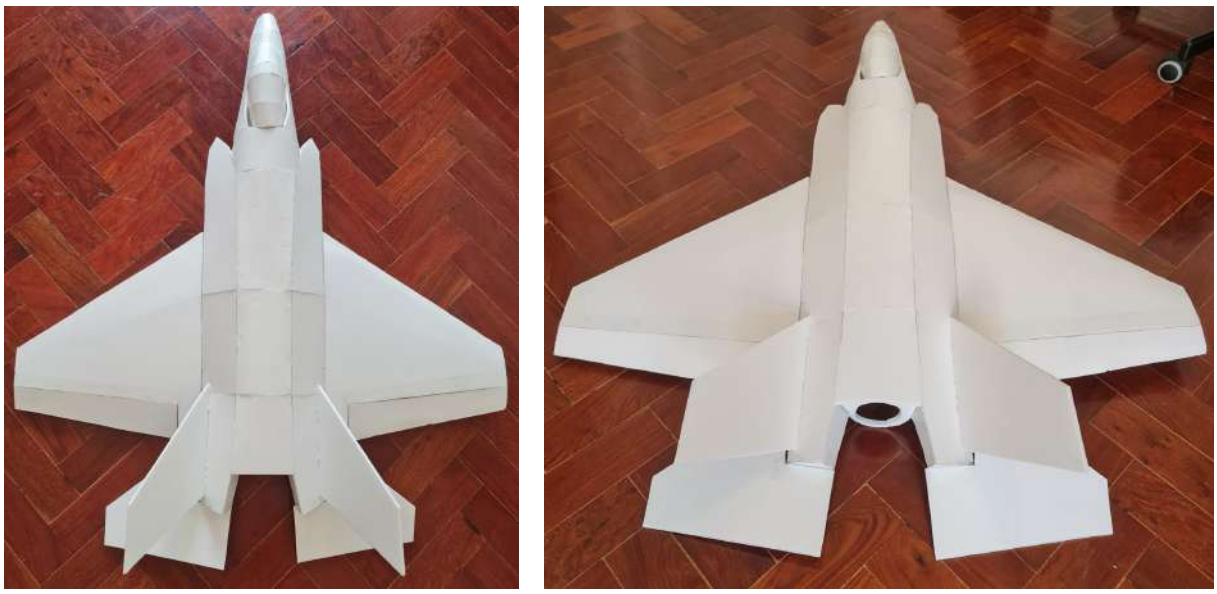

(a) F35 Top Plan View

(b) F35 Back view

Figure 4.19: F35 Rear Wings Installation

Getting a final rear configuration as shown in the Figure 4.19,

A circumferential hole was also installed at the rear of the model, as can be seen in the Figure 4.19, for the installation of a longitudinal support inside the model to attach it to the force balance for analysis in the wind tunnel.

Figure 4.20: F35 Front Overview

Finally, in Figure 4.21, a conical tip was added to the tip of the aircraft in order to eliminate stagnation points and reduce the Drag Coefficient as much as possible, as well as a transparent cabin in acetate paper, molded especially for the Model F35 with the help of a pump. of heat and mold, a very time-consuming process, to finish the construction process the entire aircraft was painted in the color ”Black Matt”, to guarantee a finish both at an aesthetic and aerodynamic level of reference.

Figure 4.21: F35 Aircraft Final - Front View

In the following figure 4.22 we can see the final front-left view of the F35 Test Aircraft.

Figure 4.22: F35 Aircraft Final - Left View

As in the following figure 4.23 we can see the final front-right view of the F35 Test Aircraft.

Figure 4.23: F35 Aircraft Final - Right View

Chapter 5

Calibration of Force Balance

This chapter describe and discuss the calibration of the force balance, where it is possible to see all the process, reported with pictures and also the data collected to calculate the equations for the axial force for the different angles measured in each bar of the force balance.

5.1 Structure Assembly

In Figure 5.1, it is possible to observe the position of the balance of forces in the wind tunnel, as well as its proper level position.

Figure 5.1: Positioning the Balance of Forces in the Wind Tunnel

The calibration procedure, as well as all its calibration steps, can be consulted in the appendix B.4.

With the help of the structure shown in the Figure 5.2, it was possible to place weights to produce forces in the 3 positions of space, applying known loads in the 3 directions, as well as producing the 3 possible moments, besides those pure forces and moments in ”x”, ”y” and ”z” axes, composed Force + Moment loads were also applied. Timing the time between each load application, as forces in the order of 20N were expected, 5N weights were applied every 30 seconds, and the measured values were recorded, this process will be described with more detail latter.

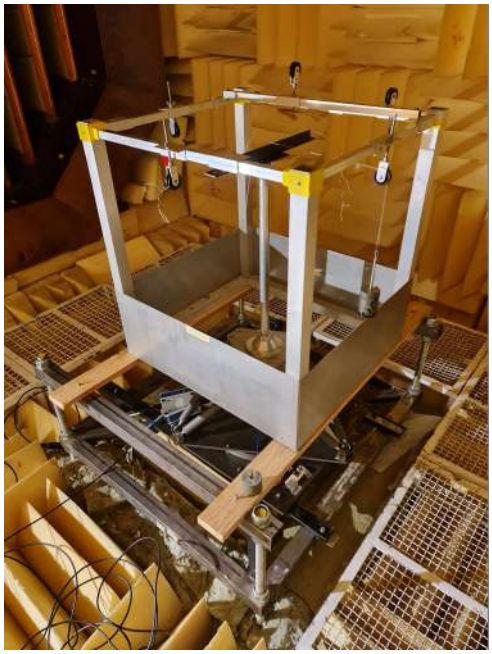

Figure 5.2: Calibration Structure

In the Figure 5.3 and 5.4 we can see examples of the various arrangements of applied forces, applied in all possible axes and moments, for a real modeling of the equations bars.

(a)

(b)

Figure 5.3: Force and Moment Calibration Process

When it came to simple, pure forces, only in one direction, a weight of 5N was added every 30 seconds. Initially, for 30 seconds, the scale was left without any weight just to stabilize the bars, then every 30 seconds 5N of weight were added, until we get 25N of total weight.

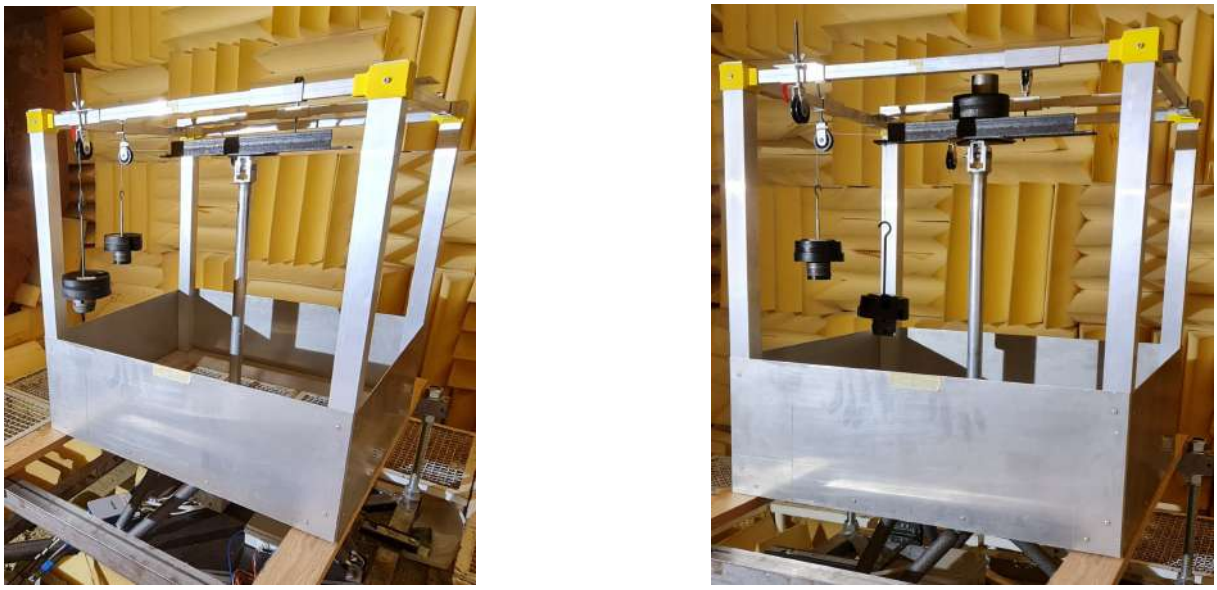

(a) (b)

Figure 5.4: Force and Moment Calibration Process

5.2 Calibration Results

In this section, some examples of the results obtained during the calibration will be presented, three measurements were made, for each applied force, that is, 2 graphs were recorded for each calibration round, and there were 3 calibration rounds, which makes a total of 60 graphs, because both positive and negative forces and moments were recorded, as well as the interaction between pure forces, conjugated forces, and finally conjugated forces and moments, totaling more than 252 792 lines of data in excel sheet. In the end, a weighted average was made between the 3 calibration rounds, and these median values were the values in MATLAB for the final calculation.

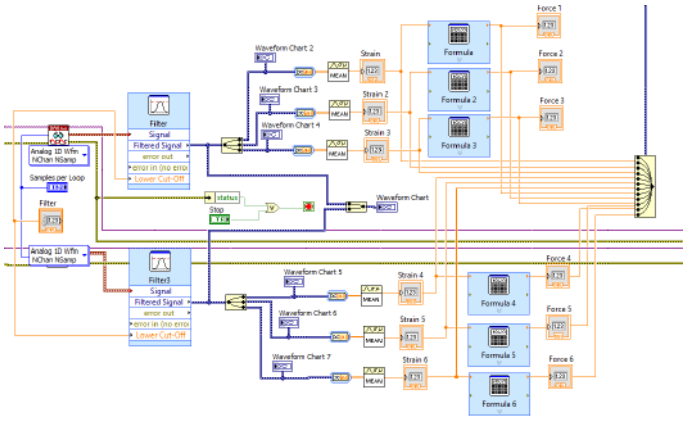

Figure 5.5: Calibration Block Diagram used for the Present Master Thesis

In the figure 5.6 we can see the example of the results measured when the known loads were applied along the positive Fx axis. Each level of the graph corresponds to a new load of 5N applied, and the horizontal distance of the new level, corresponds to 30 seconds of waiting to stabilize the values and have a stable reading of the results.

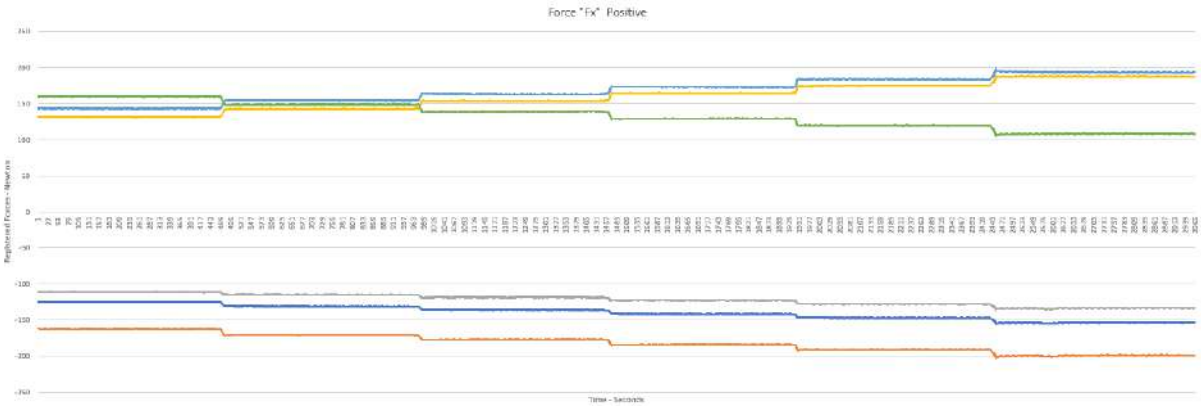

Figure 5.6: Calibration Results for Force ”Fx” Positive

In the figure 5.7 it is possible to observe the variation of axial force in each bar a when the application of a pure moment, every 30 seconds, each new level of the graph corresponds to a new load of 5N applied to increase the moment, in this case for positive My, always keeping the same 20cm moment arm.

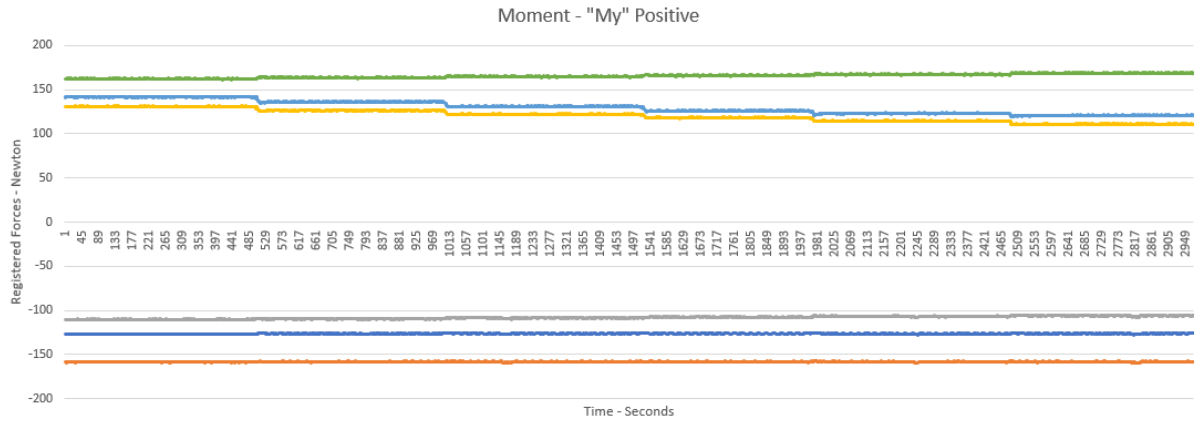

Figure 5.7: Calibration Results for Moment ”My” Positive

It is important to mention that, in the conjugated forces, as I only have two arms, and it was necessary to change the weights in 3 places at the same time, so, there were small oscillations in the load/weight transitions, as seen in Figure 5.8, between 2871 and 2953 seconds. However, the results of these oscillations have been excluded to not affect the accurate calibration.

In figure 5.8, the application of joint forces begins, which allows to know the influence when 2 forces are applied in this situation, an interval of 1 minute was expected between each level of applied load of 0N, 5N, 10N, 15N, 20N and 25N, between each new load applied, as 2 forces take longer to stabilize, and therefore the waiting time interval was greater.

Figure 5.8: Calibration Results for Compose Forces ”Fx” and ”Fz” Negative

In figure 5.9, calibration assignments were made for combined forces and moments, with the same time interval of 60 seconds, and force interval of 0N, 5N, 10N, 15N, 20N and 25N, at the same time in all forces studied in the case. Thus, we obtain a more realistic reading of the expected values, as well as their influence between the bars for the various configurations of forces and moments applied.

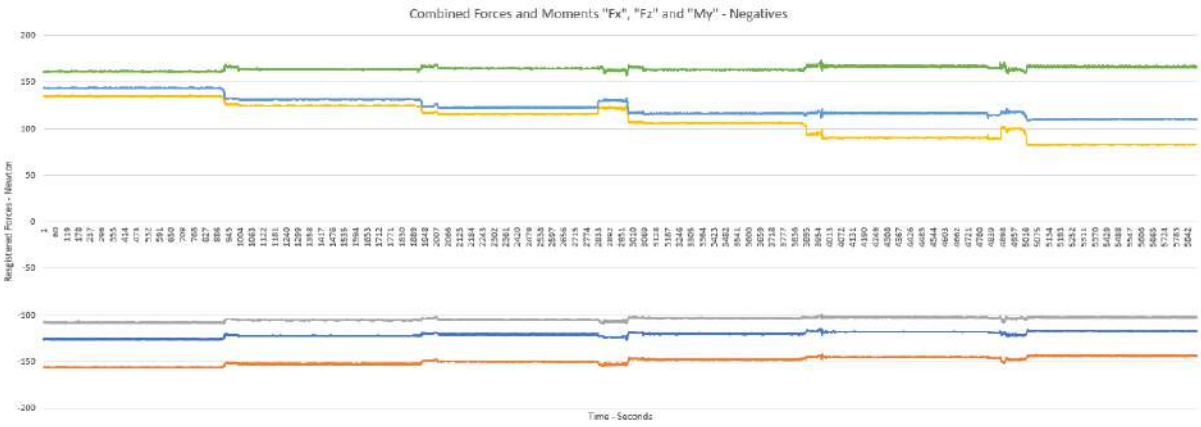

Figure 5.9: Calibration Results for Combined Forces and Moments ”Fx”, ”Fz” and ”My” Negative

This is the closest example of the reality of an aircraft in which several forces and moments of different values interact on the aircraft body, lift forces, drag forces, self-weight forces and trust forces.

5.3 Calibration Equations

In this section, the equations calculated in MATLAB will be presented, which through the results obtained in the calibration with known weights and distances. These equations define the behavior of axial forces present in the six sensing bars of the force balance, so we will have six equations, one for each bar. Thus, it will be possible to obtain an effort value, taking into account the arrangement of each bar, inclination and the relationship between them. By propagation of moments equations, transfer the forces to the aircraft, thus removing all the efforts produced by the aircraft in the given flight conditions.

After obtaining the axial forces of each bar, MATLAB makes the relationship between the forces of each bar and the axis system in the connection zone between the scale and the aircraft, calculating the equations between each axial force of the bar with the respective possible force or moment, that is, the 3 possible forces in space and the 3 possible moments in space, so we will finally have an adequate reading of the experimental values.

In Table 5.1, it is possible to observe the equations taken after the calibration process, in which the sum of each respective column, multiplied by each of the respective R_i coefficients, totals the complete equation referring to each Force or Moment.

Table 5.1: Calibration Equations Table - Matlab

	$F_x =$	$F_y =$	$F_z =$	$M_x =$	$M_y =$	$M_z =$
R1 $\times R1$	+0.039749	-0.000065	-0.102022	-0.001536	0.006397	0.002170
R1 $\times R2$	+0.017968	-0.015064	-0.231213	-0.039004	-0.002957	-0.005484
R1 $\times R3$	-0.015450	+0.014426	+0.510499	+0.064462	+0.022320	+0.005279
R1 $\times R4$	-0.004836	-0.053372	-0.012153	+0.000732	+0.007835	-0.013509
R1 $\times R5$	+0.052008	+0.045984	-0.000288	+0.009384	+0.006963	+0.015859
R1 $\times R6$	-0.029576	-0.011702	+0.129095	-0.009448	-0.003455	-0.004845
R1	+8.545607	+1.750138	-27.634322	+0.378073	+1.864908	+0.542115
R2 $\times R2$	+0.020524	0.000515	-0.015919	-0.005249	+0.002221	+0.003340
R2 $\times R3$	-0.067400	+0.011259	+0.140278	+0.007701	+0.008212	-0.012178
R2 $\times R4$	+0.002482	+0.032503	+0.057360	-0.027367	+0.024796	+0.003091
R2 $\times R5$	+0.020106	-0.036729	+0.079243	+0.027476	-0.006450	-0.004350
R2 $\times R6$	+0.002310	+0.007616	+0.176130	+0.016596	+0.007991	+0.005967
R2	-2.243770	-1.017825	-68.204507	-8.423457	-2.596759	-1.726986
R3 $\times R3$	+0.049769	-0.022136	-0.068205	+0.005642	-0.007426	+0.007216
R3 $\times R4$	-0.035867	-0.075349	+0.057011	+0.051144	-0.031130	-0.012303
R3 $\times R5$	+0.011606	+0.084114	-0.195879	-0.039781	+0.012244	+0.013994
R3 $\times R6$	-0.00800	-0.006182	-0.305435	-0.030340	-0.017522	-0.007920
R3	+2.714959	-1.706731	+142.710898	+13.865601	+7.864380	+1.247445
R4 $\times R4$	-0.029096	-0.010015	+0.016568	-0.002579	+0.002436	-0.001058
R4 $\times R5$	+0.054919	+0.025389	+0.069790	-0.001827	-0.000035	-0.001316
R4 $\times R6$	+0.001889	+0.042596	+0.067477	-0.004585	+0.003212	+0.008817
R4	-4.020534	-17.185061	-11.483799	+2.657462	+0.314671	-3.494100
R5 $\times R5$	-0.024838	-0.018454	-0.047382	+0.004812	-0.002326	+0.002619
R5 $\times R6$	-0.020661	-0.045468	-0.016433	-0.004186	-0.011310	-0.010250
R5	+13.769822	+17.945426	-1.900994	+1.009014	+3.745591	+3.891537
R6 $\times R6$	+0.006561	+0.005658	-0.034938	+0.004571	-0.000066	+0.002573
R6	-3.430904	-2.084197	+16.096012	-1.967351	+0.262324	-1.034487
$\sum_{i=R1\times R1}^{R6}$	$F_x Equation$	$F_y Equation$	$F_z Equation$	$M_x Equation$	$M_y Equation$	$M_z Equation$

Chapter 6

Longitudinal and Lateral Derivatives

In this chapter, the results obtained in the study of both models in the wind tunnel, CFD-XFLR5 software are presented, the Longitudinal and Lateral aerodynamic derivatives are presented as well as a detailed quantitative and qualitative discussion of the results.

6.1 Test Aircraft

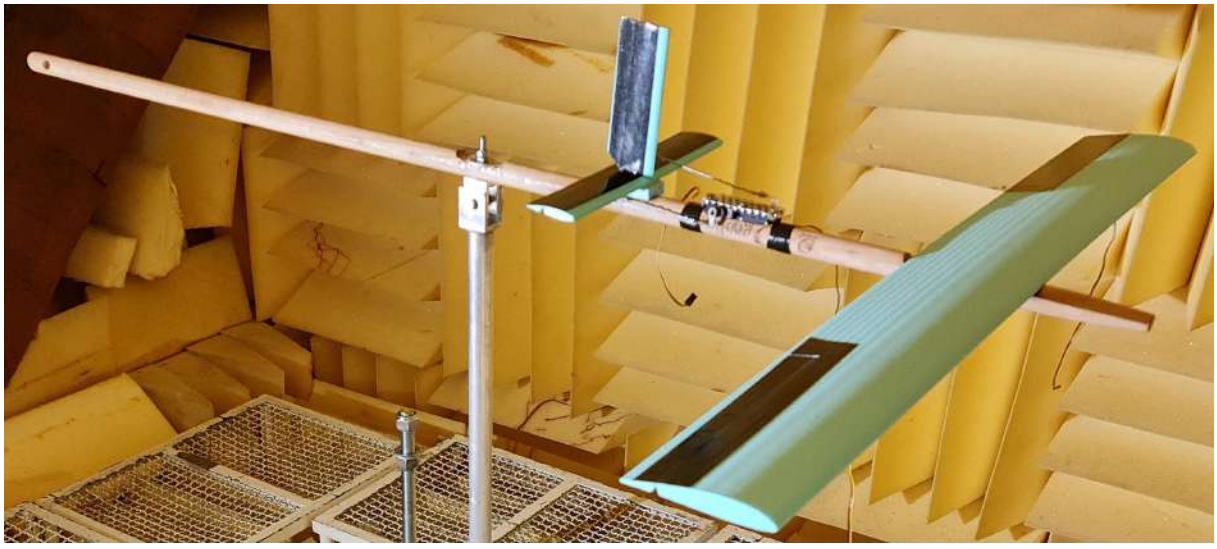

Figure 6.1: Real Test Aircraft Geometry and Mass Distribution

The test aircraft design and construction process is described and presented in the previous chapter **4.1** and **4.2** respectively, here the numerical and quantitative details of the test aircraft will be presented, as well as the results obtained.

In Figure 6.2 we can see the final result of the aircraft 3D model UAV fixed wing. Constructed from the real model that its possible to see in figure 6.1, respecting the detail of all measures and areas.

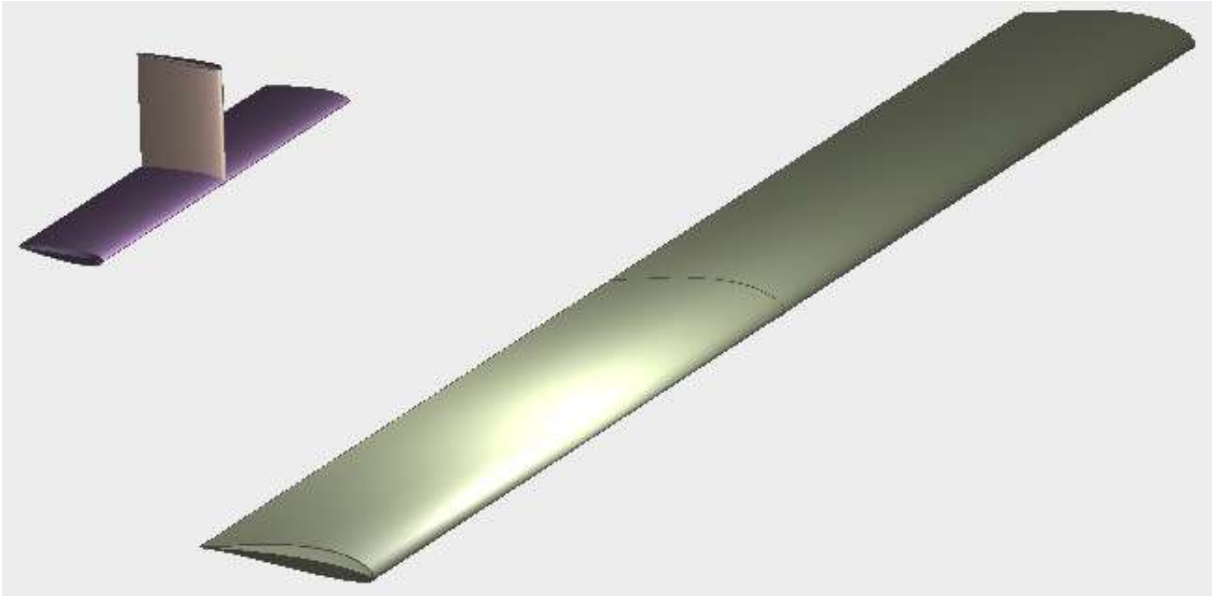

Figure 6.2: CFD Test Aircraft Model

6.1.1 Test Aircraft Geometry

The airfoil used for the wing was the ”SD 7062”, pictured in Figure 6.3, is a wing that is applied in UAV that has capability of modification for a variety of applications, it is a highly suitable airfoil for low Reynolds numbers that will be the case for the research development of this thesis.

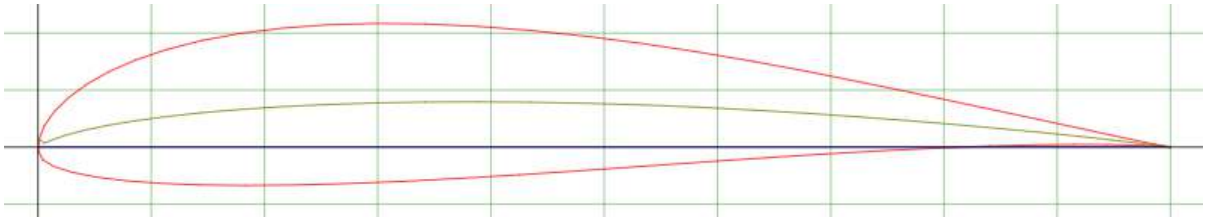

Figure 6.3: Profile SD 7062

For the tail wing, the most appropriate airfoil was the ”NACA 0015” represented in the Figure 6.4, which meets the essential conditions for actuation in low Reynolds numbers.

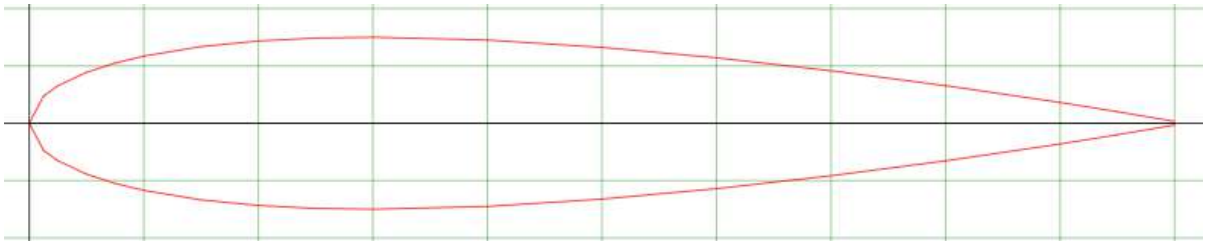

Figure 6.4: Profile NACA 0015

NACA profiles are airfoils for aircraft wings developed by the National Advisory Committee for Aeronautics (NACA, USA). This is the most famous profile series used in aircraft construction [32].

The shape of NACA profiles is described by a series of numbers after the word "NACA". The numbers from this series can then be entered into equations to accurately generate the wing section (its profile) and determine its properties. All dimensions in % are understood to be % of the chord length, this chord being the straight line connecting the leading edge and trailing edge, unless otherwise specified [33].

Using the "SD 7062" airfoil for the main wing, the following wings are built in XFLR5, and for the tail wing and fin "NACA 0015", with a small negative angle to make the stability airplane workout. The present aircraft was specially designed for this thesis, taking into account the inertia of the servomechanisms as well as the distances that allowed its full stability and best possible performance, a slight inclination of $-0.02rad$ was also incorporated in the rear stabilizer to maximize the Longitudinal stability as well as all its effect on the pitch moment, so the weight was also portrayed to assimilate as much as possible to a UAV with a $1m$ wingspan.

6.1.2 Test Aircraft Input Values for Calculations

The small UAV fixed wing used for research has a mass of 1.200 kg and a wingspan of 1 m, and it was created specially for this case of study, in Table 6.1 to 6.4 we can see the output aircraft characteristics and also the air properties, the Inertia values presented in the Table 6.1 were calculated in the XFLR5.

Table 6.1: Inertia Aircraft Table

Values Test Aircraft	
Wing Span	1 m
Wing Area	0.125 m^2
Root Chord	0.125 m
Aspect Ratio	8
I_x	0.05516 $Kg.m^2$
I_y	0.04487 $Kg.m^2$
I_z	0.09962 $Kg.m^2$
I_{xy}	0.00225 $Kg.m^2$

Analyzing the dynamics of rotational flight requires knowledge of the aircraft moments of inertia. A common method for experimental determination of moments of inertia is swinging an aircraft on a pendulum. The moment of inertia about each axis is determined individually by positioning the axis of interest parallel to the axis of rotation of the pendulum. For large scale aircraft, a compound pendulum is used to calculate the moments of inertia about the roll and pitch axes, I_x and I_y, as well as the product of inertia, I_{xz}. Due to the size and handling difficulties of a large aircraft, a bifilar torsional pendulum is used to measure the moment of inertia about the yaw axis, I_z. The moment of inertia of the pendulum about the axis of rotation can be determined from geometry, mass and the period of the system for each pendulum type.

Table 6.2: Test Aircraft Values

Values Test Aircraft	
UAV Mass	1.200 Kg
CoG$_x$	0.04671 m
CoG$_y$	0.0000 m
CoG$_z$	0.007381 m

The known moment of inertia of the pendulum apparatus is then subtracted from the moment of inertia of the complete system resulting in a measurement of the moment of inertia of the aircraft about the pendulum axis of rotation. The moment of inertia about the parallel axis passing through the aircraft center of gravity can finally be determined using the parallel axis theorem. For small-scale UAVs where it is possible to position the aircraft sideways, all moments of inertia can be determined using a single type of pendulum. After measurement of aircraft inertial properties and geometry, the Vortex Lattice Method (VLM) was used to obtain a preliminary model of the aircraft dynamics. As shown in next Chapter, parameter estimation from flight test data simulation will be used for identification of a useful and accurate flight dynamics model, VLM will be used to supplement the information gained from the flight test data simulation. Additionally, flight test design benefits from knowledge of the aircraft dynamic modes for design of control inputs.

Table 6.3: Reference Values - Test Aircraft

Test Aircraft	
Velocity	10 m/s
Angle of Attack	0 $degrees$

The XFLR5 software, was used to develop preliminary estimates of the aircraft dynamics, VLM was used to provide estimates of the aircraft dynamic modes. Specifically, its stability analysis capabilities were used to determine estimates of the linear stability and control derivatives. Only the stability derivatives were used for analysis, however, because VLM typically overestimates the control derivatives. When control surfaces are detected, viscous effects not modeled in VLM become significant causing over-prediction of control authority. The stability analysis in XFLR5 also provides the linearized longitudinal and lateral-directional state matrices which will be used to provide a preliminary estimate of the dynamic modes of the projected aircraft.

Table 6.4: Air Properties - Test Aircraft

Test Aircraft	
Density	1.225 kg/m^3
Viscosity	1.51*10^{-5} m$^2/s$

6.1.3 Test Aircraft Results

This section is divided into two subsections, the XFLR5 subsection where the qualitative results obtained in XFLR5 are commented, and the wind tunnel subsection, where the results obtained in the wind tunnel are qualitatively commented as well.

XFLR5

First, we analyse the airfoil characteristics using XFLR5 viscous analyses Real Fluid, in Figures 6.7 to 6.10, we can see the final aircraft 3D model in which inertia loads were added to the model for a better representation, closer to reality, to take into account the presence of the minimum fuselage that provides the union between the main wing and the tail wing, so the results are closer to the real test model with less variation in the aerodynamic derivatives to be calculated, from the results obtained in the XFLR5 in relation with wind tunnel results.

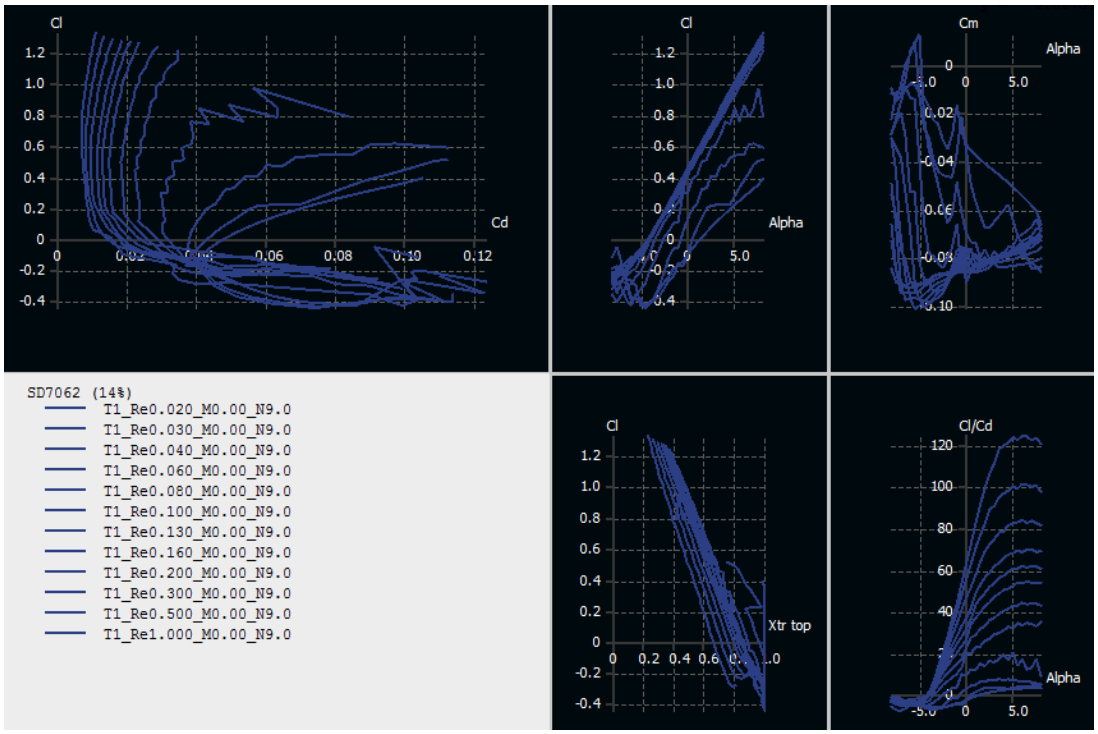

Figure 6.5: Graphics Foil in 2D for SD 7062 Analysis relative to Test Aircraft

After successfully analyzing the main wing, the tail wing was added, which gives the aircraft longitudinal stability, controlling its balance and weight distribution for the different angles of attack. This analysis is extremely important because in this way we can represent a model and report its behavior creating similarities with the real environment. The analysis was carried out for an viscous fluid, that is, a real fluid that confers characteristics of a viscosity, simulating the real environment that allows the geometric and aerodynamic characteristics of the supporting profile to be portrayed in greater detail. The analyses with the main wing and also the tail wing, that completes the longitudinal stability, both were analysed in XFLR5, working together as in a real aircraft. In Figure 6.5 and 6.6, we can see two representative

lines, the pink line representing the tail wing the longitudinal stabilizer, and the blue line representing main wing, also is illustrated all the results that was obtained by the numerical analysis in XFLR5.

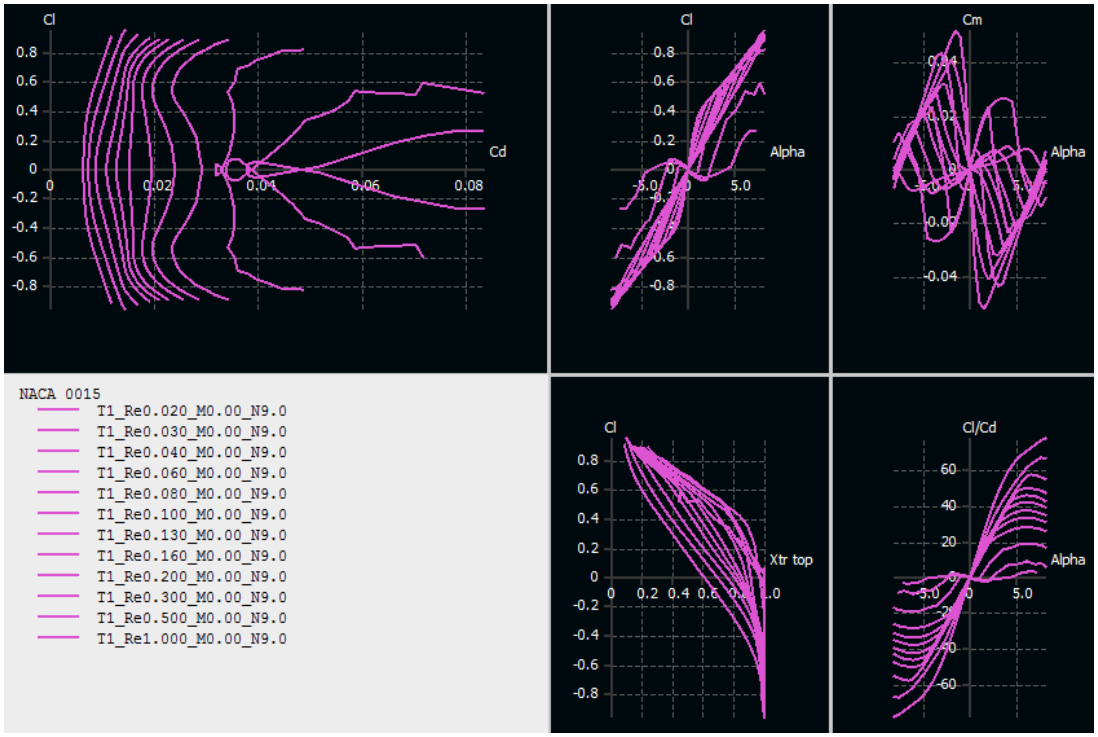

Figure 6.6: Graphics Foil in 2D for NACA 0015 Analysis relative to Test Aircraft

The following results were obtained for the distribution of the Pressure Coefficient C_p along the surface of the supporting wings, in which the red represents the Pressure Coefficient with the highest value, positive pressure coefficient which implies value above atmospheric pressure and the blue represents the value of the lowest Pressure Coefficient, negative pressure coefficient which implies value below atmospheric pressure, in the attached Figures 6.7 to 6.10 it is only possible to observe the upper part of the wings because I consider it to be the most important part of an airfoil for the production of lift, and due to this high contribution to generate lift, it is the part of the supporting surface where more will be performed study work and its specificity, the pressure coefficients distributions are represented in the following Figures 6.7 to 6.10.

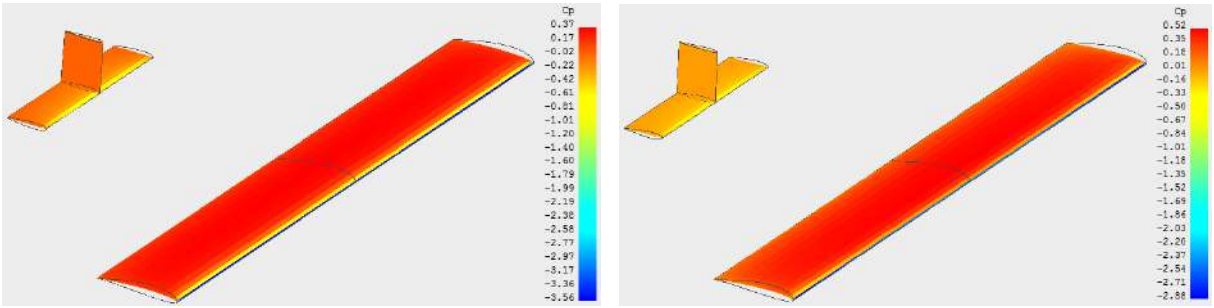

(a) $\alpha = -2°$ (b) $\alpha = 0°$

Figure 6.7: C_p Distribution for Different Angles of Attack $\alpha = -2°$ and $\alpha = 0°$

It should be noted throughout the process that the greater the angle of attack, the lower the pressure coefficient on the upper surface of the airfoil, since the analysis was performed with viscous fluid, in Real Fluid due to an angle of attack increase, imply that the ”micro turbulence” inside the boundary layer close to the airfoil upper surface will increase, until the point that the boundary layer of the flow detaches from the upper surface of the airfoil and the body becomes in a non-fuselated body, due to the excessive increase in the angle of attack and, consequently, the separation of the boundary layer from the upper surface of the airfoil occurs, creating stall, but since this analysis and study was performed to small angles of attack $-2° < \alpha < 3°$, we will not have boundary layer separation. **It is very important to emphasize that this analysis of the UAV was carried out in viscous fluid analysis, in what is called Real Fluid**, in Perfect Fluid inviscid fluid it would be different since we never experience boundary layer separation and we will always have zero drag as long as the body is closed.

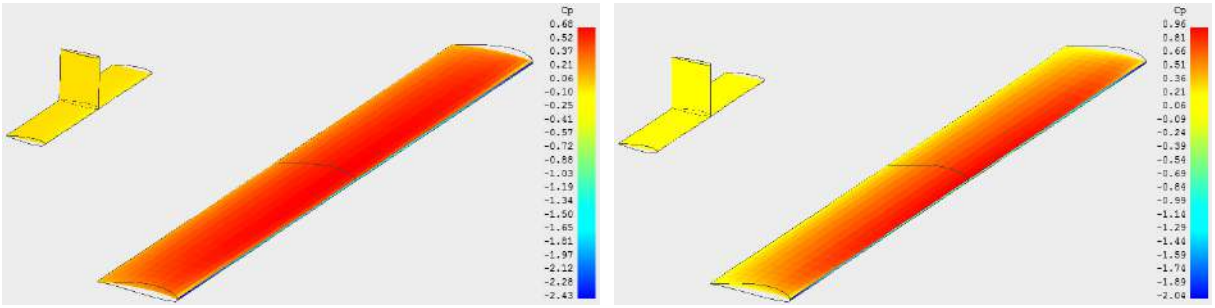

(a) $\alpha = 1.5°$ (b) $\alpha = 3°$

Figure 6.8: C_p Distribution for Different Angles of Attack $\alpha = 1.5°$ and $\alpha = 3°$

It is important to point out that all the calculations of the present thesis was carried out for small angles of attack between the values $-2° < \alpha < 3°$ to avoid any kind of separation of the boundary layer from the wing surface of the profile, and thus obtain the best possible results, however, we present the values up to 11º just to visualize the differences in the pressure coefficient on the airfoil surface.

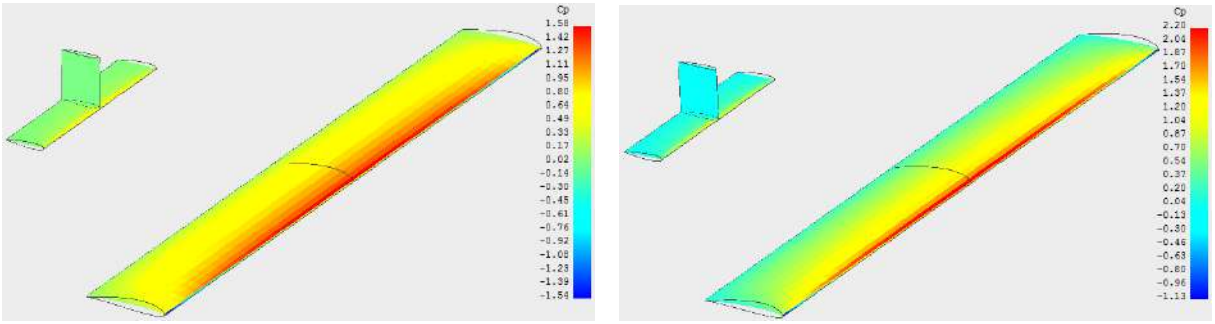

(a) $\alpha = 5°$ (b) $\alpha = 7°$

Figure 6.9: C_p Distribution for Different Angles of Attack $\alpha = 5°$ and $\alpha = 7°$

However, for a better understanding of the dynamics surrounding the surfaces of the model, images of the variation of C_p with α for larger angles of attack were added in Figure 6.9 the results of C_p are presented for $\alpha = 5°$ and $\alpha = 7°$ respectively, and in Figure 6.10 for $\alpha = 9°$ and $\alpha = 11°$, so we have a

better understanding of the behavior of the Pressure Coefficient C_p for higher Angles of Attack α.

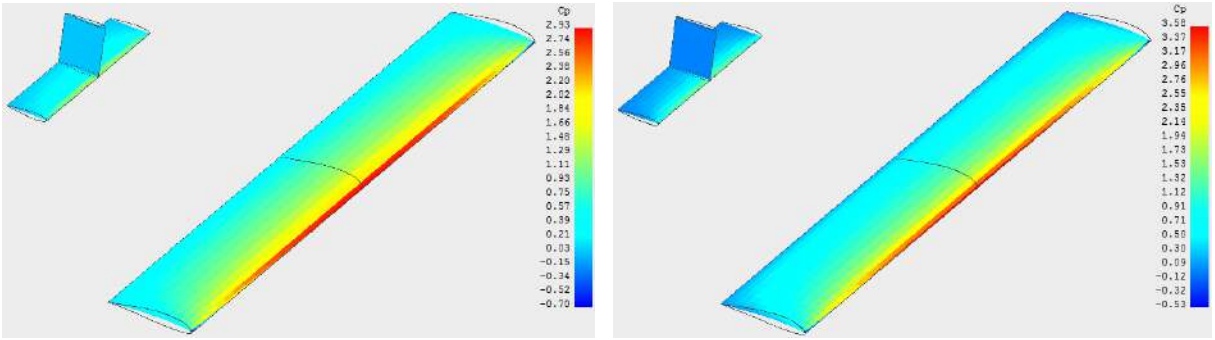

(a) $\alpha = 9°$ (b) $\alpha = 11°$

Figure 6.10: C_p Distribution for Different Angles of Attack $\alpha = 9°$ and $\alpha = 11°$

In the following graphs present in Figure 6.11 we can observe the variations of the different aerodynamic coefficients, with the variation of the angle of attack between $-2° < \alpha < 11°$.

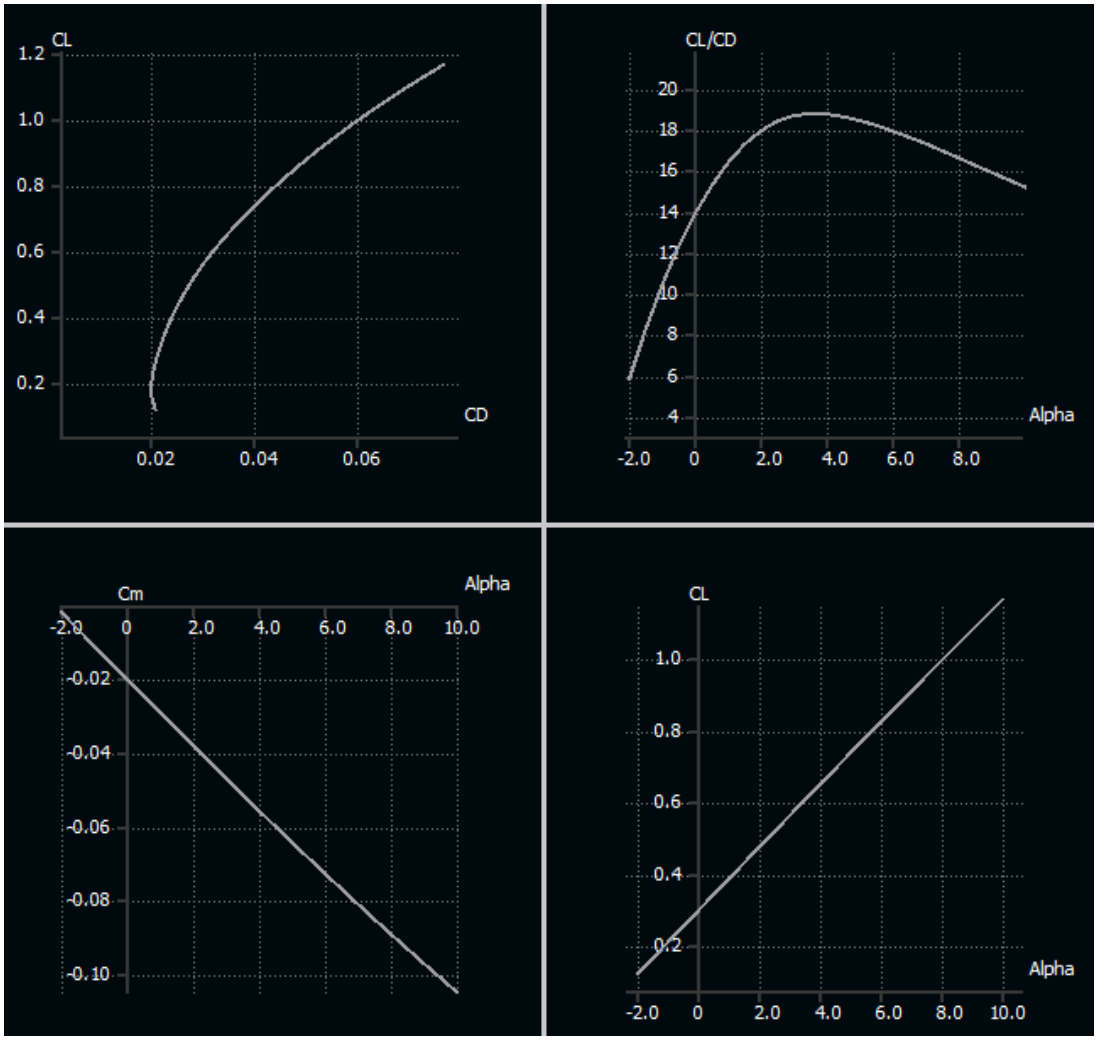

Figure 6.11: 3D Aerodynamic Coefficients Graphics C_L ,C_D, C_m, with variation of $-2° < \alpha < 11°$

Wind Tunnel

In this chapter, the process of collecting data from the experiment is presented, in order to obtain the results with the greatest possible consistency. In the following Figure 6.12 it is possible to observe the installed set up, the aircraft model under analysis as well as the force balance fixed in the wind tunnel.

Figure 6.12: Test Aircraft Geometry and Inertia Distribution

In this experiment, the forces are being measured with certainty at the base of the balance, precisely in each of the bars, and after the calibration process, the axial force equations of each bar were calculated in order to interpret their interaction, thus calculating forces measured at the base of the balance. Therefore, it is not necessary to propagate moments, as the forces measured at the base of the scale due to the forces applied to the aircraft are measured as a subtraction between the value measured in the sensors of the scale and the reference values (values measured without flow, tunnel of wind off), as the values collected is the difference between the final value, with flow, subtracting the reference value, and the result is the force acting on the aircraft.

It is only necessary to estimate the value of C_D through empirical formulas, because it is not possible to calculate the C_D on the balance, it is a value that will have to be approximately calculated.

This is just an example of the observed reference values, reference values were always observed before starting the wind tunnel, later, an arithmetic average was calculated due to the oscillations observed in the figure 6.13, to determine the average reference value , to later be subtracted from the average value of the results obtained with the wind tunnel in operation.

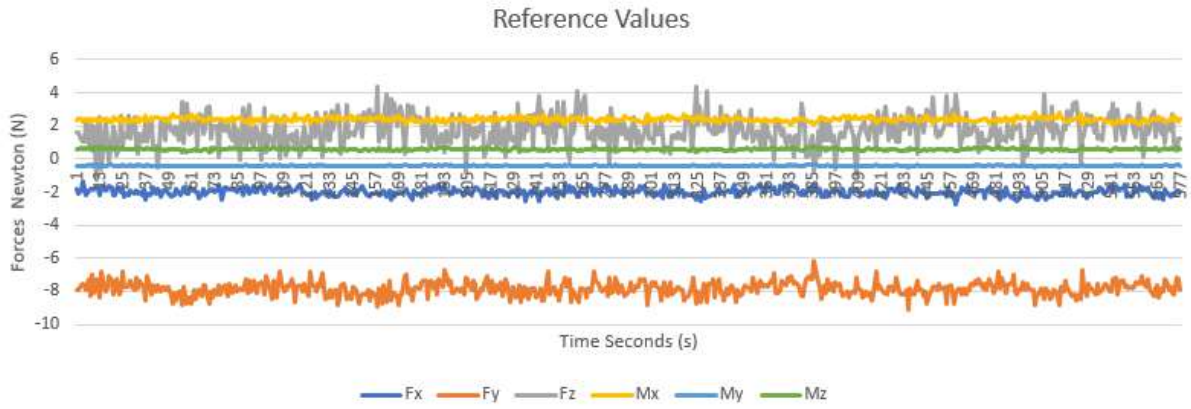

Figure 6.13: Reference Values for Zero Speed in Wind Tunnel

As previously mentioned, the average values of the observed readings were calculated for each of the measured forces, with the action of the wind tunnel, it is possible to observe the results obtained in the Table 6.5.

Table 6.5: Test Aircraft - Mean Values for Different Velocities

	$F_x(N)$	$F_y(N)$	$F_z(N)$	$M_x(N.m)$	$M_y(N.m)$	$M_z(N.m)$
Reference Value	-1.9914426	-7.8532205	1.7368939	2.3938353	-0.4106173	0.5910726
6.3 m/s	-2.4930362	-5.4903101	-0.6614839	1.8437092	-0.3549904	0.8142319
10 m/s	-3.2440922	-3.7034423	-3.1889875	1.5205711	-0.2578103	1.00309
15 m/s	-3.9121159	-1.6561105	-5.3802852	0.9113611	0.0430932	0.8452989

Subsequently, the difference between the value measured by the reference value was calculated, this difference is the correct value of the forces read on the scale for the different flight configurations.

Afterwards, it is necessary to calculate the Aerodynamic Lift and Pitch Coefficients of the respective forces.

$$C_L = \frac{L}{\frac{1}{2}\rho S V^2} \tag{6.1}$$

$$C_m = \frac{M}{\frac{1}{2}\rho S \bar{c} V^2} \tag{6.2}$$

To calculate the Drag Coefficient, it was necessary to use empirical expressions taking into account the 2 dimensions Drag Coefficient (2D) and 3 dimensions Drag Coefficient (3D),

Table 6.6: Test Aircraft - Aerodynamic Coefficients From Wind Tunnel

Velocity	C_L	C_m
6.3 m/s	0.313257517	-0.058124423
10 m/s	0.643380434	-0.15966772
15 m/s	0.929590744	-0.474081172

$$C_{D_{3D}} = C_{D_{2D}}^{Friction} + C_{D_{2D}}^{Pressure} + C_{D_{3D}}^{InducedDrag} \tag{6.3}$$

Admitting pressure gradient equal zero, $C_{D_{2D}}^{Pressure} = 0.004$, elliptical circulation distribution and also leading edge transition,

$$C_{D_{3D}} = 2 \times 0.074 \times (R_e)^{-0.2} + 0.004 + \frac{C_L^2}{\pi \times 8} \tag{6.4}$$

Using the appropriate empirical formulas it is possible to calculate the Reynolds Number and the Drag Coefficient, presented in the following Table 6.7,

Table 6.7: Test Aircraft - Aerodynamic Coefficients

Velocity	C_L	C_m	R_e	C_D
6.3 m/s	0.313257517	-0.058124423	52152.31788	0.024762516
10 m/s	0.643380434	-0.15966772	82781.45695	0.035840129
15 m/s	0.929590744	-0.474081172	124172.1854	0.052555835

To finally be able to build the graph to determine their corresponding aerodynamic derivatives.

Velocity (m/s)	CD
6.3	0.024762516
10	0.035840129
15	0.052555835

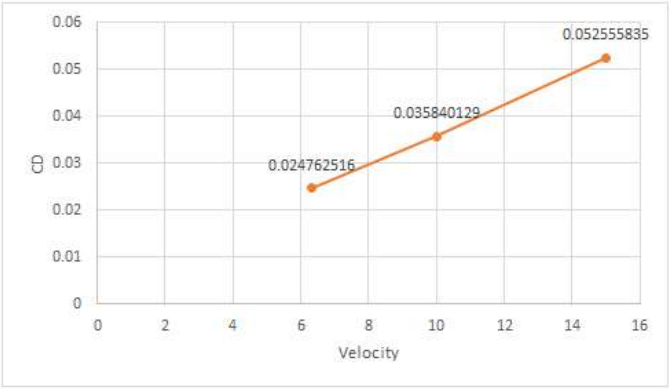

Figure 6.14: C_{D_u}

Velocity (m/s)	CL
6.3	0.313257517
10	0.643380434
15	0.929590744

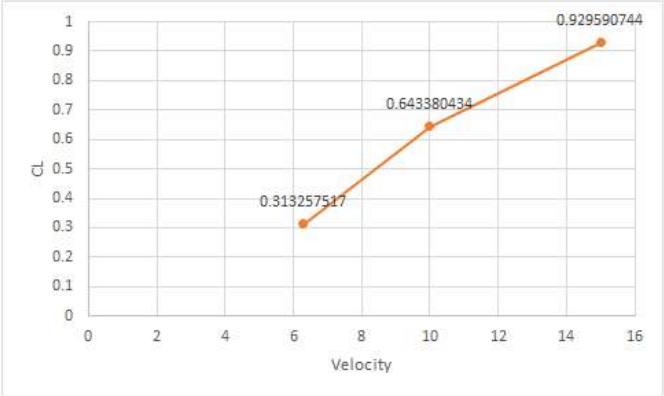

Figure 6.15: C_{L_u}

Velocity (m/s)	Cm
6.3	-0.058124423
10	-0.15966772
15	-0.474081172

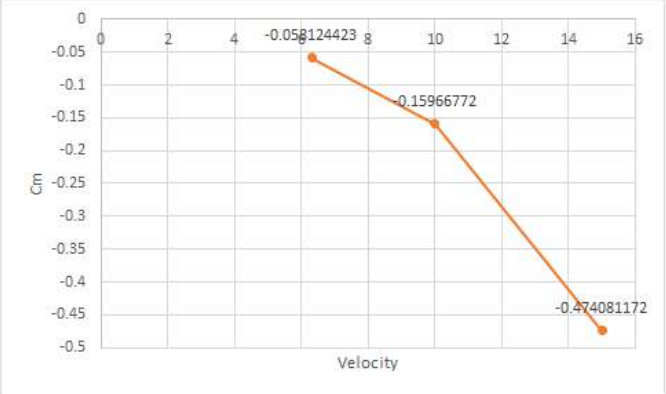

Figure 6.16: C_{m_u}

This is just an example for 1 case, this process repeats for all the aerodynamic derivatives and stability derivative that will be presented and compared all in the next Chapter 6.1.4.

6.1.4 Test Aircraft Discussion of Numerical and Qualitative Model Analysis

XFLR5

Table 6.8: Stability Derivatives Test Aircraft - XFLR5

Longitudinal Derivatives				Lateral Derivatives			
Dimensional		Non-dimensional		Dimensional		Non-dimensional	
X_u	0.0020	C_{X_u}	0.0026	Y_v	-0.0027	C_{Y_β}	-0.0036
X_w	0.2274	C_{X_α}	0.2970	Y_p	-0.0004	C_{Y_p}	-0.0010
X_q	0.0037	C_{X_q}	0.0786	Y_r	0.0011	C_{Y_r}	0.0029
Z_u	0	C_{Z_u}	0	L_v	-0.0005	C_{L_β}	-0.0007
Z_w	-0.0926	C_{Z_α}	-0.1210	L_p	-0.0051	C_{L_p}	-0.0135
Z_q	-0.0037	C_{Z_q}	-0.0786	L_r	0.0001	C_{L_r}	0.0004
M_u	8.27E-6	C_{M_u}	8.65E-5	N_v	0.0011	C_{N_β}	0.0014
M_w	-0.0008	C_{M_α}	-0.0091	N_p	0.0001	C_{N_p}	0.0004
M_q	-0.0015	C_{M_q}	-0.2516	N_r	-0.0004	C_{N_r}	-0.0011

In previous Table 6.8 we can see the resume of all the result obtained in this study, in Appendix A.1, it´s possible to see the support calculations and also the table data taken from XFLR5.

We obtain all the Non-Dimensional derivatives values with the u and α using the "Finite Difference" method to better estimate them, and for the Non-Dimensional derivatives values with the q, p and r we use analytical equations to better estimate them. Also is necessary to say that we use the $\alpha_0 = 0$ as the angle of reference, and the $u_0 = 10m/s$, as the velocity reference, making the small variances around this values, it´s all detailed explained in Appendix A.1. The results of the experimental model are very satisfied and close with what is expected, the fly conditions are represented in chapter 6.1.2.

Comparing Table 6.8 with Table 6.9 we obtain very similar values, comparing the XFLR5 results and Wind Tunnel results, X_u and C_{X_u} are practically the same values however, with opposite signals, probably due to the signals convention used, but the results are really well approximated, Y_p and C_{Y_p} just a small difference probably due to rounding, M_w and C_{M_α} we obtain a difference in one decimal place, but with the same numbers, that´s excellent results.

All the derivatives in order a q, p and r are the same values, since we use the same analytical method to calculate them.

Since we use different methods, XFLR5 and Wind Tunnel, to estimate the aerodynamic derivatives, and in the end we obtain really well approximated values, its a case to say that all the experience where very successful, different model collectors and in the end practically the same results.

Wind Tunnel

Table 6.9: Stability Derivatives Test Aircraft - Wind Tunnel

Longitudinal Derivatives				Lateral Derivatives			
Dimensional		Non-dimensional		Dimensional		Non-dimensional	
X_u	-0.0024	C_{X_u}	-0.0032	Y_v	-0.0069	C_{Y_β}	-0.0091
X_w	0.6982	C_{X_α}	0.9120	Y_p	N/A	C_{Y_p}	N/A
X_q	N/A	C_{X_q}	N/A	Y_r	N/A	C_{Y_r}	N/A
Z_u	-0.0542	C_{Z_u}	-0.0708	L_v	-0.0294	C_{L_β}	-0.0385
Z_w	-0.3565	C_{Z_α}	-0.4657	L_p	N/A	C_{L_p}	N/A
Z_q	N/A	C_{Z_q}	N/A	L_r	N/A	C_{L_r}	N/A
M_u	-0.0045	C_{M_u}	-0.0478	N_v	-0.0023	C_{N_β}	-0.0030
M_w	-0.0087	C_{M_α}	-0.0916	N_p	N/A	C_{N_p}	N/A
M_q	N/A	C_{M_q}	N/A	N_r	N/A	C_{N_r}	N/A

N/A means Not Applicable, just for Wind Tunnel calculation procedure.

In previous Table 6.9 we can see the resume of all the result obtained in this study, in Appendix B.1, it´s possible to see the support calculations.

We obtain all the Non-Dimensional derivatives values with the u and α using the ”Finite Difference” method to better estimate them, and for the Non-Dimensional derivatives values with the q we use analytical equations to better estimate them. Also is necessary to say that we use the $\alpha_0 = 0$ as the angle of reference, and the $u_0 = 10m/s$ as the velocity reference, making the small variances around this values, the fly conditions are represented in chapter 6.1.2, it´s all detailed explained in Appendix B.1. The results of the experimental model are very satisfied and close with what is expected.

Comparing Table 6.8 with Table 6.9 we obtain very similar values, comparing the XFLR5 results and Wind Tunnel results, X_u and C_{X_u} are practically the same values however, with opposite signals, probably due to the signals convention used, but the results are really well approximated, Y_p and C_{Y_p} just a small difference probably due to rounding, M_w and C_{M_α} we obtain a difference in one decimal place, but with the same numbers.

All the derivatives in order a q p and r are the same values, since we use the same analytical method to calculate them.

Since we use different methods, XFLR5 and Wind Tunnel, to estimate the aerodynamic derivatives, and in the end we obtain really well approximated values, its a case to say that all the experience where very successful, different model collectors and in the end practically the same results.

Control Derivatives

Table 6.10: Control Derivatives Test Aircraft - XFLR5 and Wind Tunnel

XFLR5 Control Derivatives				Wind Tunnel Control Derivatives			
Dimensional		Non-dimensional		Dimensional		Non-dimensional	
X_{δ_e}	-0.0008	$C_{X_{\delta_e}}$	-0.0001	X_{δ_e}	-0.0018	$C_{X_{\delta_e}}$	-0.0002
Y_{δ_r}	0.0084	$C_{Y_{\delta_r}}$	0.0011	Y_{δ_r}	0.0199	$C_{Y_{\delta_r}}$	0.0026
X_{δ_a}	0	$C_{X_{\delta_a}}$	0	X_{δ_a}	0.0022	$C_{X_{\delta_a}}$	0.0003
Z_{δ_e}	-0.0568	$C_{Z_{\delta_e}}$	-0.0074	Z_{δ_e}	-0.0510	$C_{Z_{\delta_e}}$	-0.0067
L_{δ_r}	0	$C_{L_{\delta_r}}$	0	L_{δ_r}	0.0041	$C_{L_{\delta_r}}$	0.0005
Z_{δ_a}	0	$C_{Z_{\delta_a}}$	0	Z_{δ_a}	0.0083	$C_{Z_{\delta_a}}$	0.0011
M_{δ_e}	-0.0201	$C_{M_{\delta_e}}$	-0.0209	M_{δ_e}	0.0009	$C_{M_{\delta_e}}$	0.0010
N_{δ_r}	-0.0004	$C_{N_{\delta_r}}$	-0.0004	N_{δ_r}	-0.0004	$C_{N_{\delta_r}}$	-0.0004
M_{δ_a}	0	$C_{M_{\delta_a}}$	0	M_{δ_a}	-0.0004	$C_{M_{\delta_a}}$	-0.0004

In previous Table 6.10 we can see the resume of all the result obtained in this study, in Appendix A.3 and Appendix B.3 it´s possible to see the support calculations in excel and also the table data taken from XFLR5. It´s necessary to say that we use the $\alpha_0 = 0$ as the angle of reference, and the $u_0 = 10m/s$ as the velocity reference, the fly conditions are represented in chapter 6.1.2. The signal system used for the orientation and characterization of the positive and negative directions of the ailerons, elevator and fin, is represented in Figure 3.1. Comparing values from Table 6.10, obtained from XFLR5 and Wind Tunnel, we can see that, all the control derivatives obtained by the δ_e variation, are practically the same, very similar, with just a small variance, that show that the dimensions and characteristics were completely recreated from XFLR5 to Wind Tunnel. The precision obtained from the results show that. In δ_r variation we observe a small difference, but practically the same values, as observe in Table 6.10. In δ_a we get zero in XFLR5, because they don't have variation, that explain the zero result. In Figure 6.17 it´s possible to observe the δ_a variation in XFLR5.

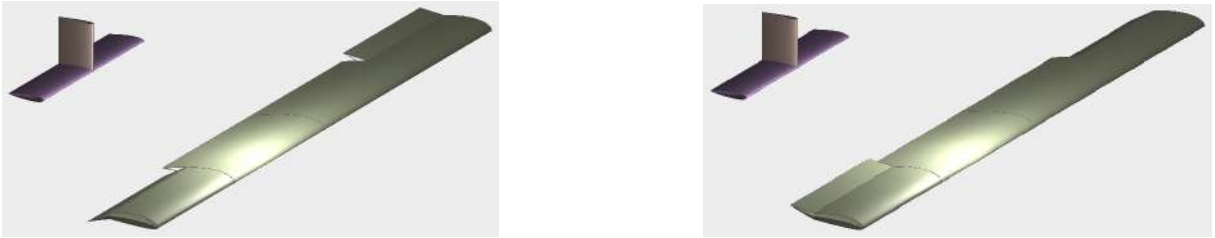

(a) Anti-Clock Rotation

(b) Clock Rotation

Figure 6.17: Test Aircraft δ_a Variation

6.2 F35 Aircraft

Figure 6.18: F35 Aircraft Wind Tunnel Assembly

The F35 aircraft design and construction process was described and presented in the previous chapter **4.3** and **4.4** respectively, here the numerical and quantitative details of the test aircraft will be presented, as well as the estimated aerodynamic derivatives obtained.

6.2.1 F35 Aircraft Geometry

In this section, the geometry and specifics of the Model F35 Aircraft will be described, images will be presented with the constructive details of the aircraft as well as its front, rear, left, right and bottom views. In Figure 6.19 a clear perspective of the right side view F35 Aircraft is presented.

Figure 6.19: F35 Aircraft Cruise Flight

As the F35 Aircraft Model, it is a model built on symmetrical profiles specially designed for this master's thesis, it is not possible to have a defined geometry for the aircraft's wings, it can only be guaranteed that it is a profile model symmetrical wing, with a geometric specificity for highly maneuverable aircraft.

In Figure 6.20 it is possible to have a clear view of the front views F35 Aircraft, as well as its air intakes to feed the engines, it´s aerodynamics of a supersonic aircraft adapted to small Reynolds numbers Aircraft.

(a) Front View (b) Low View

Figure 6.20: F35 Aircraft

The fixed-wing aircraft consists of a fuselage and two fully symmetrical wings, which give it high maneuverability, as well as high support, compared to the real model, the area of both wings was increased proportionally to guarantee the generation of lift since this model fly at low speeds so it needs more area to generate enough lift and fly.

In Figure 6.21, it is possible to observe the straight alignment of the two wings, as well as the same angle for the vertical stabilizer on both sides, to note its high symmetry.

Figure 6.21: F35 Aircraft Back View

This chapter describes the geometry of the F 35 aircraft, which later on will be calculated in quantitative terms, its stability derivatives, as well as its response characteristics in terms of forces applied to the aircraft. In the end, it is intended to have a description and prediction of its behavior in flight, with the assigned geometry, allowing a greater accuracy in the prediction of its behavior in flight.

6.2.2 F35 Aircraft Input Values for Calculations

In this section, the measured and characterized values of the F35 Test Aircraft will be presented. For the calculations, in Table 6.11, it is possible to observe the characteristic values of the air properties, representing the best possible reality taking into account the place where the tests were carried out as well as the height relative to sea level.

Table 6.11: Air Properties - F35 Aircraft

F35 Test Aircraft	
Density	1.225 kg/m^3
Viscosity	1.51*10^{-5} m$^2/s$

In the Table 6.12 it is possible to observe the measured values characteristic of the aircraft, measured directly after the construction of the model so that the results are as realistic as possible and error-free.

Table 6.12: F35 Model Specifications

F35 Test Aircraft	
Wing Span	950 mm
Flying Weight	1.235 Kg
Wing Loading	37 $gram/dm^2$
Aspect Ratio	6.4
Wing Area	33.37 dm^2
Center of Gravity	11.5 cm from the beginning of the wing root

In the table 6.13 it is possible to observe the characteristic reference values assumed, in order to calculate the stability derivatives. Were considered these values because they are the ones that best describe the aircraft in cruise flight, so there is a better approximation in order to generate the autopilot equations, in consequence they will be insert in the analytical model of equations for small perturbations, so that, the autopilot will performs an accurate response in order to correct the altitude and stabilize the cruise flight. These equations will predict how much it will be necessary to flex the ailerons or rudder, in order to balance the flight again, and maintain cruising flight stability. The more accurate the stability derivatives are calculated, better the prediction of correction, how much it will be necessary to flex/perform the ailerons, therefore, the faster and more efficient the aircraft stabilization will be, after a small disturbance generated by the wind, or by the change in the position of masses inside the plane.

Table 6.13: Reference Values - F35 Aircraft

F35 Test Aircraft	
Velocity	10 m/s
Angle of Attack	0 $degrees$

6.2.3 F35 Aircraft Results

This section presents the wind tunnel subsection, where the results obtained in the wind tunnel are qualitatively commented.

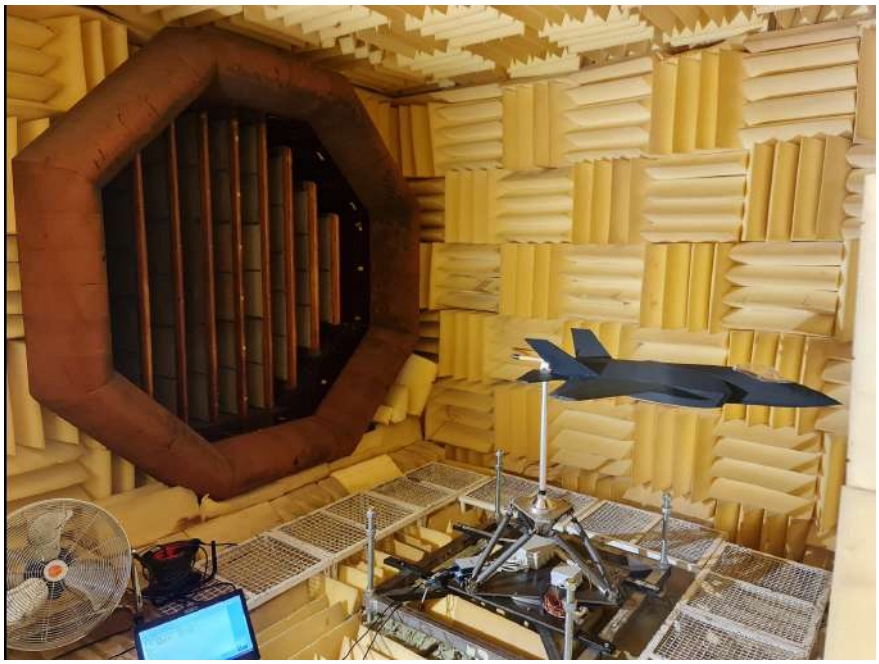

Figure 6.22: Wind Tunnel F35 Aircraft

To calculate the stability derivatives in the F35 Aircraft, the reference values observed in Figure 6.23 were used, they are the values read in the force balance only with the weight of the aircraft, with the wind tunnel turned off, so they are the average values for each one of the forces that will be subtracted from the values with the Wind Tunnel in operation that allowed to calculate the real values that are being created by the aircraft.

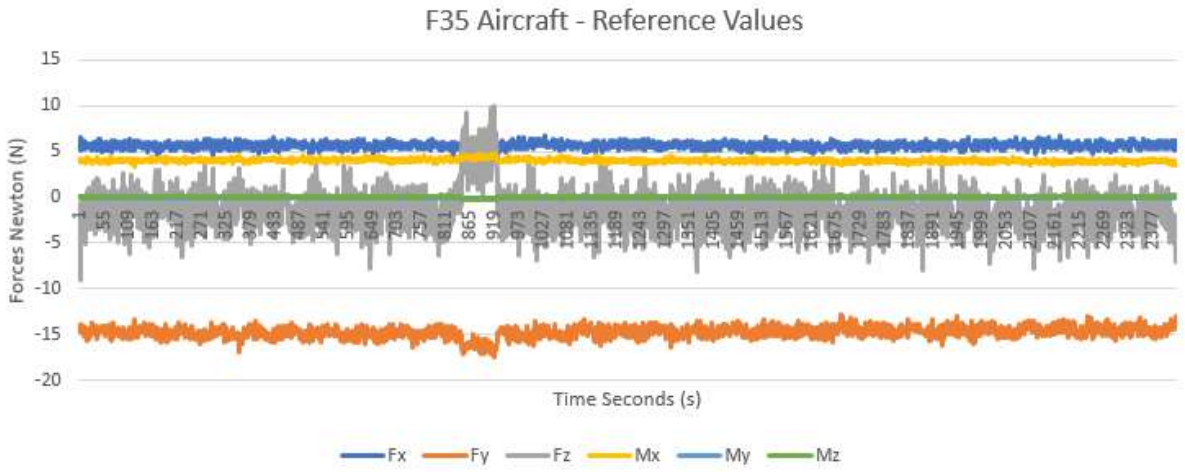

Figure 6.23: F35 Aircraft - Reference Values

Wind Tunnel

In the previous chapter of calculating the stability derivatives for ”Test Aircraft”, the values were first calculated in CFD and later we obtained their validation in the Wind Tunnel, taking advantage of this verification we can calculate with certainty the derivatives in the ”F35 Aircraft” with great certainty of the results obtained without their validation in CFD.

Figure 6.24: F35 Aircraft in Wind Tunnel

Here, we use the same process described in section 6.1.3 in the Wind Tunnel subsection. Exactly the same procedure, however without having the validation comparison previously made between the CFD and the Wind Tunnel for Test Aircraft.

In the table 6.14, the values of C_L and C_m obtained in the balance of forces are presented.

Table 6.14: F35 Aircraft - Aerodynamic Coefficients From Wind Tunnel

Velocity	C_L	C_m
6.3 m/s	0.293236093	-0.100281345
10 m/s	0.315918853	-0.081049705
15 m/s	0.334786727	-0.044046167

Using the values read on the force balance of C_L and C_m, it is possible to calculate the Reynolds number, and with these three values of aerodynamic coefficients it is possible to estimate the value of the Drag Coefficient C_D, using the same process and formulas and the same assumptions assumed in the Test Aircraft, elliptical circulation distribution, leading edge transition, pressure gradient equal to zero, and $C_{D_{2D}}^{Pressure} = 0.004$. In Table B.2 it´s possible to see the final calculated values.

This is just an example for a case, for the calculation of the aerodynamic coefficients, to later calculate the stability derivatives, this process is repeated for all the stability derivatives calculated.

Table 6.15: F35 Aircraft - Aerodynamic Coefficients

Velocity	C_L	C_m	R_e	C_D
6.3 m/s	0.293236093	-0.100281345	108476.8212	0.021982435
10 m/s	0.315918853	-0.081049705	172185.4305	0.021246957
15 m/s	0.334786727	-0.044046167	258278.1457	0.020701376

In Figure 6.25, it is possible to observe the variations of the forces according to the increase in speed of the aircraft, as well as their changes of level according to the increase of the speed, they were stabilized for two minutes to calculate an average of all the values read for a correct reading after each speed. Each color represents a force, the most relevant being the gray color that represents "F_z" and consequently the Lift, the axis system being considered that makes the "F_z" axis is positively directed towards the ground, and the more negative the value of "F_z" greater Lift is generated.

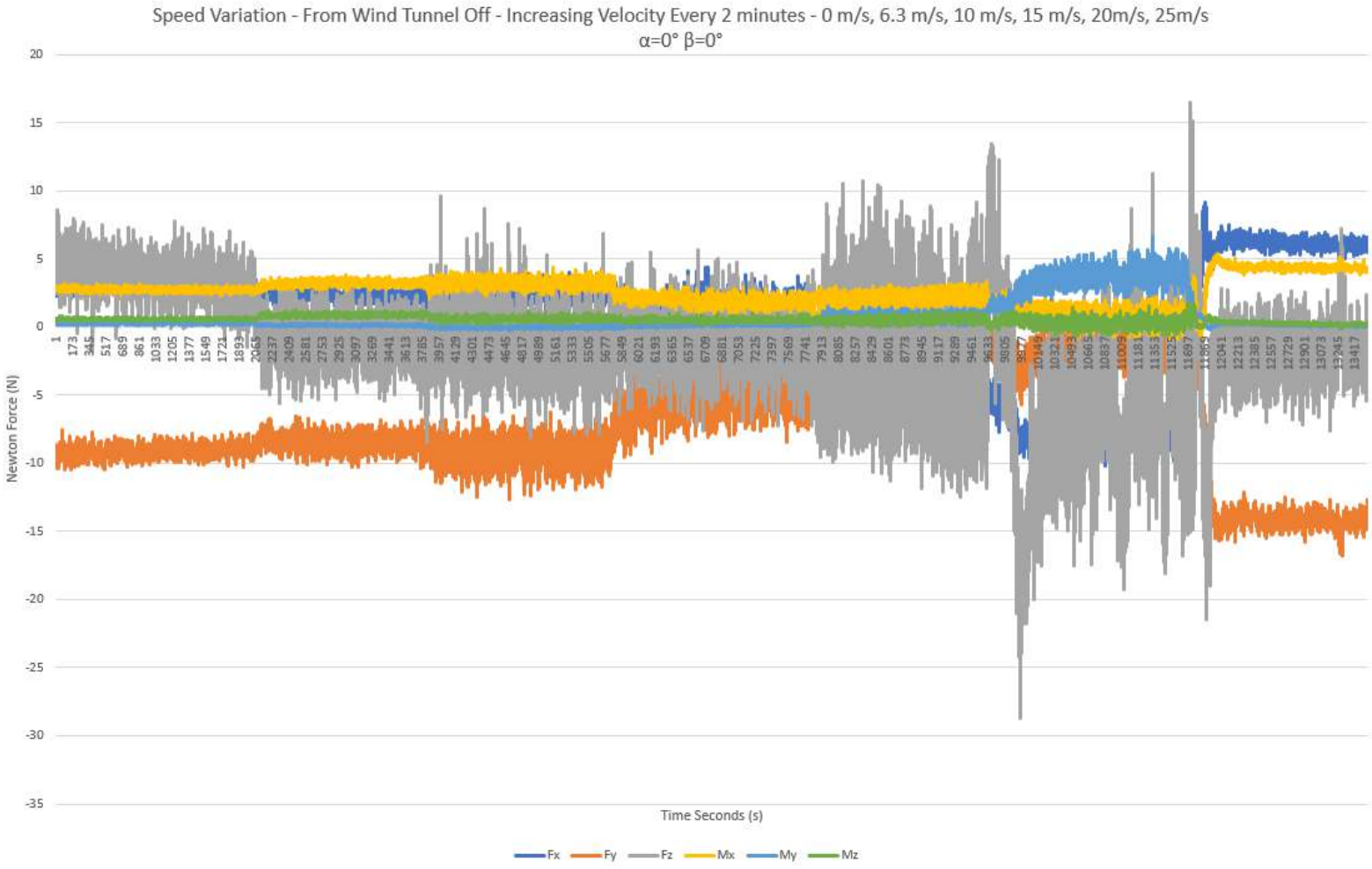

Figure 6.25: F35 Aircraft Speed Variation - 0 m/s, 6.3 m/s, 10 m/s, 15 m/s, 20m/s, 25m/s, 0 m/s

6.2.4 F35 Aircraft Discussion of Numerical and Qualitative Model Analysis

Wind Tunnel

Table 6.16: Stability Derivatives F35 Aircraft - Wind Tunnel

Longitudinal Derivatives				Lateral Derivatives			
Dimensional		Non-dimensional		Dimensional		Non-dimensional	
X_u	0.0003	C_{X_u}	0.0001	Y_v	-0.0236	C_{Y_β}	-0.0116
X_w	0.4257	C_{X_α}	0.2083	Y_p	N/A	C_{Y_p}	N/A
X_q	N/A	C_{X_q}	N/A	Y_r	N/A	C_{Y_r}	N/A
Z_u	-0.0098	C_{Z_u}	-0.0047	L_v	-0.1056	C_{L_β}	-0.0517
Z_w	-0.1249	C_{Z_α}	-0.0611	L_p	N/A	C_{L_p}	N/A
Z_q	N/A	C_{Z_q}	N/A	L_r	N/A	C_{L_r}	N/A
M_u	0.0034	C_{M_u}	0.0064	N_v	-0.0082	C_{N_β}	-0.0040
M_w	-0.0051	C_{M_α}	-0.0097	N_p	N/A	C_{N_p}	N/A
M_q	N/A	C_{M_q}	N/A	N_r	N/A	C_{N_r}	N/A

N/A means Not Applicable, just for Wind Tunnel calculation procedure.

It´s necessary to say that we use the $\alpha_0 = 0$ as the angle of reference, and the $u_0 = 10m/s$ as the velocity reference. The signal system used for the orientation and characterization of the positive and negative directions of the Forces, Moments and all the signal conventions are represented in Figure 3.1. In Appendix B.3 it´s possible to see the support calculations in excel.

After calculating the results in the XFLR5 and having them validated in the Wind Tunnel, it is clear that there is real and high confidence in the results obtained in the Wind Tunnel for the F35 Aircraft, knowing that the proximity obtained in Test Aircraft results, confirmed that the readings on the force balance are very realistic and coherent, with a high degree of accuracy. From what we can conclude that the results obtained in the wind tunnel by the F35 Aircraft were a success, the aircraft withstood the tests up to a speed of 25m/s, about 90km/h, without any damage, maintaining its aerodynamic and structural characteristics.

The results obtained in the Wind Tunnel for the F35 Aircraft, read on the balance of forces, are really within the range of expected values for this type of UAV, as well as its signs and dimensions, are really within the expected, as well as its order of magnitude. All this demonstrates that the experimental procedure was a success!

Chapter 7

Conclusions

Presents the overall conclusions and introduces future work to improve the estimations of the aerodynamic stability derivatives.

7.1 Achievements

Dear reader, If you happen to find an error in this master's thesis, GREAT, probably they exist, that means that you understand the subject, and also, that I didn't have enough time to find it.. :)

We want to make a point of saying that all these results were fully transcribed from the balance of forces and XFLR5 in full for the present master's thesis, we did not make any adjustments to look like better values, they were completely the results obtained in the readers, completely transcribed, in full. We noticed some small errors that could easily have been corrected with new readings, however, lacking the opportunity to repeat the tests, we had to assume them, repairing and highlighting the small errors, as experimental reading errors.

We actually obtained similar values, which were practically identical, and since we obtain the values from different methods, XFLR5-CFD and Wind Tunnel, and in the end, they were really close values, which is an entirely satisfactory result, considering that different reading methods were used, CFD in a virtual reading model with a virtual model, creating a real model, recreated in full to be coupled to the scale of forces and obtain results in the Wind Tunnel, are incredible results, mainly in the derivatives of control in Test Aircraft.

Just a value that is consider ridiculous, probably due to a reading error in the balance of forces, obtained the $C_L = 2$ when $\alpha = +5°$, just in one reading, we have reviewed the results over and over again and have not found the fault, probably a reading error on the scale that generate this value.

In the construction of the F35 Aircraft, in order to confirm the reading on the balance of forces, and to confirm the validity of the readings, contrary to the Test Aircraft, in the F35 Aircraft the depth rudder δ_e was flexed downwards, positive deflection as per convention, observing the expected, the C_m with negative values, however with positive slope, which demonstrates a correct reading of the balance of forces in the pitch moments.

At Test Aircraft, we are very pleased with the results, as they coincide with the predicted values when designing it, as can be seen in the Design chapter.

The major achievements of the present work was overcome, establish the necessary model for the construction of an adequate evaluation model UAV Fixed Wing. Also achieved the proposed objectives of ”Estimation of Aerodynamic and Control Derivatives of Small Fixed-Wing Aircraft using Numerical Simulations and Wind Tunnel Experiments”, a small introduction was made of all the formulas and concepts that have to be taken into account, the respective equations of reference to be used, as well as the construction of a model for the calculation and representation of the final supported system for the calculation of stability derivatives, all that remains is to wish that this Thesis is within the expected, fulfilling all the proposed objectives.

These two aircraft models, ”Test Aircraft” and ”F35 Aircraft”, were the first two aircraft models to be tested in the Wind Tunnel with balance of forces at Instituto Superior Técnico, and perhaps in Portugal.

7.2 Future Work

The future work will be to get the F35 Aircraft to fly because a value of 70N was read on the scale, with $\alpha = +5^{\circ}$ and the F35 Aircraft weighs 1.235Kg, approximating 12N, it is irrevocable proof that it will fly, with an EDF engine and respective servos and necessary electronic material, as well as the Test Aircraft that proved through readings and controls that it will fly too.

For an angle of attack equal to zero, we were able to generate approximately 8N, cruising speed, just increase the angle of attack a little bit to generate enough lift to fly.

This Thesis will be the first study about the ”Estimation of Aerodynamic and Control Derivatives of Small Fixed-Wing Aircraft using Numerical Simulations and Wind Tunnel Experiments”, in future it will be developed a deeper study about the different subjects that will need to take into account. During my life, it is intended to deepen the study on the calculation of stability derivatives for numerical and analytical analysis in a UAV Fixed Wing Aircraft´s, which in the future will be a necessary output background for my professional life, about the continuation of this present topic.

A analysis and calculation of the stability derivatives and control derivatives was made in wind tunnels and CFD-XFLR5, thank you Portugal.

Bibliography

[1] R. Jategaonkar. *Flight vehicle system identification: a time domain methodology,*. Virginia: American Institute of Aeronautics and Astronautics/Aerospace Press, 2^{nd} edition, 2015.

[2] J. R. Azinheira. Controlo de voo - sebenta. Instituto Superior Técnico, 2021.

[3] B. Etkin and L. D. Reid. *Dynamics of Flight: Stability and Control*. John Wiley and Sons, $3^{nd}edition$ edition, 1996.

[4] J. Oliveira. Apontamentos de estabilidade de voo. Instituto Superior Técnico, 2019.

[5] H. X. iao. A dual-euler method for solving all-attitude angles of the aircraft. *China Flight Test Establishment*, 1993.

[6] R. R. C. Javier García-Heras Carretero, Francisco Javier Sáez Nieto. Aircraft trajectory simulator using a three degrees of freedom aircraft point mass model. *Air Navigation Research Group*, 2013.

[7] R. Metha. The principles of physics. volume 11, page 378.

[8] B. M. Simmons. System identification of a nonlinear flight dynamics model for a small, fixed-wing uav. Master's thesis, Faculty of the Virginia Polytechnic Institute and State University, 2018.

[9] N. R. P. 1168. Application of parameter estimation to aircraft stability and control. Technical report, NASA, National Aeronautics and Space Administration, 1986. Richard E. Maine and Kenneth W. Iliff.

[10] R. de long and J. Mulderf. Accurate estimation of aircraft inertia characteristics from a single suspension experiment. *Delft University of Technology, Delft, the Netherlands*, 1987.

[11] B. Etkin and L. D. Reid. *Dynamics of flight: stability and control.* Wiley New York, $3^{nd}volume$ edition, 1996.

[12] E. A. Morelli and V. Klein. *Aircraft system identification: theory and practice*. VA: Sunyte Enterprises, 2^{nd} edition, 2016.

[13] P. V. D. Clinton E. Brown and J. W. Kloetzli. Measurements and analysis of the forces acting on a small aircraft flying in the upwash of a large aircraft. *HYDRONAUT1CS , INCORPORATED*, 1978.

[14] C. Bil. *Stochastic trajectory optimisation for aircraft in air combat*. researchgate, 2022.

[15] V. de Brederode. *Aerodinâmica Incompressível: Fundamentos*. IST Press, 2^{nd} edition, Junho de 2018.

[16] O. A. A. H. Ahmed EA1 *, Hafez A1 and A.-E. HM1. Modelling of a small unmanned aerial vehicle. *Advances in Robotics Automation*, 2015.

[17] D. A. Caughey. Introduction to aircraft stability and control course notes for mae 5070. Technical report, Sibley School of Mechanical Aerospace Engineering, Cornell University Ithaca, New York 14853-7501, 2011.

[18] B. A. W. *Aircraft Dynamic Stability and Response*. Elsever, 1980. ISBN 0-08-024768-7.

[19] R. Jan. *Airplane Flight Dynamics and Automatic Flight Controls*. Roskam Aviation and Engineering Corporation, second printing edition, 1979. Library of Congress Catalog Card Number: 78-31382.

[20] H. Auchter. *Brook Taylor, der mathematiker und philosoph; beiträge zur wissenschaftsgeschichte der zeit des Newton-Leibniz-streites*. Würzburg, K. Triltsch, 1937.

[21] E. C. de Oliveira. *Funções Especiais com Aplicações*. Editora Livraria da Fisica, , note = ISBN 8-588-32542-X edition.

[22] D. C. Fraser. *"On the Graphic Delineation of Interpolation Formulae"*. Journal of the Institute of Actuaries, , note = 43 (2): 235–241 edition, January 1, 1909.

[23] I. Newton. *Principia*. Lemma V, book iii edition, (1687).

[24] F. Lessman. *Finite Difference Equations*. Springer, 1992. ISBN 0-486-67260-3.

[25] W. H. Mason. "configuration aerodynamics,". *Virginia Tech*, 2009.

[26] V. Blacksburg. "about xflr5 calculations and experimental measurements,". *Presentation document*, 2009.

[27] B. Dunbar. *What Are Wind Tunnels?* National Aeronautics and Space Administration - NASA, 2018.

[28] J. B. Barlow. *Low-Speed Wind Tunnel Testing*. Wiley, 3^{nd} edition edition, 2022.

[29] A. Oliveira. *Design, Construction, Calibration and Testing of a Wind Tunnel Force Balance*. IST, 2020.

[30] N. Hall. *Force Balance*. National Aeronautics and Space Administration - NASA, 2021.

[31] L. W. Traub and C. Coffman. Efficient low-reynolds-number airfoils. *JOURNAL OF AIRCRAFT*, page 17, 2019. DOI: 10.2514/1.C035515.

[32] K. W. e. R. P. EN Jacobs. *"As características de 78 seções de aerofólio relacionadas a partir de testes no túnel de vento de densidade variável"*. NACA, 1933.

[33] J. D. A. Jr. *"Fundamentos da aerodinâmica"*. NACA, terceira ed edition. capítulo 4.

Appendix A

Excel Final Results - XFLR5

The values used as a reference to calculate the derivatives for the Test Aircraft:

Table A.1: Test Aircraft - Data From Excel - XFLR5

Variable	Reference Value
Density:	1.225 Kg/m^3
Speed:	10 m/s
Chord:	0.125 m
Areas:	0.125 m^2
Angle of attack:	0 $Degrees$

In the next pages, it´s possible to observe our excel results.

A.1 Tables - Stability Derivatives - Test Aircraft - XFLR5

Freestream speed : 10.000 m/s

alpha	Beta	CL	CDi	CDv	CD	CY	Cl	Cm	Cn	Cni	QInf	XCP
-2.000	0.000	0.121356	0.001006	0.029524	0.030530	0.000000	-0.000000	-0.001537	-0.000000	-0.000000	10.0000	0.0482
-1.500	0.000	0.165687	0.001463	0.029369	0.030832	0.000000	-0.000000	-0.006185	-0.000000	-0.000000	10.0000	0.0512
-1.000	0.000	0.210000	0.002081	0.029298	0.031379	0.000000	-0.000000	-0.010819	-0.000000	-0.000000	10.0000	0.0530
-0.500	0.000	0.254287	0.002859	0.029017	0.031876	0.000000	-0.000000	-0.015419	-0.000000	-0.000000	10.0000	0.0541
0.000	0.000	0.298542	0.003797	0.028739	0.032535	0.000000	-0.000000	-0.020000	-0.000000	-0.000000	10.0000	0.0549
0.500	0.000	0.342756	0.004893	0.028467	0.033360	0.000000	-0.000000	-0.024557	-0.000000	-0.000000	10.0000	0.0555
1.000	0.000	0.386922	0.006149	0.028196	0.034345	0.000000	-0.000000	-0.029088	-0.000000	-0.000000	10.0000	0.0560
1.500	0.000	0.431032	0.007563	0.028377	0.035939	0.000000	-0.000000	-0.033618	-0.000000	-0.000000	10.0000	0.0563
2.000	0.000	0.475080	0.009133	0.028373	0.037506	0.000000	-0.000000	-0.038107	-0.000000	-0.000000	10.0000	0.0566
2.500	0.000	0.519057	0.010860	0.028933	0.039793	0.000000	-0.000000	-0.042596	-0.000000	-0.000000	10.0000	0.0569
3.000	0.000	0.562956	0.012742	0.029095	0.041837	0.000000	-0.000000	-0.047036	-0.000000	-0.000000	10.0000	0.0571
3.500	0.000	0.606769	0.014778	0.029625	0.044403	0.000000	-0.000000	-0.051467	-0.000000	-0.000000	10.0000	0.0573
4.000	0.000	0.650490	0.016966	0.029943	0.046908	0.000000	-0.000000	-0.055855	-0.000000	-0.000000	10.0000	0.0575
4.500	0.000	0.694111	0.019305	0.030356	0.049661	0.000000	-0.000000	-0.060216	-0.000000	-0.000000	10.0000	0.0576
5.000	0.000	0.737624	0.021794	0.030887	0.052681	0.000000	-0.000000	-0.064549	-0.000000	-0.000000	10.0000	0.0578

Figure A.1: Speed 10 m/s

Alpha = 0°

alpha	Beta	CL	CDi	CDv	CD	CY	Cl	Cm	Cn	Cni	QInf	XCP
0.000	0.000	0.298542	0.003797	0.049605	0.053401	0.000000	-0.000000	-0.020686	-0.000000	-0.000000	6.0000	0.0549
0.000	0.000	0.298542	0.003797	0.041160	0.044957	0.000000	-0.000000	-0.020379	-0.000000	-0.000000	7.0000	0.0549
0.000	0.000	0.298542	0.003797	0.035976	0.039773	0.000000	-0.000000	-0.020226	-0.000000	-0.000000	8.0000	0.0549
0.000	0.000	0.298542	0.003797	0.032080	0.035877	0.000000	-0.000000	-0.020096	-0.000000	-0.000000	9.0000	0.0549
0.000	0.000	0.298542	0.003797	0.028739	0.032535	0.000000	-0.000000	-0.020000	-0.000000	-0.000000	10.0000	0.0549
0.000	0.000	0.298542	0.003797	0.026813	0.030609	0.000000	-0.000000	-0.019923	-0.000000	-0.000000	11.0000	0.0549
0.000	0.000	0.298542	0.003797	0.024909	0.028706	0.000000	-0.000000	-0.019844	-0.000000	-0.000000	12.0000	0.0549
0.000	0.000	0.298542	0.003797	0.023704	0.027501	0.000000	-0.000000	-0.019807	-0.000000	-0.000000	13.0000	0.0549
0.000	0.000	0.298542	0.003797	0.022560	0.026356	0.000000	-0.000000	-0.019774	-0.000000	-0.000000	14.0000	0.0549
0.000	0.000	0.298542	0.003797	0.021415	0.025212	0.000000	-0.000000	-0.019741	-0.000000	-0.000000	15.0000	0.0549

Figure A.2: $\alpha = 0°$

A.2 Tables - Control Derivatives - Test Aircraft - XFLR5

Freestream speed : 10.000 m/s

	alpha	Beta	CL	CDi	CDv	CD	CY	Cl	Cm	Cn	Cni	QInf	XCP
-18º Up	0.000	0.000	0.165412	0.009640	0.033026	0.042666	-0.000000	0.000000	0.356681	-0.000000	0.000000	10.0000	-0.2228
0º Reference	0.000	0.000	0.298542	0.003797	0.028739	0.032535	0.000000	-0.000000	-0.020000	-0.000000	-0.000000	10.0000	0.0549
+18º Down	0.000	0.000	0.432844	0.012076	0.034455	0.046531	-0.000000	0.000000	-0.397466	0.000000	0.000000	10.0000	0.1615

Figure A.3: δ_e Variation

Freestream speed : 10.000 m/s

	alpha	Beta	CL	CDi	CDv	CD	CY	Cl	Cm	Cn	Cni	QInf	XCP
Clockwise	0.000	0.000	0.279640	0.030940	0.041893	0.072833	-0.002359	0.129008	-0.014458	-0.002111	0.000866	10.0000	0.0525
Reference	0.000	0.000	0.298813	0.003803	0.028744	0.032547	-0.000000	0.000000	-0.019962	0.000000	0.000000	10.0000	0.0549
Anticlockwise	0.000	0.000	0.279640	0.030940	0.041892	0.072832	0.002359	-0.129008	-0.014459	0.002111	-0.000866	10.0000	0.0525

Figure A.4: δ_a Variation

Freestream speed : 10.000 m/s

	alpha	Beta	CL	CDi	CDv	CD	CY	Cl	Cm	Cn	Cni	QInf	XCP
-18º Right	0.000	0.000	0.301742	0.005680	0.030340	0.036020	-0.019761	-0.000424	-0.028524	0.007593	0.007584	10.0000	0.0586
Reference	0.000	0.000	0.298813	0.003803	0.028744	0.032547	-0.000000	0.000000	-0.019962	0.000000	0.000000	10.0000	0.0549
+18º Left	0.000	0.000	0.301742	0.005680	0.030327	0.036007	0.019761	0.000424	-0.028530	-0.007593	-0.007584	10.0000	0.0586

Figure A.5: δ_r Variation

A.3 Excel - Control Derivatives - Test Aircraft - XFLR5

Figure A.6: Test Aircraft δ_e Variation

Variação dos Ailerons - Delta_a

X_Delta_a=	0
Z_Delta_a=	0
M_Delta_a=	0

Alpha = 0º
Velocidade = 10 m/s

C_X Delta a= - CD_Delta_a	0
CZ_Delta a = - Cl_Delta a =	0
Cm_Delta a =	0

Calculo das derivadas Dimensionais devido a variação

Densidade:	1.225 Kg/m^3
Velocidade:	10 m/s
Corda:	0.125 m
Area S:	0.125 m^2
Alpha:	0 º Graus

Delta_a (Graus)	CD
18	0.072832
0	0.032547
-18	0.072832

negativo, aileron esquerdo para baixo, sentido horario

CD_Delta_a = 0

Delta_a (Graus)	CL
18	0.27964
0	0.298813
-18	0.27964

CL_Delta_a = 0

Delta_a (Graus)	Cm
18	-0.014459
0	-0.019962
-18	-0.014459

Cm_Delta_a = 0

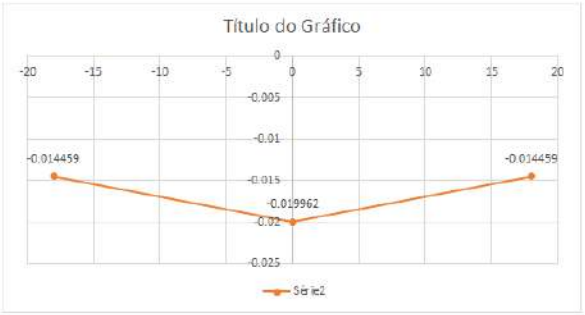

Figure A.7: Test Aircraft δ_a Variation

Variação do Fin - Rudder - Delta_r

Y_Delta_r =	0.008405286
L_Delta_r =	0
N_Delta_r =	-0.000403708

Alpha = 0º
Velocidade = 10 m/s

C_Y Delta r=	0.001097833
CL_Delta r =	0
Cn_Delta r=	-0.000421833

Calculo das derivadas Dimensionais devido a variação

Densidade:	1.225 Kg/m^3
Velocidade:	10 m/s
Corda:	0.125 m
Area S:	0.125 m^2
Alpha:	0 º Graus

Delta_r (Graus)	Cy
18	0.019761
0	0
-18	-0.019761

negativo, para a porta, fletido direita

CY_Delta_r =	0.00109783

Delta_r (Graus)	CL
18	0.301742
0	0.298813
-18	0.301742

CL_Delta_r =	0

Delta_r (Graus)	Cn
18	-0.007593
0	0
-18	0.007593

Cn_Delta_r =	-0.00042183

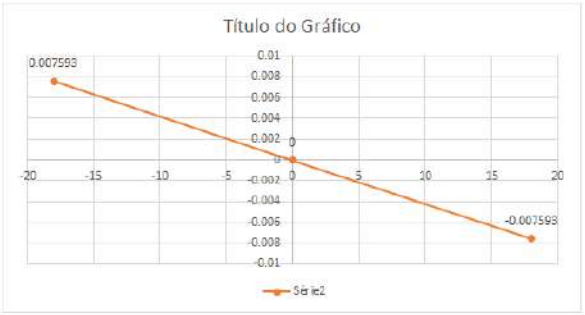

Figure A.8: Test Aircraft δ_r Variation

Appendix B

Excel Final Results - Wind Tunnel

The values used as a reference to calculate the derivatives for the Test Aircraft:

Table B.1: Test Aircraft - Data From Excel - Wind Tunnel

Variable	Reference Value
Density:	1.225 Kg/m^3
Speed:	10 m/s
Chord:	0.125 m
Areas:	0.125 m^2
Angle of attack:	0 $Degrees$

And the values used as a reference to calculate the derivatives for the F35 Aircraft:

Table B.2: F35 Aircraft - Data From Excel - Wind Tunnel

Variable	Reference Value
Density:	1.225 Kg/m^3
Speed:	10 m/s
Chord:	0.26 m
Areas:	0.3337 m^2
Angle of attack:	0 $Degrees$

In the next pages, it´s possible to observe our excel results.

B.1 Excel - Stability Derivatives - Test Aircraft - Wind Tunnel

Figure B.1: Test Aircraft Speed Variation

X_w=	0.698267358
Z_w=	-0.356556788
M_w=	-0.008773457

Cx_a = CL_1 - CD_a = 0.912023

Cz_a = - (CL_a + CD_1) = -0.46571

Cm_a = -0.09167

Para Alpha = 0º

CL_1= 0.915071

CD_1= 0.052687

	CD3d	CL	Cm	Re
-5	0.17914	-2.00386	-0.05812	82781.46
0	0.052687	0.915071	-0.15967	82781.46
5	0.199266	2.126332	-0.47408	82781.46

Velocity 10 m/s

Alpha (Graus º)	CD
-5	0.023274523
0	0.035840129
5	0.05375304

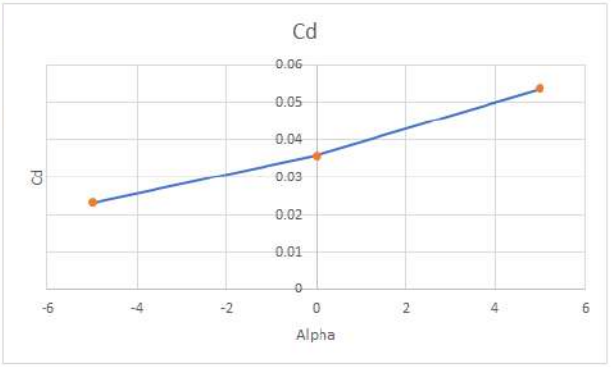

Cd_a 0.003048

Velocity 10 m/s

Alpha (Graus º)	CL
-5	-2.003862853
0	0.915070524
5	2.126332371

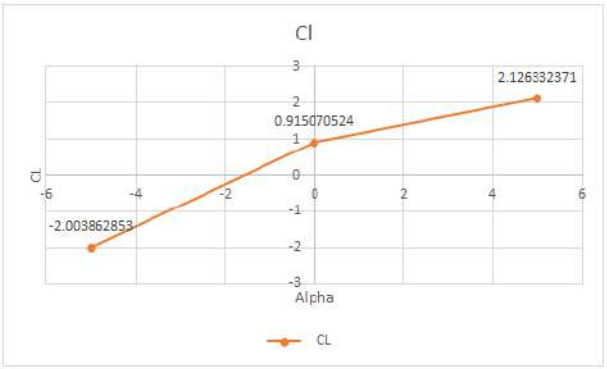

CL_a= 0.41302

Velocity 10 m/s

Alpha (Graus º)	Cm
-5	0.383096402
0	-0.04788432
5	-0.533640293

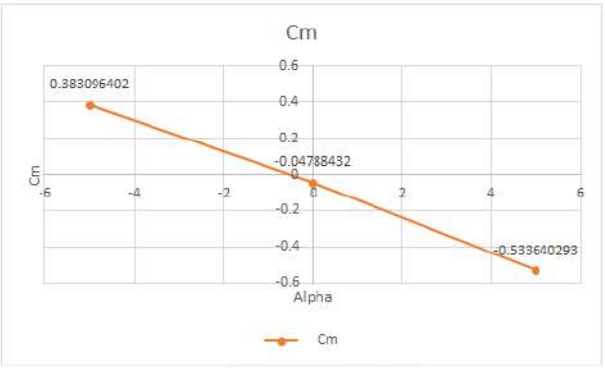

Cm_a= -0.09167

Figure B.2: Test Aircraft Angle of Attack Variation

L_v=	-0.0294992
N_v=	-0.0023591
Y_v=	-0.0069419

	CY	CL	Cn
U=10ms e a=0º B=-5º	0.330868	1.233042	0.025334
U=10ms e a=0º B=0º	0.404827	0.917405	-0.00114
U=10ms e a=0º B=5º	0.240198	0.847746	-0.00548

Velocity 10 m/s

Beta (Grausº)	CL
-5	1.233042
0	0.917405
5	0.847746

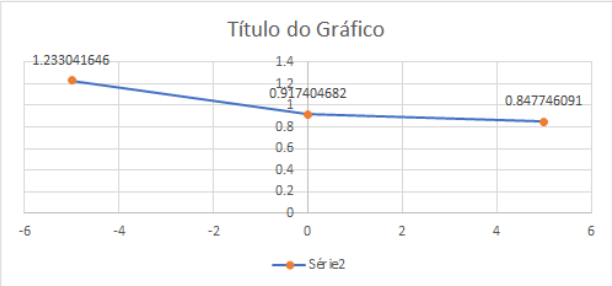

CL_B=	-0.03853

Velocity 10 m/s

Beta (Grausº)	Cn
-5	0.025334
0	-0.00114
5	-0.00548

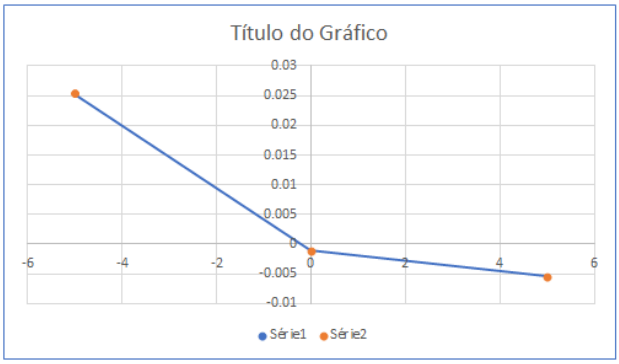

Cn_B=	-0.00308

Velocity 10 m/s

Beta (Grausº)	Cy
-5	0.330868
0	0.404827
5	0.240198

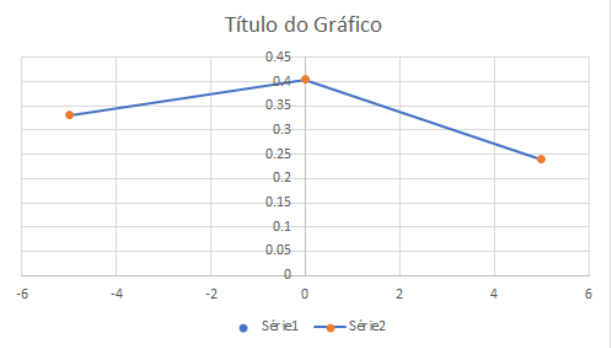

CY_B=	-0.00907

Figure B.3: Test Aircraft β Variation

Variation q

Clq=(Clq)asa + (Clq)cauda

(CLq)total= 0.078654

(CMq)total= -0.25169

(CZq)= -0.07865

(Clq)tail= 0.071504

(Cmq)tail= -0.22881

Xq=	**0.0037637**
Zq=	**-0.0037637**
Mq=	**-0.0015055**

lt=	0.4	m	
St=	0.02	m^2	V_H= 0.512
c=	0.125	m	corda da asa
S=	0.125	m^2	area asa
at=	0.069827889	\rad	

derivada do cl do estabilizador horizontal em ordem a alpha

ct=	0.06	m	corda da cauda
lt_barra=	0.38375		
d=	0.4	m	distancia Leasa - Lecauda
VH_barra=	0.4912		

Calculo do at:

at= 0.069827889

Alpha (Graus)	CL
-2	-0.14028
-1.5	-0.10523
-1	-0.07017
-0.5	-0.03509
0	0
0.5	0.035086
1	0.070166
1.5	0.105232
2	0.140278
2.5	0.175298
3	0.210284
3.5	0.245229
4	0.280128
4.5	0.314974
5	0.34976
5.5	0.384479
6	0.419125
6.5	0.453692
7	0.488173

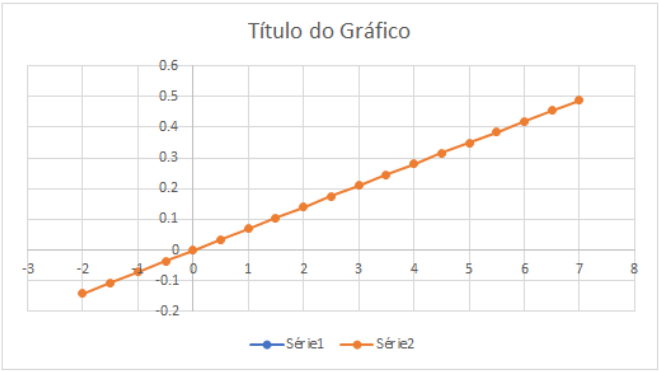

Figure B.4: Test Aircraft Pitch Moment Variation

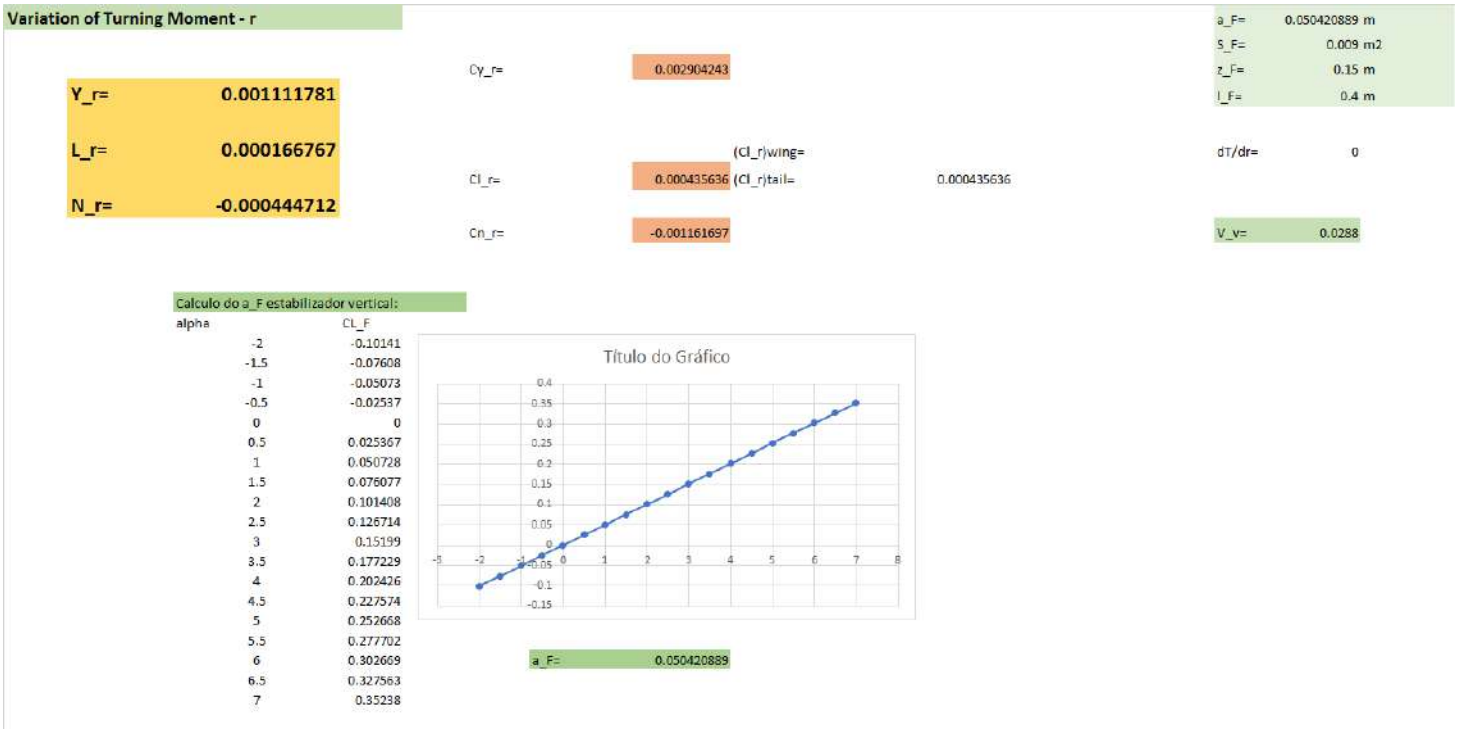

Figure B.5: Test Aircraft Turning Moment Variation

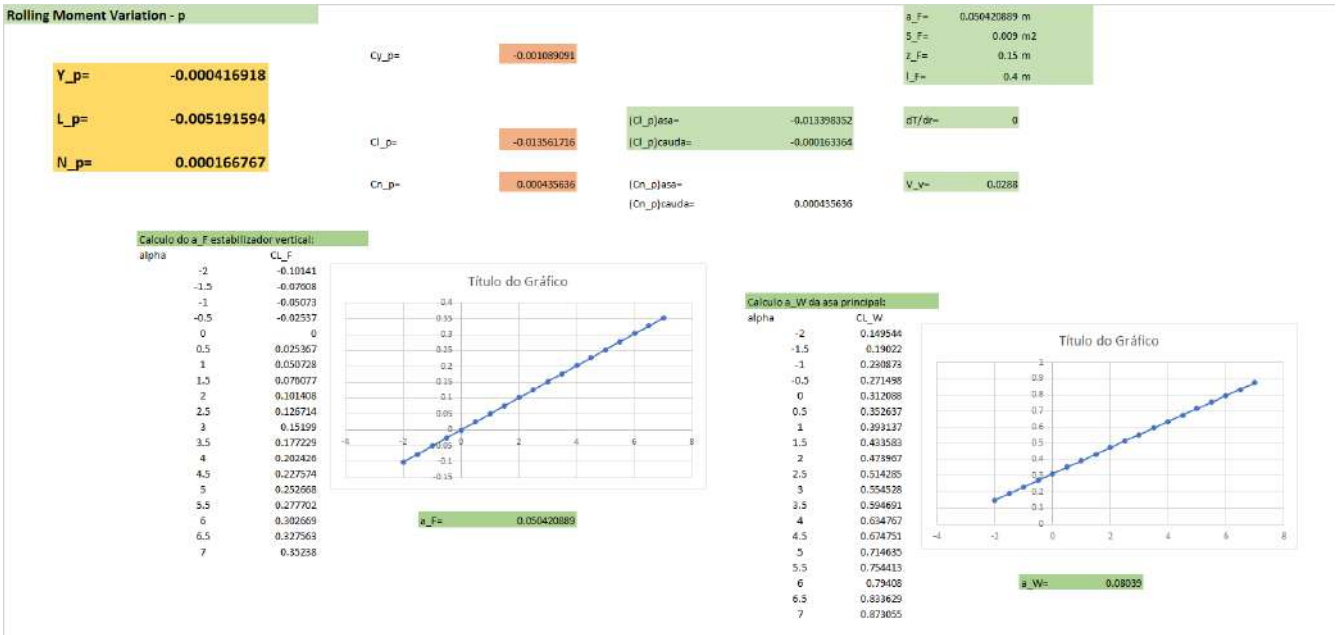

Figure B.6: Test Aircraft Rolling Moment Variation

B.2 Excel - Stability Derivatives - F35 Aircraft - Wind Tunnel

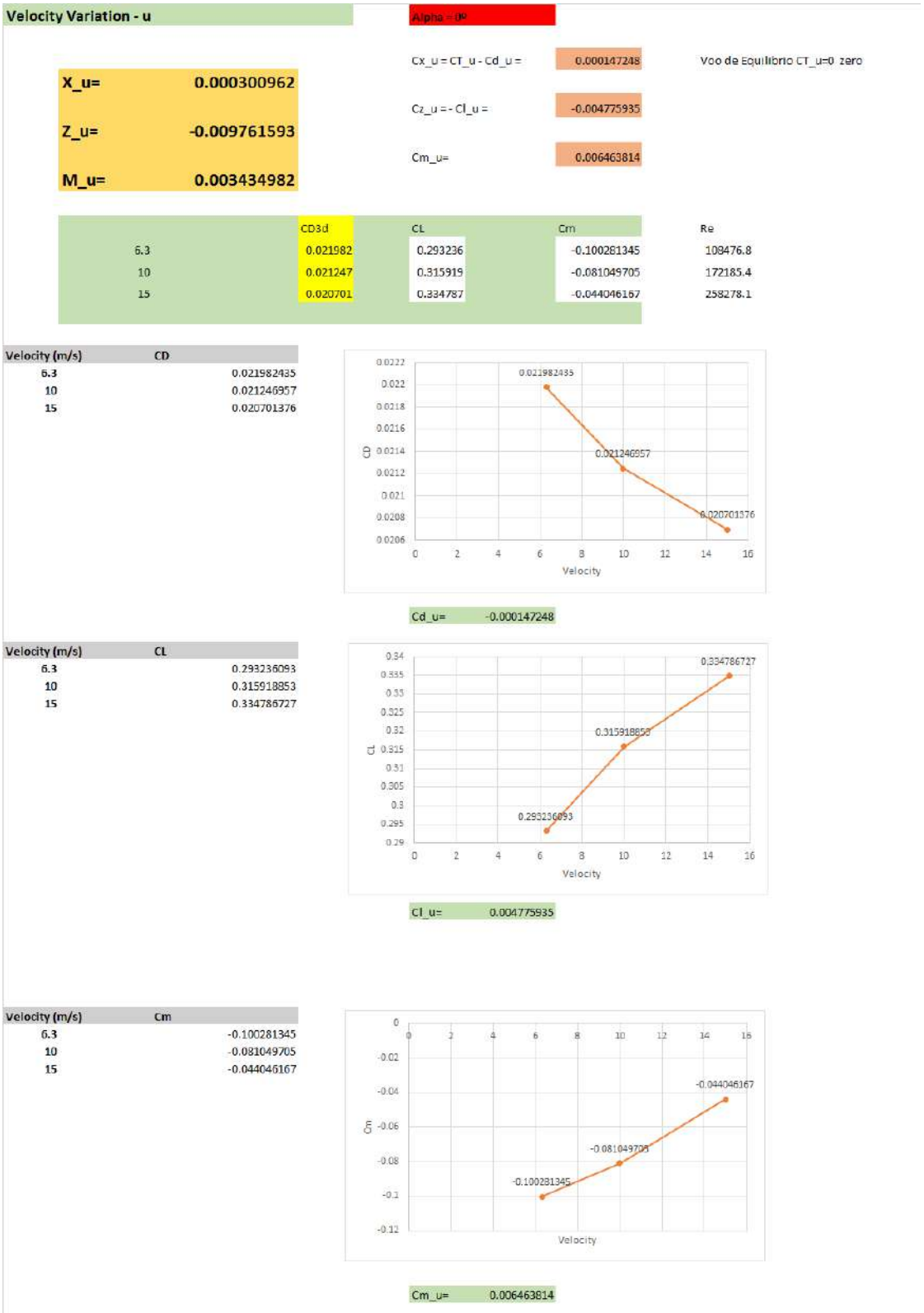

Figure B.7: F35 Aircraft Speed Variation

Para Alpha = 0º

CL_1=	0.2086963
CD_1=	0.0190088

Cx_a = CL_1 - CD_a =	0.208294
Cz_a = - (CL_a + CD_1) =	-0.0611
Cm_a =	-0.00968

X_w=	0.4257357
Z_w=	-0.124874
M_w=	-0.005145

	CD3d	CL	Cm	Re
-5	0.017601	-0.09045	0.075186	172185.4
0	0.019009	0.208696	-0.01919	172185.4
5	0.02162	0.330418	-0.02163	172185.4

Velocidade de 10 m/s

Alpha (Grausº)	CD
-5	0.017601365
0	0.019008818
5	0.021619818

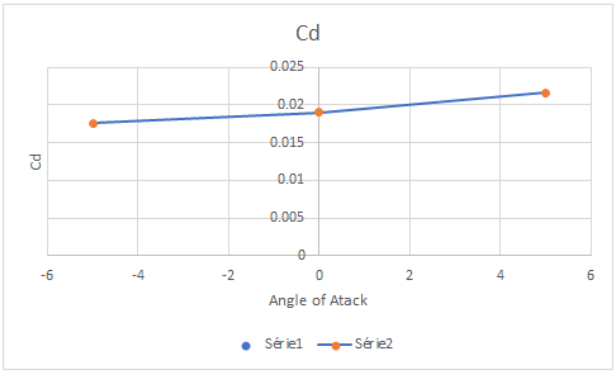

Cd_a	0.000402

Velocidade de 10 m/s

Alpha (Grausº)	CL
-5	-0.090448908
0	0.208696312
5	0.33041752

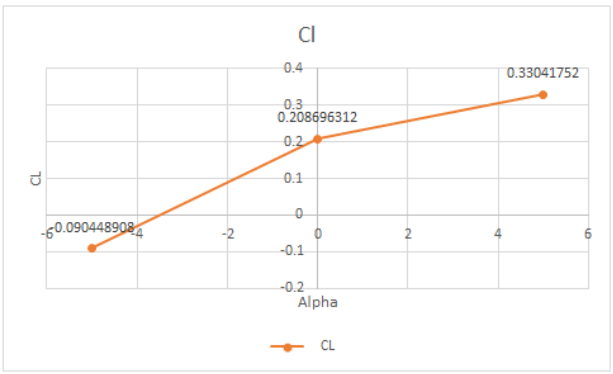

CL_a=	0.042087

Velocidade de 10 m/s

Alpha (Grausº)	Cm
-5	0.075186029
0	-0.019190504
5	-0.021634353

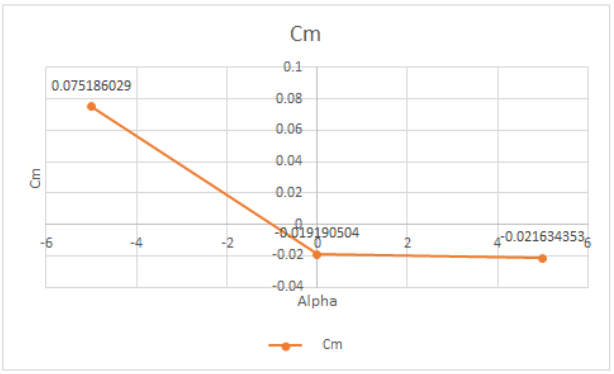

Cm_a=	-0.00968

Figure B.8: F35 Aircraft Angle of Attack Variation

L_v=	-0.1056486
N_v=	-0.008258
Y_v=	-0.0236363

	CY	CL	Cn
U=10ms e a=0º B=-5º	0.236136	0.758669	0.031794
U=10ms e a=0º B=0º	0.511013	0.511013	0.019511
U=10ms e a=0º B=5º	0.120493	0.241775	-0.00861

Velocidade de 10 m/s

Beta (Graus º)	CL
-5	0.758669
0	0.511013
5	0.241775

CL_B= -0.05169

Velocidade de 10 m/s

Beta (Graus º)	Cn
-5	0.031794
0	0.019511
5	-0.00861

Cn_B= -0.00404

Velocidade de 10 m/s

Beta (Graus º)	Cy
-5	0.236136
0	0.511013
5	0.120493

CY_B= -0.01156

Figure B.9: F35 Aircraft β Variation

Figure B.10: F35 Aircraft Pitch Moment Variation

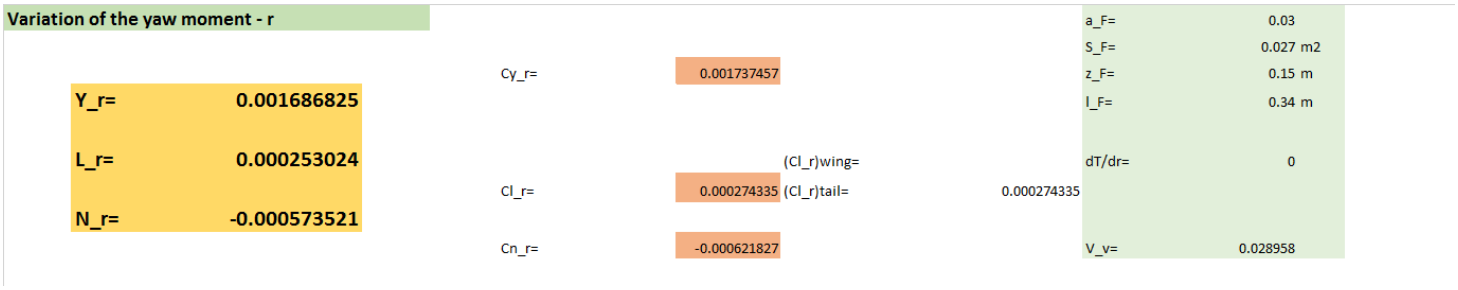

Figure B.11: F35 Aircraft Yaw Moment Variation

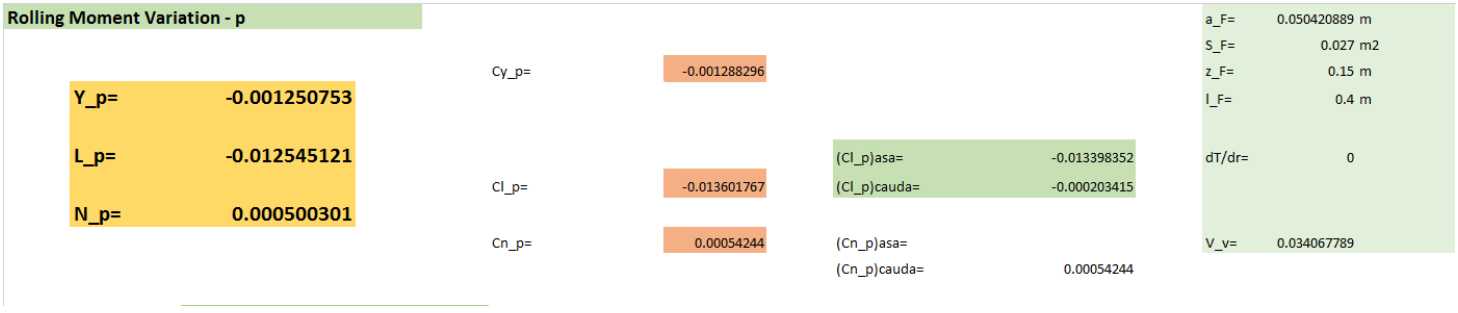

Figure B.12: F35 Aircraft Rolling Moment Variation

B.3 Excel - Control Derivatives - Test Aircraft - Wind Tunnel

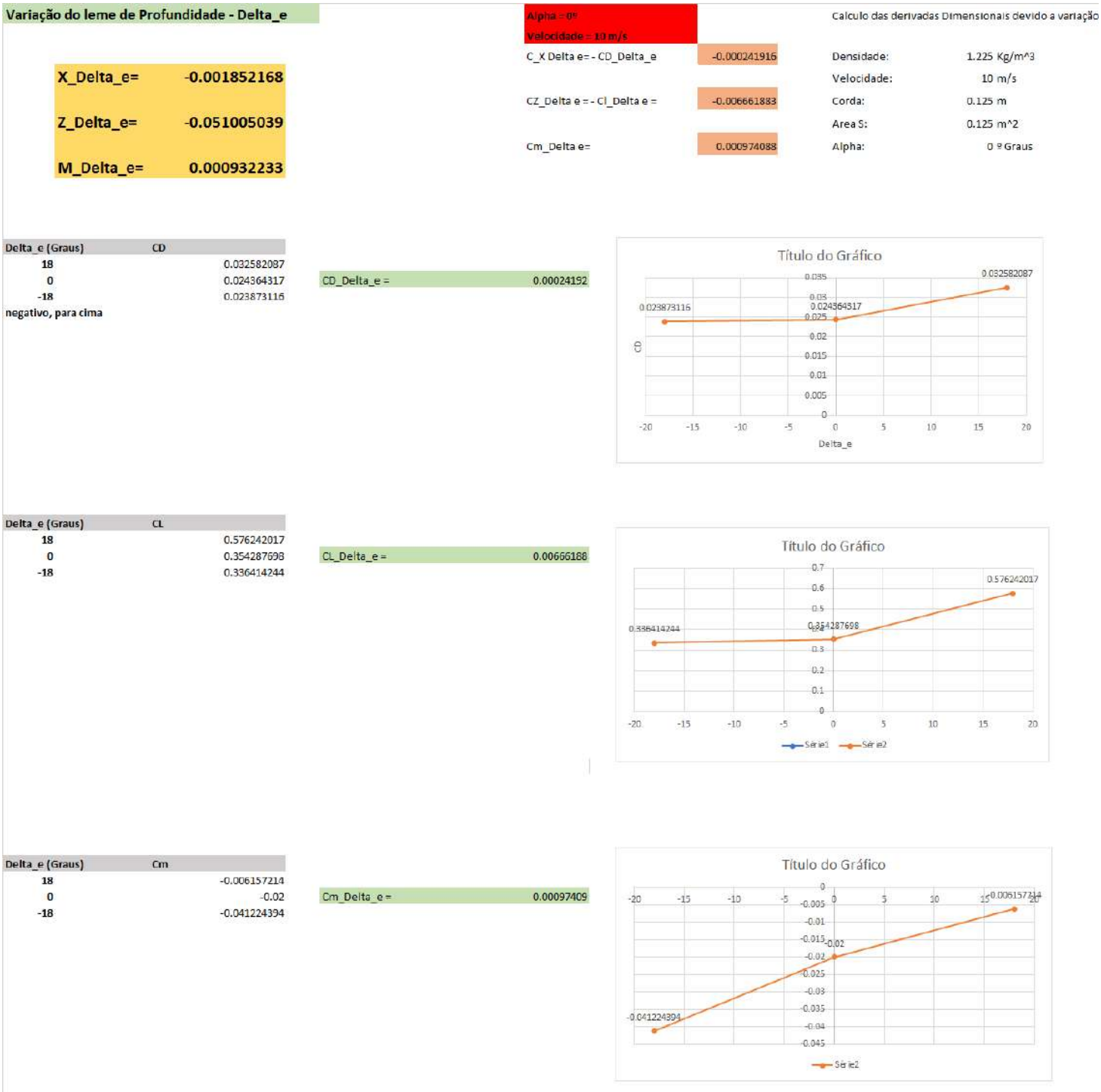

Figure B.13: Test Aircraft δ_e Variation

Variação dos Ailerons - Delta_a

X_Delta_a=	0.002169609
Z_Delta_a=	0.008304692
M_Delta_a=	-0.000359325

Alpha = 0º
Velocidade = 10 m/s

C_X Delta a= - CD_Delta_a	0.000283378
CZ_Delta a = - Cl_Delta a =	0.001084694
Cm_Delta a =	-0.000375458

Calculo das derivadas Dimensionais devido a variação

Densidade:	1.225 Kg/m^3
Velocidade:	10 m/s
Corda:	0.125 m
Area S:	0.125 m^2
Alpha:	0 º Graus

Delta_a (Graus)	CD
18	0.066253219
0	0.032547
-18	0.07645481

negativo, aileron esquerdo para baixo, sentido horario
Mx+

CD_Delta_a = -0.00028338

Delta_a (Graus)	CL
18	0.293348
0	0.298813
-18	0.332397

CL_Delta_a = -0.00108469

Delta_a (Graus)	Cm
18	-0.029083498
0	-0.019962
-18	-0.015566994

Cm_Delta_a = -0.00037546

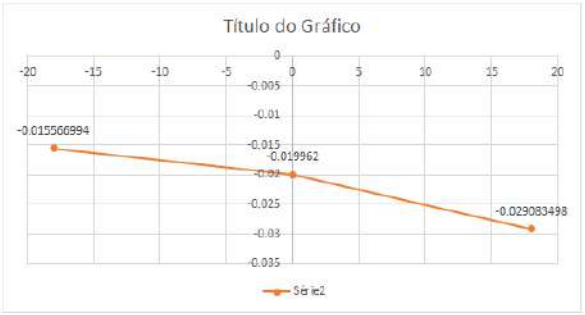

Figure B.14: Test Aircraft δ_a Variation

Variação do Fin - Rudder - Delta_r

Y_Delta_r =	0.019865148
L_Delta_r =	0.004082483
N_Delta_r =	-0.000385806

Alpha = 0º
Velocidade = 10 m/s

C_Y Delta r=	0.002594632
CL_Delta r =	0.000533222
Cn_Delta r=	-0.000403128

Calculo das derivadas Dimensionais devido a variação

Densidade:	1.225 Kg/m^3
Velocidade:	10 m/s
Corda:	0.125 m
Area S:	0.125 m^2
Alpha:	0 º Graus

Delta_r (Graus)	Cy
18	0.0007252
0	0
-18	-0.092681538

negativo, para a porta, fletido direita

CY_Delta_r = 0.00259463

Delta_r (Graus)	CL
18	0.307833
0	0.298813
-18	0.327029

CL_Delta_r = -0.00053322

Delta_r (Graus)	Cn
18	-0.000564858
0	0
-18	0.013947734

Cn_Delta_r = -0.00040313

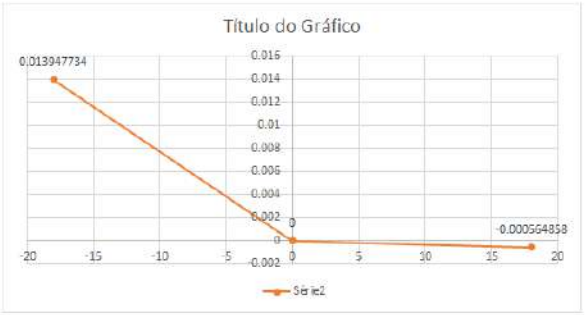

Figure B.15: Test Aircraft δ_r Variation

B.4 Procedure Guide for Balance of Forces

The following steps are required to initialise and operate the aerodynamic force balance:

1. Set the aerodynamic force balance inside the wind tunnel test near to the nozzle and over a additional structure to place the top of the flange exactly under the lower limit of nozzle;

2. Align the force balance with the nozzle so that the X axis of the force balance is parallel to the axis of symmetry of the nozzle. Then level the moving platform by adjusting the rubber supports at the bottom of the force balance, use a spirit level or similar on all edges;

3. Level the top of alpha adjustment with a spirit level or similar. Then, run the attitude sensor calibration script with the sensor on the current position of the top surface and aligned with the lateral surface edge. This reset the values of roll, pitch and yaw to zero;

4. Set the desired angle of attack using the pitch value of the attitude sensor as reference. The angle of side-slip follows the same methodology, but taking the yaw. The rotating collar is fix by three clamps in each vertex of the fix platform;

5. Mount the test model on the force balance and verify the nozzle limits influence on the model;

6. If the attitude of the model during the experiment is a parameter of study, the sensor should be placed in a part of the model that does not influence its aerodynamics (within the model if possible). Then reset the attitude sensor values for the current position running the calibration script again;

7. Place the pitot tube support in the front of the force balance and adjust the height to ensure the flow interference between plate and model do not occur. Then align the pitot tube with the flow;

8. Connect the sensing bars cable in the DAQ boards. Three sensing bars per DAQ board and follow the numeration of the cable (1, 2, 3, 4, 5, 6) with the numeration of the two DAQ boards (ch0, ch1, ch2, ch0, ch1, ch2);

9. Connect the three USBs to the hub, power the hub and connect it to the computer outside;

10. Open the LabVIEWTM file and verify that the first psychical channel corresponds to the DAQ board with the sensing bar 1, 2, 3 and the second physical channel to the other and check the order of the channels in each physical channel;

11. The force balance is ready for the experiments. Run both acquisition files in simultaneous and start with 0 airspeed. Change the frequency to the desired velocity. Take some time between velocities to identify the corresponding quantities and average them in data treatment;

12. Remove the test model and repeat the exact sequence to take the contribution of the structure under the influence of the flow to the forces and moments.